Available online at www.sciencedirect.com
ScienceDirect
Physics Reports 437 (2006) 1–54
PHYSICS REPORTS
www.elsevier.com/locate/physrep

Mesoscopic models of biological membranes

Maddalena Venturoli[a], Maria Maddalena Sperotto[b], Marieke Kranenburg[c], Berend Smit[a,c,*]

[a] *Centre Européen de Calcul Atomique et Moleculaire (CECAM), Ecole Normale Supérieure, 46 Allée d'Italie, 69007 Lyon, France*
[b] *Biocentrum, The Technical University of Denmark (DTU), Kgs. Lyngby, Denmark*
[c] *Van't Hoff Institute for Molecular Sciences, University of Amsterdam, Nieuwe Achtergracht 166, 1018 WV Amsterdam, The Netherlands*

Accepted 19 July 2006

editor: M.L. Klein

Abstract

Phospholipids are the main components of biological membranes and dissolved in water these molecules self-assemble into closed structures, of which bilayers are the most relevant from a biological point of view. Lipid bilayers are often used, both in experimental and by theoretical investigations, as model systems to understand the fundamental properties of biomembranes. The properties of lipid bilayers can be studied at different time and length scales. For some properties it is sufficient to envision a membrane as an elastic sheet, while for others it is important to take into account the details of the individual atoms. In this review, we focus on an intermediate level, where groups of atoms are lumped into pseudo-particles to arrive at a coarse-grained, or mesoscopic, description of a bilayer, which is subsequently studied using molecular simulation.

The aim of this review is to compare various strategies to coarse grain a biological membrane. The conclusion of this comparison is that there can be many valid different strategies, but that the results obtained by the various mesoscopic models are surprisingly consistent. A second objective of this review is to illustrate how mesoscopic models can be used to obtain a better understanding of experimental systems. The advantage of coarse-grained models is that these can be simulated very efficiently, so that phenomena involving large systems, or requiring a large number of simulations, can be studied in detail. This is illustrated with the study of the relation between the phase behavior of a membrane and the structure of the phospholipids, and the membrane structural changes due to molecules (such as alcohols, cholesterol and anesthetics) adsorbed to the membrane. We then discuss the effect of transmembrane peptides on the local structure of a membrane and the mechanism of vesicle fusion and fission.

PACS: 87.16.Dg; 87.17Aa; 87.15.Kg

Keywords: Biological membranes; Mesoscopic models; Dissipative particle dynamics

Contents

* Corresponding author. Centre Européen de Calcul Atomique et Moleculaire (CECAM), Ecole Normale Supérieure, 46 Allée d'Italie, 69007 Lyon, France.
E-mail address: b.smit@cecam.fr (B. Smit).

0370-1573/$ - see front matter © 2006 Elsevier B.V. All rights reserved.
doi:10.1016/j.physrep.2006.07.006

1. Introduction to biomembranes

Biological membranes are soft condensed matter structures which surround the cell and its inner organelles. They maintain relevant concentration gradients by acting as selective filters toward ions and molecules. Besides their passive role, they also host a number of metabolic and biosynthetic activities [1].

Over the years, our view of the structure of a membrane has evolved significantly since the first model of a biomembrane was presented by Gorter and Grendel in 1925 [2]. Gorter and Grendel performed experiments showing that a biomembrane is a very thin biomolecular structure, made of a double layer of lipid molecules, the so-called lipid bilayer. Then, in 1935, Danielli and Davson [3] developed the first model which took into account the presence of proteins in membranes—in fact proteins were thought to form a spread on each side of the lipid bilayer. It was not until 1972 that Singer and Nicolson [4] formulated the "fluid mosaic" model, on which the modern view of biomembranes is based. The fluid mosaic model describes the biomembrane as a fluid bilayer, which is composed of many types of lipids, and where proteins are embedded or attached. The molecules are free to move on the bilayer plane, thus imparting a liquid (or fluid) character to the membrane. Also, because of the great variety of the lipid and protein molecules of which it is composed, the membrane looks like a mosaic.

Subsequent refinements of the fluid mosaic model were suggested, based on the results of experimental and theoretical studies focusing on some specific aspects of membrane structure. Israelachvili [5] refined the Singer and Nicholson model by suggesting that proteins and lipids need to 'adjust' to each other (see the concept of 'hydrophobic matching' discussed in Section 3.3) thus causing a possible modulation of the lipid bilayer thickness. A further refinement was made by Sackmann [6] who stressed the role played by the cytoskeleton and the glycocalyx. Both these models view the membrane as a complex, highly cooperative and heterogeneous system, which displays dynamic and structural properties on many length- and time scales [7]. A schematic model of a membrane is shown in Fig. 1. The non-random molecular organization of membranes is vital for some biological processes and can be affected by physical and chemical factors which, in turn, can affect the functioning of the entire cell. During the last decades, it has been possible to make further progresses in unraveling the relation between membrane structure and organization

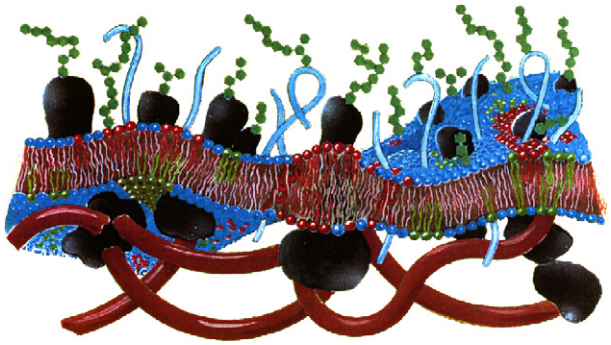

Fig. 1. A schematic drawing illustrating the complexity of a biological membrane.

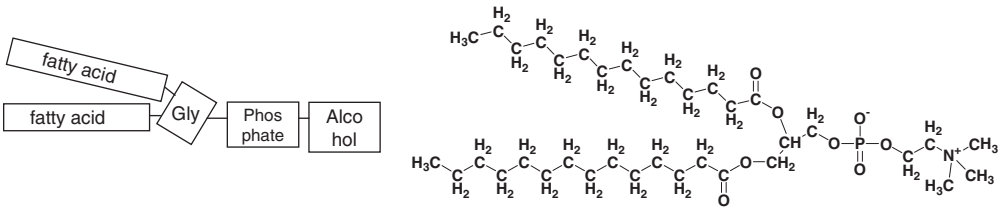

Fig. 2. Schematic drawing of a typical phospholipid (left), and the chemical structure of a specific phospholipid molecule, dimyristoylphosphatidylcholine (DMPC) (right). 'Gly' denotes the glycerol group.

(and membrane shape and shape transformation), and membrane biological functioning [6,8]—which is the ultimate goal of biomembrane science.

Because of the complexity of biomembrane structures, it is often necessary to investigate simplified systems: reconstituted lipid bilayers composed of one or two lipid species, and with embedded natural proteins, sterols, or artificial peptides, provide a model system for biological membranes. Understanding the physics of such simplified membranes can yield further insight into their biological function, can help to understand the cause of diseases, and can finally lead to the development of new therapeutics. Therefore, reconstituted membranes are extensively investigated by a number of experimental methods, based on spectroscopy, microscopy, fluorescence, scattering, and calorimetry, as well as by theoretical methods. In particular, the use of theories, modeling and computer simulations [9], has become an important and necessary tool for understanding the structure–function relation: not only the results from theories and model studies may provide a framework of interpretation of experimental data, but can also serve as a source of inspiration for future experiments.

Cell membranes are made of three major types of lipids, the phospholipids, cholesterol and glycolipids, where the phospholipids are one of the most abundant types. The backbone of a phospholipid is the glycerol group to which a hydrophilic headgroup and two hydrocarbon chains are connected—as schematically illustrated in Fig. 2. The head group consists of a phosphate group and an alcohol group. The hydrocarbon chains may vary in length and typically contain between 12 and 20 carbon atoms; also, they can be unsaturated or saturated, depending on the presence or not of one or more double bonds between consecutive carbon atoms. One of the most common types of phospholipids found in biomembranes are the phosphatidylcholines (PC). The chemical structure shown in Fig. 2 refers to a specific PC called dimyristoylphosphatidylcholine (DMPC); DMPC is one of the lipid types which are usually considered for making reconstituted membranes.

The characteristic of these biomembrane lipids is that they are amphiphilic molecules made of a hydrophilic (water loving, polar) head group and one or two hydrophobic (water repellent, non-polar) hydrocarbon chains. Because of this amphiphilic nature, when lipids are dissolved in water at sufficiently high concentrations, they spontaneously self-assemble into structures where the lipid 'tails' shield themselves from the polar environment of the water, while the polar head groups prefer the contact with water. Depending on the shape of the lipids, different structures may form

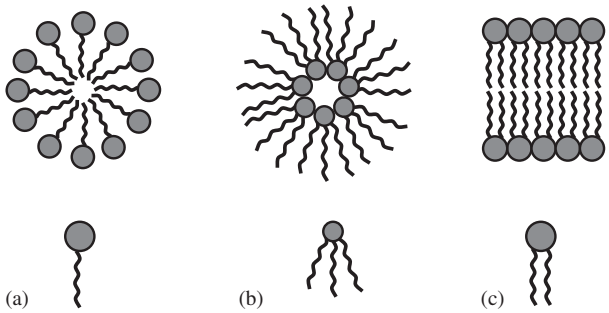

Fig. 3. Possible structures formed by the self-assembly of lipid molecules in water: (a) micelle; (b) inverted micelle; and (c) bilayer. The filled circles represent the polar hydrophilic head groups of the lipids, and the wavy lines the hydrophobic acyl-chains.

(see Fig. 3) [10–13]. Lipids are a special form of amphiphilic molecules and the structures shown in Fig. 3 can also be observed in surfactant solutions or special types of block co-polymers. The formation of these structures is caused by the hydrophobic effect [14,15], but also van der Waals attractive forces, electrostatic interactions, and the formation of hydrogen bonds contribute to the stabilization of these structures [16,17]. The understanding of the physical–chemical aspects of these structure is a very active area of research.

Of course, among these structures, the bilayer has received particular attention from the bio-community. At this point, it is important to mention that a bilayer of lipids is a very much simplified model system of real membranes. Nevertheless, understanding the physical-chemistry of these model membranes is of relevance for the more complex biological systems. These simplified systems are therefore extensively studied, both experimentally as well as from a theoretical point of view.

Seen from a macroscopic point of view, biomembranes are stable and flexible thin sheets, about 50 Å thick. Biomembranes are fluid structures, which, in macroscopic terms, means that they do not exhibit sheer restoring forces. At the molecular level, the bilayer forming molecules undergo translational and rotational diffusion typical of a thick oil [18]. The structure and the physical properties of membranes depend on the properties of the lipid molecules (such as the head group types or the length and unsaturation of the acyl chains) and of the membrane-associated proteins. For example, the degree of unsaturation of the acyl chains is an important control parameter for the fluidity of biomembranes, hence for their flexibility.

The reconstituted one-component lipid bilayers show a complex behavior which is the result of the many degrees of freedom present in these systems. Therefore, depending on the time and length scales one is interested in, to model such systems it may be necessary to neglect some of the degrees of freedom and approximate others in an effective way, to be able to study the behavior of the systems as function of, for example, temperature, or composition.

Biomembrane phenomena have been studied theoretically with the help of lattice [19,20], interfacial [21], or phenomenological models [22–24]. Although these types of modeling are not computationally time demanding, the disadvantages of the lattice and phenomenological models cited above is that they do not picture the membrane as a three-dimensional structure embedded in a three-dimensional space—and therefore cannot be used to investigate a number of phenomena or processes related, for example, to out-of-plane membrane changes, such as what happens during the fusion of two cells. A fully atomistic description can be obtained via simulations methods such as molecular dynamics (MD) or the Monte Carlo technique (MC). These all-atom simulations give important information on the structural and dynamic properties of lipid bilayers. For an overview of the results of these types of simulations, we refer to [25–27] and references therein. Atomistic MD simulations are, however, computationally very expensive to investigate membrane phenomena which occur on the mesoscopic time and length scales. In fact, recently Brannigan et al. [28] have given an estimate of the time required to simulate a small patch of a cell membrane for just 1 ms by MD on atomistic models: 46 years. As there are many important phenomena that occur beyond this time and length scale, we either wait many years before the computers have become sufficiently fast, or develop an alternative approach that aims to bridge the time and length scales involved in these phenomena. One approach is to coarse grain the system by integrating out those atomic coordinates that are not relevant for the problem being studied. For example, by approximating the molecular components of a system by a set of ‘particles’, or ‘beads’, where each ‘bead’ represents a cluster of atoms whose details are not important to the process under investigation. The bead-based mesoscopic models

are an example of coarse-grained models. Of course, in such an approach it is assumed that we know which atomic aspects are important and which ones can be neglected. In practice, however, our knowledge is not sufficient to a priori identify which aspects are essential. In addition, there is no universal recipe available that turns an all-atom model into a coarse grained model. These two aspects are the motivation behind this review. In recent years many different approaches have been published with different aims and different recipes to coarse grain lipid bilayers. Section 2 is devoted to the presentation of the types of coarse-grain models which have been used to study model membranes. In this section we aim to illustrate and compare the various approaches that have been used to coarse grain a membrane system. The interesting aspect is that these models have been developed with very different applications in mind. These applications range from the self-assembly of lipids into bilayer and vesicles, bilayer phase-changes, domain formation and growth, formation of pores, membrane budding and fission, vesicle fusion, etc. We conclude this section with a critical comparison of the different approaches.

To illustrate how mesoscopic models can be used to shed some light on important experimental questions in biomembrane systems, in Section 3 we discuss a few applications in more detail. These applications relate to the phase behavior of lipid bilayers and the structural modifications of the bilayer caused by the adsorption of molecules (e.g., alcohol, anesthetics, or cholesterol), to the effect of integral membrane proteins on the local structure of a membrane, and to the process of vesicle fusion and fission.

In a separate appendix, we describe the simulation techniques such as MD, MC and dissipative particle dynamics (DPD) that are used on these models, focusing on those computational aspects that are peculiar to bilayers (e.g., simulations are zero surface tension). In addition, we describe the methods that are used to compute various structural and mechanical properties of a bilayer.

2. Mesoscopic models

The formation and stability in water of lipid self-assembled structures is mainly due to the hydrophobic effect. In mesoscopic models of lipid-water systems, water is either modeled implicitly by the use of effective forces which act on the lipids to form aggregates and to guaranty their stability in the solvent, or water is explicitly modeled. Because implicit solvent models have recently been reviewed [28], here we will just give a short description of these models and their applications in relation to biomembranes.

2.1. Implicit solvent models

Implicit solvent models may be grouped into two main types [28]: continuum elastic-models and particle-based coarse-grained models. Because the description of continuum models is outside the scope of this review—for a review of continuum models see [28,29]—here we just mention that continuum models view a membrane as an infinitely thin elastic sheet described by its free energy of deformation. The expression for the free energy is based on the Helfrich Hamiltonian [30,31]. In short, quantities like the bending rigidity, spontaneous curvature and surface tension are used to describe the physical state of the system, and the parameters related to these quantities constitute an input to the model. Continuum models are well suited to study phenomena at macroscopic length- and time-scales, such as shape deformation of vesicles and thermal fluctuation modes of lipid bilayers. However, if one wants to study membrane phenomena occurring at the mesoscopic time and length scale, and/or if one wants to gain insight into the effect of the molecular structure of the membrane components on the physical behavior of the whole system, a particle-based approach becomes necessary. By using the latter approach, the mechanical properties of the membrane can be derived as a result of the simulation study, and do no longer constitute inputs to the model—as is the case for continuum models.

The idea of implicit solvent modeling for particle-based models is that the hydrophobic interactions are not explicitly taken into account. In this way, the computational time can be significantly reduced, since the degrees of freedom of the solvent particles, which represents a substantial fraction of the simulated system, are not explicitly taken into account. The stability of the bilayer system has, however, to be guaranteed by an external force which constrains the lipid headgroups, either by linking them to each other or by tethering them to a surface. In alternative, effective attractive potentials between the lipids can be employed to maintain macroscopic structures.

Sintes and Baumgärtner [32,33] were among the first to develop an implicit solvent coarse-grained model for lipid bilayers. Lipid molecules are modeled by flexible chains having each five monomers, where each monomer represents three or four CH_2 chemical groups. The head group of the lipids is modeled by a single monomer. The molecules

interact via hard-core potentials. To maintain the bilayer integrity, the heads of the mesoscopic molecules are tethered to some continuous sheets which also allow the molecules to diffuse freely in their proximity. Sintes and Baumgärtner validated the model for the pure lipid bilayer by reproducing the values of the average mean area per lipid and the average tilt angle obtained experimentally. The same authors also extended this model to study the lipid-mediated attractions between transmembrane cylindrically-shaped proteins [32] and truncated-cone shaped proteins [34]. The results from this study are described in more detail in Section 3.3.

In analogy to a previously developed mesoscopic model for Langmuir monolayers, Lenz and Schmid [35] developed a mesoscopic implicit solvent model for pure lipid bilayers with saturated lipids. Each lipid is made of a six-bead tail, with beads of equal size, and a larger lipid head-group bead. The lipid beads interact via a truncated Lennard–Jones potential. The solvent-induced bilayer stability is obtained by considering two types of approaches. The first approach consists in forcing the lipids to form bilayers by confining their heads to two parallel planes—as in the model of Sintes and Baumgärtner. An advantage of this approach is that it does not require great computational effort. A limitation of the approach is the fact that the planes which confine the head-group beads do limit the bilayer deformations and undulations. This limitation is overcome in the second approach because the bilayer is stabilized by a surrounding gas of 'phantom' solvent beads, which do not interact with each other, but only with the lipid head-group beads. Both models are validated by reproducing qualitatively the abrupt changes that a order parameter, for example the area per lipid, shows when saturated lipid bilayers undergo a gel–fluid phase transition.

A particular implementation of the so-called "tethered models" is the multiscale approach of Ayton and Voth [36]. These authors discretize the area of the membrane into a number of finite small elements that are represented by particles bonded together in two dimensional elastic sheets. The time-evolution of these particles is studied by the DPD simulation technique. The parameterization of the conservative force bonding the particles together is done by performing preliminary atomistic MD simulations of a DMPC bilayer, and by tuning the coarse-grain model parameters to reproduce the area compressibility, density, area per lipid and bilayer thickness of the atomistic system [37].

Another implicit-solvent modeling approach consists in incorporating the hydrophobic interactions into effective lipid–lipid interactions resulting from attractive pair potentials (e.g. van der Waals). However, these types of effective interactions may lead to the formation of membranes which are not fluid at any considered temperature [38–40]. A solution to this problem is to adopt multi-body potentials, as Drouffe et al. [38] did. According to their approach, a model membrane is made of anisotropic spheres forming a sheet; the spheres interact both via an orientation dependent pair-potential, and via isotropic many-body potentials between the particles, which account for the hydrophobic interactions. Using many-body potentials, Drouffe et al. [38] were able to maintain the membrane in the fluid phase. It is worth mentioning that, using the approach described above, Drouffe et al. were able to self-assemble a vesicle a decade before it was possible to self-assemble a membrane or a vesicle by explicit-solvent simulations, either based on atomistic models [41,42] or on mesoscopic ones [43].

Noguchi and Takasu [39,44–46] also used multi-body potentials, with the lipid molecule represented by a rigid chain consisting of one hydrophilic and two hydrophobic beads. To hold the system together, an attractive multi-body potential acts between the hydrophobic beads. This model was validated by verifying that, depending on the temperature considered, the mesoscopic molecules assemble into micelles or vesicles [39]. By decreasing temperature, the formed structures evolve from many small micelles to larger micelles, branched thread-like micelles, and finally to fluid vesicles. Studies on the kinetics of self-assembly predicted the formation of intermediate 'stalk' structures, which were previously suggested by other investigations [47]. Brownian dynamics studies of the molecular mechanism of membrane fusion [44] also detected the formation of a 'stalk' intermediate, from which the fusion proceeds. The vesicle fusion process is described in Section 3.4.

Models that consider the lipids as rigid molecules may show limitations in reproducing the elastic properties of real lipid membranes, resulting in bilayers with a much higher bending rigidity. Improvements of the rigid-lipid models to allow for molecular flexibility [48,49] resulted in bilayers with the correct bending rigidity. To study phenomena that are sensitive to the flexibility of the lipids, Wang and Frenkel extended the Noguchi and Takasu model to flexible lipid molecules [50], and studied the phenomenon of spontaneous pore formation in lipid bilayers [51]. Experiments performed at relatively low tension on a membrane at thermal equilibrium [52] suggest that the spontaneous pore formation (without rupture of the membrane) is a two-stage process: first a molecular-sized metastable defect forms, which then acts as the seed for the nucleation of a larger pore. Molecular simulations can be used to provide informations about the microscopic structure of the defects. Atomistic simulations would require very large stresses to induce a pore formation—and consequently could result in membrane rupture [53]—therefore Wang and Frenkel [51] have used

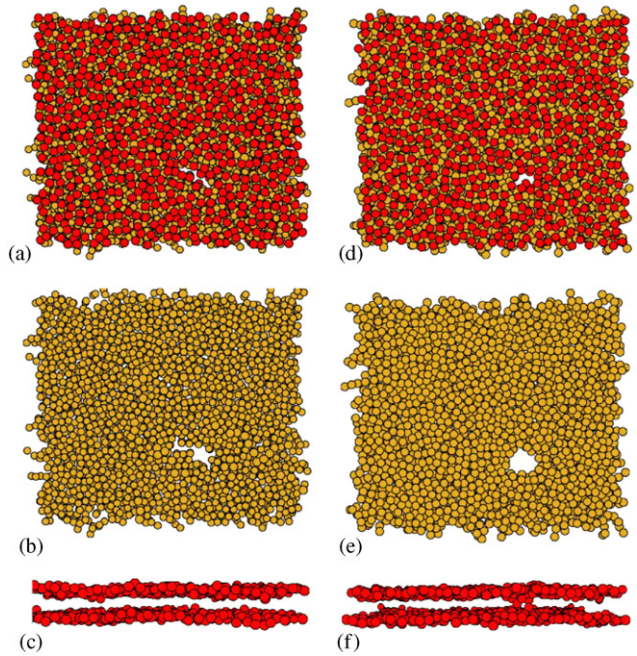

Fig. 4. Membrane with a hydrophobic (left) and a hydrophilic (right) pore. Hydrophilic particles are depicted in red and hydrophobic ones in yellow (color online only). Reused with permission from Zun-Jing Wang and Daan Frenkel [51]. Copyright 2005, American Institute of Physics.

a mesoscopic model studied with Monte Carlo simulations to monitor pore nucleation under constant lateral stresses that are lower than those needed to rupture the membrane. These simulations show that both 'hydrophobic' and 'hydrophilic' pores can form, where 'hydrophobic'/'hydrophilic' refers to a pore with a rim covered with hydrophobic/hydrophilic groups, respectively, as illustrated in Fig. 4. In fact, the incipient pores are hydrophobic but, as the lateral size of the pore nucleus becomes comparable with the molecular length, the pore becomes hydrophilic. Small pores instead remain hydrophobic, and show deviations form a circular shape, due to thermal fluctuations. The growth and closure of hydrophilic pores depends on the competition between the surface tension of the membrane and the line tension at the pore rim. The estimated values of the latter from the shape of the computed free-energy barrier for the nucleation of pores is in good agreement with experimental data.

From a computational point of view, the use of a multi-body potential is inconvenient. Recently, it was shown that a stable fluid phase of particle-based coarse-grained lipid bilayers with implicit solvent can also be obtained using only pairwise interactions [40,54–56]. Like the Noguchi and Takasu model, the Farago [54] model represents the lipids as rigid molecules composed of three beads, two hydrophobic and one hydrophilic. It is also an implicit solvent model but, unlike its predecessor, it does not rely upon many-body interactions to hold the amphiphiles together, but rather on pair-interactions. The model was validated by investigating with Monte Carlo simulations the phase behavior of lipid bilayers as a function of the projected area (i.e., the area density of the lipids). Upon increasing the projected area (which is analogous to increasing the temperature) it was found that the model membrane undergoes a solid–fluid phase transition. In the solid phase the lipids are not mobile and they pack in hexagonal order. In the fluid phase the lipids are free to diffuse in the membrane plane. Also, the elastic behavior of the system was characterized by calculating the surface tension and the bending modulus from the spectrum of thermal undulations of the fluid membrane [54,57]. The value of the bending modulus found using this model is in the same range of experimental values for pure lipid bilayers [58]. Interestingly, Farago found that at low area densities another transition occurs from negative to positive surface tension, which is accompanied by the formation of pores in the membrane—as previously predicted by theoretical arguments [59]—and which involves lipid flip-flop, a suggested connection also based on experimental evidence [60].

Farago et al. [61] have extended this implicit solvent model to capture the self-assembly of cationic lipid-DNA (CL-DNA) gene delivery complexes. CL-DNA complexes are interesting from the biotechnological point of view because of their potential use as nonviral transfection vectors in gene therapy [62] and because they have low toxicity,

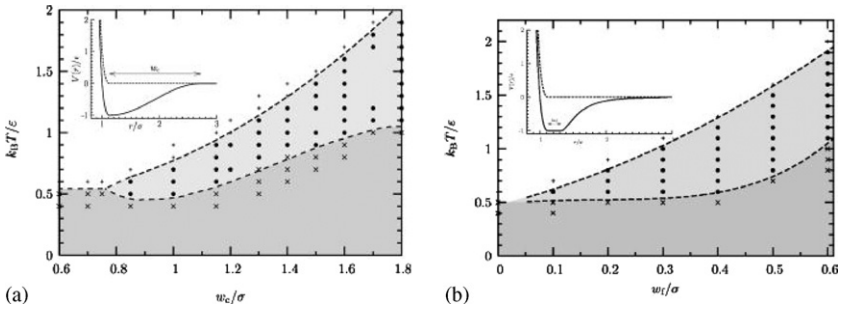

Fig. 5. Phase diagrams of model lipid bilayers obtained using the implicit solvent model of Cooke and Deserno [40]. Gel (crosses) and fluid (full circles) phases are obtained as a function of temperature and of the width (w_c) of the range of attraction for two types of pair potential (inset in the figures). Reused with permission from Cooke and Deserno [40]. Copyright 2005, American Institute of Physics.

non-immunogenicity, and are easy to produce. Therefore, to recognize structures of CL-DNA complexes may strongly advance the understanding of their function. Farago et al. predicted a dependence of the spacing between DNA chains on the concentration of CLs which is in excellent agreement with X-ray diffraction experimental data. Also, they found that at high concentrations of CLs, the large electrostatic pressure induces the formation of pores in the membrane, through which the DNA molecules may escape the complex. They relate this observation to the origin of recently observed enhanced transfection efficiency of lamellar CL-DNA complexes at high charge densities.

Cooke et al. [49] implemented a coarse-grained model of lipids with implicit solvent and showed that pairwise interactions are sufficient to produce a stable fluid bilayer. In this model the lipids are represented by a trimer with one head bead and two tail beads, linked by a finite extensible nonlinear elastic (FENE) potential and subjected to a bond bending potential to control the chain flexibility. The main feature of this model is that the hydrophobic effect is taken into account by using a simple attractive two-body potential between the lipid tails, whose range can be varied while all the other interactions are repulsive. Using MD and a Langevin thermostat on this coarse-grained model, Cooke and co-workers constructed the phase diagram of preassembled bilayers as a function of temperature and of the range of the attraction between the lipid tails. The phase diagram (Fig. 5) shows that a fluid phase is present, which is stabilized by increasing the attraction range, while it disappears below a critical range (gas-phase), and that a transition to the gel phase can be reproduced with decreasing temperature. The model also shows that the attractive interaction leads to self-assembled bilayer whose aggregation properties matches the ones of the preassembled bilayers at the same temperature and attraction range, although the phase boundaries are slightly broadened in the case of self-assembled bilayers. Moreover Cooke and Deserno [40] have shown that the key feature of the model is the range of the attraction potential, and not its specific functional form as illustrated by the phase diagrams of Fig. 5.

Also Brannigan et al. [48] find that a sufficiently broad pairwise attractive potential leads to a stable fluid bilayer without explicit solvent. The difference with the model of Cooke et al. is that Brannigan and co-workers applied the attractive potential between special “interface” beads, which connect the hydrophilic head bead to the hydrophobic tails beads. These special beads are meant to mimic the effect of hydrophobic interactions and to control the interfacial tension in the absence of solvent. Both models were able to reproduce bilayers with a bending rigidity in the experimental range for lipid bilayers. Cooke et al. [49] have also shown that the value of the bending rigidity (at zero tension) can be tuned via the range of the attractive potential, to which it is related by a monotonous linear dependence.

Recently, Cooke and Deserno [63] extended their coarse-grain model to investigate the effect of lipid shape on the curvature of the lipid aggregates. By varying the size of the lipid headgroup, these authors could model lipids with noncylindrical shapes. These lipids aggregate into the typical structures experimentally observed for noncylindrical (or nonbilayer) lipids [64], including spherical micelles and branched wormlike micelles. They also showed that curvature-induced lipid sorting occurs in mixed system with pronounced curvature, but that the coupling between lipid shape and membrane curvature has a weak effect in biologically sized systems.

A promising approach to derive the effective interactions between coarse-grained molecules is based on the inverse MC method [65]. The procedure consists in performing (small) atomistic simulations of the system one wants to parameterize from which the radial distribution functions (RDFs) between pairs of centers which will represent the interaction sites in the coarse-grained model calculated. Different methods have been used to reconstruct the effective

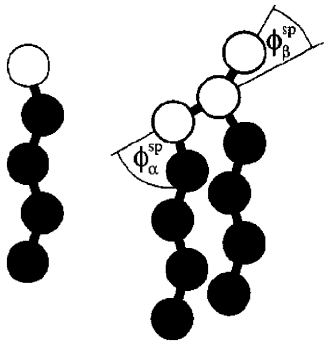

Fig. 6. Coarse-grain model of Goetz and Lipowsky [74] for amphiphilic molecules with one or two hydrophobic tails. Hydrophilic beads are represented in white and hydrophobic ones in black. Reused with permission from Rüdiger Goetz and Reinhard Lipowsky [74]. Copyright 1998, American Institute of Physics.

potentials from the RDFs [65–67]. In general, an iterative procedure is used by comparing the RDFs of the atomistic and coarse-grained simulations, using tabulated potentials for the coarse-grained model, until convergence is reached. By construction, the RDFs of the coarse-grained model match those of the atomistic simulations. Lyubartsev [68] applied this method to construct a implicit solvent model for lipids and lipid bilayers. Coarse-grained lipids are formed by one headgroup consisting of two beads to which two tails of four beads each are attached. The effective pairwise interaction potentials are derived from atomistic simulations of DMPC in water using the inverse MC procedure. The effect of the solvent is implicitly taken into account in the effective potentials. Four bead types were considered, for the choline, phosphate, glycerol and carbon groups in the lipid tails. Harmonic springs were used between beads linked together, and bond-bending potentials were neglected. Spontaneous self-assembly of these model lipids into bilayers and vesicles was obtained by using both MC and MD, with MD being more efficient. Density profiles in the bilayer were found to be in good agreement with the ones from atomistic simulations. This was not to be a priori expected, since the interaction potentials were derived using a dilute system of lipids in water and not a fully formed bilayer.

2.2. *Explicit solvent models*

In this section we review the coarse-grain models for phospholipid molecules where the solvent is explicitly treated. Among these models one can distinguish between two main types. One type is constituted by the 'bead-and-spring' models: these models aim at describing the system with as few bead types as possible; in general, two bead types are used which are either polar (hydrophilic) or hydrophobic. The beads interact with one another via effective potentials, which do not aim to represent the true nature of the underlying atomistic interactions. Electrostatic interactions are not explicitly modeled. Concerning the nonbonded interactions, they can be represented by Lennard–Jones like potentials, of by soft-repulsive potentials. These lipid models have many points in common with the earlier models developed to study the self-assembly of micelles and surfactant monolayers [69–73]. It is worth mentioning that, despite their simplicity, these models show a remarkable ability to reproduce the structural, thermodynamic and mechanical properties of lipid aggregates (e.g., bilayers and vesicles). The explicit solvent models of the other type are also based on a simplified description of the molecules, but the interactions are systematically parameterized using data obtained from atomic-resolution simulations.

2.2.1. *Empirical coarse-grained models*

Goetz and Lipowsky [74] introduced a simple coarse-grained model for lipid membranes based on a binary Lennard–Jones fluid of solvent beads and amphiphilic molecules. The amphiphiles are made of one or two hydrophobic tails attached to a headgroup made of one or more hydrophilic bead(s), as illustrated in Fig. 6. The beads are linked together by harmonic springs and the chain stiffness and headgroup geometry can be controlled by bond-bending potentials. The repulsive interactions between hydrophobic and hydrophilic beads are modeled by a repulsive soft-core potential ($\sim 1/r^9$), while attractive interactions are modeled by the Lennard–Jones potential. No electrostatic interactions are considered. Depending on concentration, spontaneous self-assembly into micelles or fluid bilayers was observed for this

coarse-grained model [74], and both MD and MC simulations techniques were used. The effect of lipid architecture (e.g., chain length or stiffness) on the structure and lateral stress distribution in the bilayer was also investigated. The elastic properties of these coarse-grain bilayers have also been studied by means of MD simulations [43]. Both bending undulations at long wave lengths and protrusion modes at molecular scales were observed (for a definition of these quantities see Appendix A.2.2), thus showing that the model is able to bridge micro and macro length scales. The bending rigidity of bilayers formed by these model amphiphiles was also studied by Den Otter and Briels [75]. Equilibrium MD was used to study bending amplitudes of the order of thermal undulations, with results in agreement with the Helfrich's expression for the free energy. Nonequilibrium MD techniques were used to explore larger bending amplitudes. Also, Den Otter [76] investigated the system size dependence of the area compressibility, showing that for large system sizes (where the bilayer thermal undulations modes become activated) the approximation based on equating the bilayer area to the projected area leads to underestimating the elastic modulus. Hence, a more accurate determination of the true bilayer area is necessary to calculate area compressibility in large bilayer patches. Using a similar model for amphiphilic molecules (single-chain), Imparato et al. [77] have shown that the bending rigidity of a two-component bilayer, in which the two amphiphiles differ only in tail length, exhibits a nonmonotonous behavior as function of bilayer composition. A similar functional dependence was found by Brannigan and Brown [56] using an implicit solvent, particle-based model.

Inspired by the modeling approach of Goetz and Lipowsky [74], Stevens [78,79] developed a model consisting of just hydrophilic and hydrophobic bead types. Lipids are built by connecting two tails of hydrophobic beads to a headgroup represented by three hydrophilic beads. Solvent particles are represented by single monomers of the same type of the headgroup beads. The particles interact via a 6–12 Lennard–Jones potential, with the same energy minimum and hard-core distance for all the pairs. Phase separation is obtained by setting the cut-off of the polar–apolar interaction to the minimum of the energy well, thus retaining only its repulsive part. Beads in the lipid are linked via soft springs—represented by a FENE potential plus the attractive part of the Lennard–Jones potential to be able to use the same integration timestep as for the nonbonded interactions. The flexibility of the lipid is controlled by harmonic bond-bending potentials which maintain the geometry of the headgroup and are used to model saturated and unsaturated lipids. The model system was studied using MD simulations and was validated by making sure that coarse-grained lipids self-assemble into a fluid bilayer if starting from a random water–lipid configuration. Stevens [79] then studied the thermotropic phase behavior of bilayers formed by model lipids of varying chain length, and found a gel-to-fluid phase transition, as further discussed in Section 3.1. The model was also used to investigate domain formation in bilayers made of a mixture of long and short lipids [80], finding that at a temperature between the melting temperatures of the short and the long lipids, gel domains form. Within these domains, a complementary organization is found, in which long lipids on one side of the bilayer are faced by short ones on the opposite side. This is in agreement with experimental findings on lipid organization in mixed bilayer [81]. This arrangement of lipid molecules minimizes the exposition of the longer lipid tails to the water environment.

Another approach to simplified coarse-grained models for amphiphilic molecules is the one of Schmid and co-workers [82–84]. This approach is based on a model used to describe polymers [85] and amphiphilic dimers [86,87]. Schmid and co-workers model the amphiphilic molecules as linear fully-flexible tetramers, consisting of soft beads, two hydrophilic and two hydrophobic, linked by a FENE potential. The solvent is modeled with soft spherical beads. All the beads have the same mass and size, corresponding approximately to three water molecules, or a propane molecule. The interactions between the beads are modeled using a soft repulsion of the Lennard–Jones type plus a short range attraction. The parameter describing the range of attraction between the beads determines the possible phase separation (self-assembly) of the amphiphiles from the solvent phase. The elastic properties (bending constant and compressibility) of bilayer stacks in the fluid lamellar phase of up to fifteen bilayers were studied using MD simulations on this model [82]. In reason of the large system size considered by Schmid and co-workers, their results could be compared with those obtained from continuum theory for smectics. The formation and dynamics of pores due to thermal fluctuations in a stack of tensionless bilayers was also studied using the same model [83,84].

In the past few years, a number of coarse-grain lipid models have been developed and studied by the DPD simulation technique [88–93]. These models are based on a simple 'bead-and-spring' representation of the lipid molecules, where the nonbonded interactions are represented by soft-repulsive potential (the expression for the related effective force is given in Eq. A.5 in Appendix). Three bead types are usually defined: hydrophobic, hydrophilic, and water-like, each with a size which approximately corresponds to the one of three water molecules. A lipid is constructed by linking hydrophilic beads (modeling the lipid headgroup) to one or two chains of hydrophobic beads (modeling the acyl chains of the lipid)

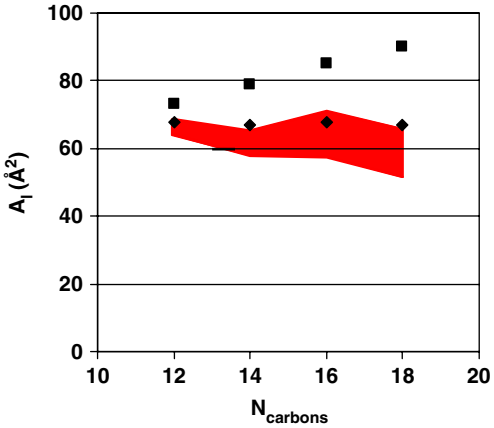

Fig. 7. Area per lipid in the fluid phase as a function of tail length obtained using the coarse-grained model of Kranenburg et al. [94] (black symbols). The squares are the values obtained using the fully flexible lipid model and the diamonds the values calculated from the model with additional bond-bending potentials. The shaded area indicates the range of the experimentally obtained values [102–107].

via harmonic springs. The chain stiffness can be tuned using bond-bending potentials. The parameters for the bonded interactions can be empirical [88,90,91] or can be derived by a mapping with atomistic simulations of phospholipids in water [94]. The difference in the strength of the nonbonded interactions is what mimics the difference between beads which represents groups of different nature (polar/apolar). The effective interaction parameter between water beads is usually derived from the compressibility of water at room temperature [95], while the repulsion parameters for a multicomponent system can be derived using the Flory–Huggins χ-parameters that represent the excess free energy of mixing [89,95,96]. It is however important to note that different authors have used slightly different sets of parameters. Nevertheless, as long as the interactions between polar and apolar beads are chosen sufficiently more repulsive than the interactions between alike beads, the model lipids are able to self-assemble into stable bilayers [88–90] and vesicles [91,92]. The self-assembly process studied with DPD shows a dynamics which is faster than the one resulting from standard MD simulations on coarse-grained models.

Groot and Rabone [89] used the DPD technique on a coarse-grained model for phospholipids with the aim to study the effect of nonionic surfactants on cell membranes. Each lipid is modeled by a three-bead headgroup, and two tails of five hydrophobic beads each. In particular, to model the phosphatidylethanolamine (PE) lipid two bead types were defined for the lipid head group, one which represents the phosphate and ethanol groups, and the other representing the glycerol group. The hydrophobic beads in the lipid tails are all of the same type. Groot and Rabone validated their model by calculating the density profiles of a coarse-grained lipid bilayer, and comparing them with those typically obtained from atomistic simulations of lipid bilayers. Also, they estimated the value of the area per lipid and the lipid lateral diffusion coefficient finding a good agreement with experimental data. Groot and Rabone [89] used their coarse-grained model to understand under which conditions the presence of nonionic surfactants causes leakage of the bilayer, and eventually cell death, via pore formation (see Section 3.2). Inspired by the approach of Groot and Rabone, and as a further validation of the DPD coarse-grained model approach, the thermotropic phase behavior of coarse-grain lipid bilayers was extensively studied by Smit and co-workers [97–101]. This topic will be further discussed in Sections 3.1 and 3.2.

The issue of tail stiffness (already discussed for the case of implicit solvent models) was also considered for DPD models of coarse-grained lipids. Kranenburg et al. [94] calculated the dependence of the area per lipid on lipid tail length. Their results show that in bilayers of fully flexible lipids the area per lipid increases with increasing tail length, while experimentally the area per lipid (above the melting temperature) slightly decreases with increasing tail length [102]. This decrease in area is attributed to the larger van der Waals interactions among the longer tails. Kranenburg et al. [94] showed that the experimental trend can be reproduced (see Fig. 7) if chain stiffness, via a bond-bending potential, is considered in the coarse-grained model. A similar dependence of the area per lipid on lipid tail length was found by Stevens [79] using the model previously described, which is based on Lennard–Jones interactions and which takes into account lipid chain stiffness. Also, the density profile of a bilayer made of coarse-grained lipids with

bond-bending rigidity is in good agreement with the one obtained from atomistic simulations [94] (see Fig. A.2 in the Appendix).

The surface tension and bending rigidity of coarse-grained bilayers studied using DPD were calculated by Shillcock and Lipowsky [90], and the dependence of these quantities on the lipid architecture was investigated. An effect of the lipid architecture on the properties of self-assembled structures was also detected by Yamamoto and Hyodo [91], who studied the formation of lipid vesicles made of model lipids with one or two hydrophobic tails. These authors found that the use of a double-tail architecture speeds up the aggregation process.

Laradji and Sunil Kumar [108] extended the DPD model to consider bilayers composed of two lipid types. They validated the model by estimating the bending modulus and line tension of domains formed by the two components and found values in reasonable agreement with experimental measurements on lipid membranes [58]. A DPD coarse-grained model for lipid bilayers with embedded peptides was also developed by Venturoli et al. [109]. This model was used to investigate lipid–protein interactions as a function of hydrophobic mismatch, as we report in more details in Section 3.3. The processes of vesicle budding and fission were also studied using DPD on coarse-grained models [110,92], as described in Section 3.4.

2.2.2. From atomistic to a coarse-grained description

In the following, we review some mesoscopic modeling approaches which aim at establishing a link between the coarse-grain representation and the underlying atomistic nature of the molecules. These models usually consider several different types of beads (not just hydrophobic and hydrophilic), and—at least some of—the model interaction parameters are derived from simulations on atomistic models. In these models, electrostatic interactions are also taken into account, and the solvent is explicitly modeled.

Marrink and co-workers [111] introduced a model for phospholipids with the aim of retaining the chemical nature of the molecular components, while defining as few bead types as possible. By doing so, they have at disposal a set of bead types with which molecules having different architecture can be easily built. According to this model, each bead has, on average, the volume of four water molecules. Also, only four interaction types are considered, polar, nonpolar, apolar, and charged. Subtypes for the charged and the nonpolar types are used to define the hydrogen-bonding characteristics of these groups. The nonbonded interactions between the sites are described by a Lennard–Jones 6–12 potential, whose parameters are calibrated using alkanes/water systems to reproduce the experimental densities, mutual solubilities and relative diffusion rates. The minimum distance of approach between two sites is set equal for all types, while for the strength of the Lennard–Jones interaction only five levels are defined, thus keeping the model simple. Electrostatic interactions for charged groups are represented by the Coulomb potential, which is screened through a relative dielectric constant (representing hydration) and shifted to the same cutoff distance used for the Lennard–Jones potentials; this results in a short range electrostatic interaction which increases the efficiency of the simulation. One of the advantages of this model is that the parameterization of the interaction potentials is not tailored to a specific lipid type, and different phospholipids can therefore be constructed from a small set of building blocks. Alkanes and lipid molecules are built by connecting coarse-grained beads via an harmonic potential, as shown in Fig. 8. The parameters for the bonded forces are derived using a mapping on atomistic MD simulations. This model can thus be seen as intermediate between the empirical models described in the previous section and the models which aim at systematically derive the interaction parameters from atomistic simulations.

Using MD simulations on this coarse-grained model, Marrink and co-workers were able to obtain self-assembly of phospholipids into a bilayer [111]. The density profiles (along the bilayer normal) obtained from the simulations on the coarse-grained model are in good agreement with results from atomistic simulations. In addition, Marrink and co-workers were able to reproduce the experimental area per DPPC and DPPE lipid. Although all the interaction parameters were optimized for room temperature (i.e., above the melting temperature of the lipids), it was also possible to model a gel phase using the same interaction parameters [112]. Formation of a nonlamellar phase induced by changes in lipid architecture was also observed [111]. This mesoscopic model was also used to study the spontaneous aggregation of DPPC into small vesicles, and to investigate vesicle structure and dynamics [113] (see Section 3.4). Motivated by the fact that nonbilayer phases seem to be involved in membrane fusion, Marrink and Mark [114] performed MD simulations on their coarse-grained model to study the complete transition pathway from a multilamellar to a nonlamellar inverted hexagonal phase, as illustrated in Fig. 9. Starting from a multilamellar configuration, the spontaneous formation of stalks between the bilayers at high temperature or reduced hydration was observed on a nanosecond timescale. Also, the stalks appear to be stable within a narrow hydration/temperature/composition range, rearranging into the rhombohedral

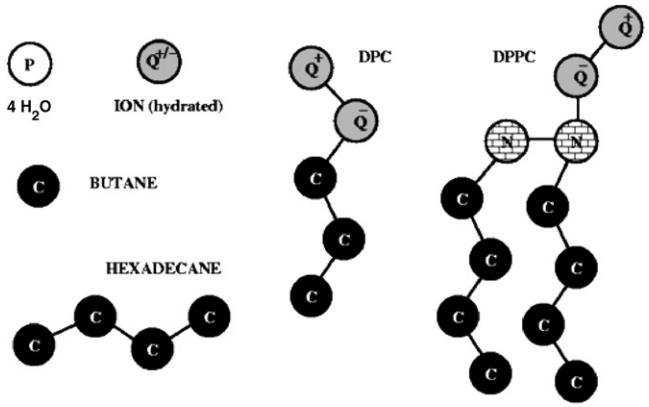

Fig. 8. Site types used to build the coarse-grained model of Marrink et al. [111]: polar (P), nonpolar (N), apolar (C), and charged (Q). To build alkanes and phospholipids the sites are linked together via harmonic springs; next nearest neighbors interact through a harmonic angle potential. Charged groups also interact through a short-range electrostatic potential. Reprinted with permission from [111]. Copyright 2004 American Chemical Society.

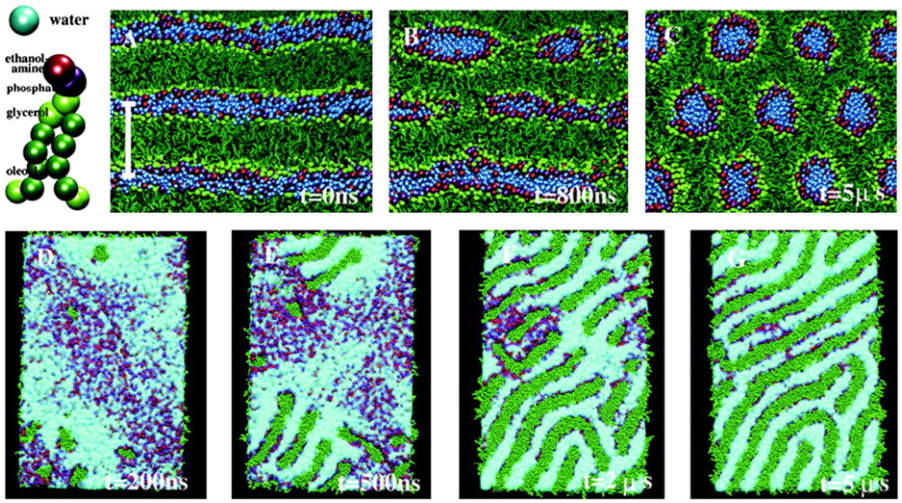

Fig. 9. Thermotropic transition from multilamellar to inverted hexagonal phase for the coarse-grained model of DOPE (shown in the top left figure) simulated by Marrink and Mark [114]. Reprinted with permission from [114]. Copyright 2004 Biophysical Society.

phase. The finding of stalk intermediates in the formation of nonlamellar phases is also supported by experimental evidence [115].

Klein and co-workers [116–118] developed a mesoscopic model which is explicitly parameterized for DMPC and considers more bead types than the model of Marrink and co-workers. Each DMPC molecule consists of 13 interaction sites, eight of which are hydrophobic (four for each tail) and five of which are hydrophilic, three for the glycerol moiety and one each for the charged choline and phosphate groups, as illustrated in Fig. 10. Water is represented by mapping three water molecules onto one interaction site. The interactions between sites are modeled via Lennard–Jones 6–4 or 9–6 potentials, combined with long-range Coulombic potential for charged groups. The parameterization of water–water interaction is calibrated to reproduce the melting temperature of water, which gives a scale for the energy, and the water density at room temperature, which sets the length scale. The interaction parameters between the beads in the lipid tails are optimized to reproduce the bulk density and vapor pressure of dodecane and nonane, while the water–tail interactions are chosen such that a water/hydrocarbon interface is well described. The remaining interactions are chosen to reproduce radial distribution functions, as obtained from atomistic simulations of DMPC bilayers. The

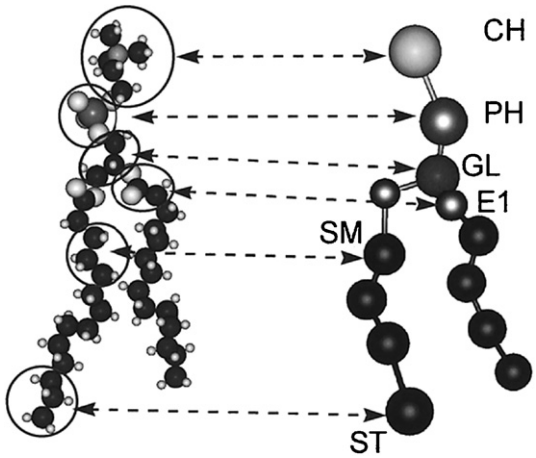

Fig. 10. Coarse-grained DMPC molecule according to the model of Shelley et al. [116]. Different bead types are used for the choline (CH), phosphate (PH), glycerol (GL), ester (E1), carbons in the tails (SM) and terminal carbon (ST) groups. Reprinted with permission from [116]. Copyright 2001 American Chemical Society.

parameterization of bonded interactions (bond-length and bond-bending potentials) are also derived from atomistic simulations of DMPC. Drawbacks of this approach are the specific parameterization for the DMPC lipid and the procedure to derive the parameters for the nonbonded interactions, which can be cumbersome and not always accurate. This procedure sometimes requires tabulated potentials of mean force (PMF), which are derived from radial distribution functions using the inverse MC method previously described for the implicit solvent model of Lyubartsev [68]. Spontaneous self-assembly of coarse-grained DMPC into a bilayer was observed, where the bilayer structural properties were in good agreement with the ones derived from atomistic simulations [117,119]. Both MD and MC were used to study this coarse-grain model, showing that MD is much more efficient than MC to simulate the self-assembly process. Self-assembly of a Langmuir monolayer of the coarse-grained DMPC was also studied [120], and the formation of a reverse hexagonal phase was observed in the presence of alkanes [117].

A limitation of the parameterization of the model was found by Shelley et al. [117] while studying the distribution in the bilayer of coarse-grained halothane (a small volatile anesthetic molecule). Results from the mesoscopic model were qualitatively different than those of a MD atomistic study [121], although better agreement was found by adjusting the nonbonded interaction parameters, showing that careful parameterization of the model is essential. The study of the interaction of small molecules (modeling general anesthetics) with lipid bilayers using the optimized coarse-grained model was further carried out by Pickholz et al. [122], as described in more detail in Section 3.2.2.

Recently, Klein and co-workers extended their coarse-grained model to include a generic hydrophobic nanotube, and studied its mechanism of insertion in a coarse-grained DMPC bilayer. Also, in an attempt to shed light on the factors that control the assembly of monomers into a biologically active oligomeric state, such as omooligomeric ion channels, Nielsen et al. [123] have carried out MD simulations on this mesoscopic model to analyze the lipid bilayer perturbation around a transmembrane hydrophobic nanotube. The results of these two studies are discussed in more detail in Section 3.3.

Another promising method to coarse-grain phospholipid bilayers from atomistic simulations was recently proposed by Izvekov and Voth [124]. These authors used a multiscale approach to systematically derive the mesoscopic potential parameters from atomistic interactions. To this end, a force-match method [125] is used to determine pairwise effective forces from atomistic MD trajectories and forces. These are used to define PMFs between coarse-grained sites. The force field is fitted using a spline interpolation of the forces computed from atomistic MD simulations, where atoms are grouped into their corresponding coarse-grained sites. By choosing a sufficiently large number of distinct atomic configurations selected along the atomistic trajectories, the system of linear equations of the fitting approach becomes overdetermined and can be efficiently solved by standard least square methods. The radial distribution functions for pairs of coarse-grain sites and the density profiles in a DMPC bilayer were found to reproduce with good accuracy the corresponding quantities computed in the atomistic simulations.

The models we have discussed so far view a bilayer as a self-assembled structure made of coarse-grained entities (i.e. the lipids). In the approach of Voth and coworkers [36,126–130], already described in the context of implicit solvent models, the membrane is instead seen as a sheet of particles, which are a discrete representation of a continuum equation. In this so-called elastic membrane model (EM) a single particle of the bilayer represents a group of several lipids, and a typical particle has a size of the order of 1 nm. At this level of coarse graining, membranes of $\sim 100\,\mathrm{nm}^2$ can be conveniently simulated, and undulations and buckling can be studied. Voth an co-workers have developed various strategies to couple the EM model to an underlying atomic (or less coarse grained) representation of the system. The simplest approach is to couple these two levels by using the atomic scale simulations to compute the input parameters for the mesoscopic simulations [37,130]. Interestingly, Voth and co-workers take multi-scale modeling one step further, in the sense that they simulate the microscopic (atomic) membrane and the EM membrane in parallel [126,129]. The results from the atomistic simulations are used to 'feed' the mesoscopic simulations, and the mesoscopic simulations are used in turn to impose the long length and time scale structural fluctuations on the atomic scale system, thus effectively generating a multi-scale model. From this approach one can also obtain insights in the role of water on the dynamics of the membrane. For example, a mapping on an EM model was developed in which water was treated implicitly [131] or was taken into account explicitly [129,130]. Comparison of the two approaches shows that with an implicit solvent the relaxation mechanism of fluctuations of the membrane are not correctly described, indicating that taking into account the hydrodynamics is essential to describe the dynamic undulation spectrum [129]. This model has also been used to study undulation forces between two membranes [130].

3. Membrane processes studied with mesoscopic models

The development of mesoscopic models has made it possible to investigate a number of biomembrane phenomena that are outside the range of time- and length-scale which one can reach with the use of atomistic models. In particular, using particle-based mesoscopic modeling approaches one can study membrane structural and mechanical properties on a macroscopic scale (for example, the membrane bending rigidity) and, at the same time, one can gain information at the molecular level by directly observing the effect of the lipid structure and dynamics on the whole microscopic and macroscopic structural organization of the membrane.

Any coarse-graining approach, by definition, simplifies the complex nature of the system it aims to model, by reducing its degrees of freedom and neglecting some of the details of the molecular structure and interactions. Nevertheless, the model should be able reproduce some of the features of the systems one wants to study. In Section 2 we have seen that different coarse-grained models for lipid molecules have been validated by testing their ability to self-assemble into stable structures (such as bilayers or vesicles) displaying the internal organization and structural properties typical of real (albeit simpler than cell membranes) lipid systems. A further step in the validation of such models may consist in investigating their thermodynamic behavior, such as thermally driven phase changes. To validate mesoscopic models of pure lipid bilayers, the thermal phase behavior of PCs obtained experimentally (see [132] for a review) can be considered, and compared to the phase behavior of coarse-grained lipid bilayers. In the following section we review some applications of coarse-grained models to the study of the phase behavior of model lipid bilayers. We also show how phase behavior can be influenced by lipid architecture, such as tail length and headgroup size. Once that a coarse-grained model is validated, the fact that it is based on a simplified molecular structure can be exploited to gain insight into the type of interactions and lipid architecture that are responsible for a particular phase behavior. The complexity of the models can then be increased by, for example, considering mixed systems composed of more than one lipid type, or containing 'impurities', such as alcohols or proteins. Studies of mixed systems will be discussed in Sections 3.2 and 3.3. Coarse-grained lipid models have also been used to investigate bilayer systems which are not in planar geometry. In particular, these approaches were used to model rather large systems containing lipid vesicles, and to address the study of the mechanism of vesicle fusion and fission. In Section 3.4 we review in detail some of these studies.

3.1. Thermotropic phase behavior of lipid bilayers

Phospholipid bilayers, even the simplest ones composed of only one lipid type, display a rich temperature phase behavior [132,133]. The stable phase at low temperature is the sub-gel phase, commonly labeled L_c. Upon heating, the transition to the gel, or $L_{\beta'}$, phase occurs. The transition from the L_c phase to the $L_{\beta'}$ phase is called the sub-transition. Both phases are characterized by having a very low lipid mobility in the bilayer plane and ordered acyl chains, which

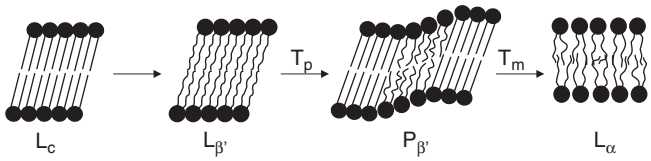

Fig. 11. Schematic representation of lipid bilayer phases at different temperatures. L_c sub-gel phase, $L_{\beta'}$ gel-phase in which the lipids are tilted, $P_{\beta'}$ ripple phase, L_α liquid crystalline phase. T_p and T_m denote the pre- and the main-transition temperature, respectively.

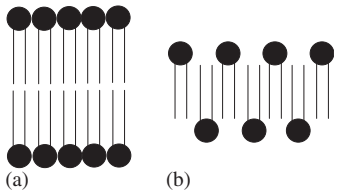

Fig. 12. Schematic representation of (a) the L_β phase and (b) the $L_{\beta I}$ phase.

can also be tilted with respect to the lipid bilayer normal; however, in the $L_{\beta'}$ phase the head groups are more hydrated than in the L_c phase, in which the lipids exhibit a long range hexagonal lattice arrangement in the bilayer plane. In the $L_{\beta'}$ phase the acyl chains also exhibit some degree of disorder. A further increase in temperature leads to the formation of the 'rippled', or $P_{\beta'}$, phase. The transition from the $L_{\beta'}$ to the $P_{\beta'}$ phase is called the pre-transition. The $P_{\beta'}$ phase is characterized by the appearance of undulations in the bilayer. Above the melting temperature, T_m, the bilayer is in the liquid-crystalline, or fluid, L_α phase. The transition from the rippled to the fluid phase is called the main transition. During the main transition, a melting of the bilayer takes place, where the lipid hydrocarbon chains become disordered and where the mobility of the lipids in the plane of the bilayer becomes fluid-like. A schematic illustration of these phases is shown in Fig. 11.

The values of the transition temperatures depend on the lipid type [132]. In general, these values increase with increasing chain length of the lipid, and decrease with increasing headgroup hydration and unsaturation of the acyl chains [1]. In the latter case, the transition temperatures are not only influenced by the number of double bonds in the chains, but also by their position along the chain. The chemical nature of the lipid headgroup may also influence the phase behavior. For example, in the case of a bilayer formed by lipids with a small head group, a gel-like phase, L_β, may appear at temperatures below the main transition, in which the tails do not tilt with respect to the bilayer normal (see Fig. 12(a)). Transition temperatures and phase behavior are also affected by the presence of impurities in the bilayer, such as other types of lipids, cholesterol, proteins, cations, or small molecules such as alcohols. For example, small amphiphilic molecules added to a pure lipid bilayer may induce a low temperature interdigitated gel-phase, $L_{\beta I}$, where the two leaflets of the bilayer interpenetrate, and the terminal methyl groups of the lipid chains in the two opposite monolayers do not face one another, but are located near the head group region of the opposing monolayer (Fig. 12(b)). Also, the presence in the bilayer of integral membrane proteins (i.e., amphipathic proteins which span the hydrophobic section of the bilayer) may affect the lipid bilayer phase behavior [20].

3.1.1. Single-tail lipid bilayers

Both single- and double-tail phospholipids can form bilayers [134]. An interesting question is whether there is a difference in the phase behavior between these two types of lipids. In Section 2 we have already described some coarse-grained models of bilayers made of single-tail lipids. Here we discuss in some detail the phase behavior of the model of Smit and co-workers, who considered a lipid model consisting of one hydrophilic head bead connected to a single tail, which spontaneously self-assemble into bilayers [88]. The phase behavior of single-tail lipids with varying chain length was investigated [97,98] using the DPD simulation technique combined with the constant surface tension MC scheme described in the Appendix (Section A.1.4). This algorithm allows to impose a tensionless state to the bilayer, permitting the spontaneous rearrangements of the bilayer area characteristic of phase transitions. To distinguish different phases, Smit and co-workers monitored the values of the area per lipid, the extent of tail overlap, and the ordering of the

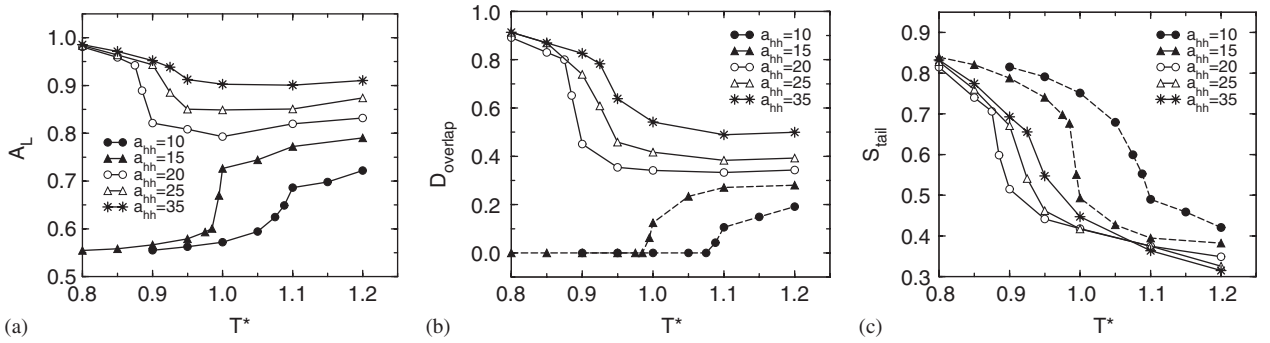

Fig. 13. (a) Area per lipid A_L, (b) extent of chain overlap $D_{overlap}$, and (c) tail order parameter S_{tail} (for the definition of these quantites see Section A.2 in the Appendix) as a function of reduced temperature T^* for different head–head repulsion parameters a_{hh}. The dashed curves show a transition from the L_β to the L_α phase, the solid curves show the transition from the $L_{\beta I}$ to the L_α phase. The results shown are for lipids with tails of eight hydrophobic beads. Similar trends were found for lipids with different chain length. From the simulations of Kranenburg et al. [98].

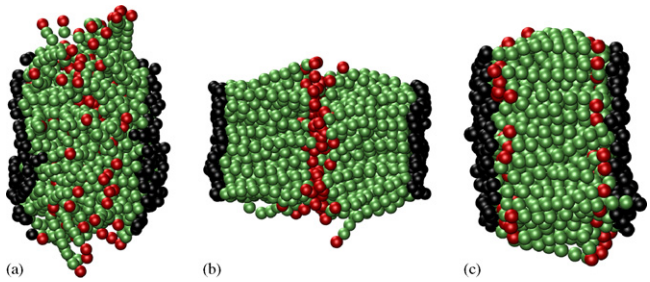

Fig. 14. Snapshots of a bilayer of single-tail lipids with nine tail beads: (a) liquid crystalline phase L_α; (b) noninterdigitated gel phase L_β; and (c) interdigitated gel phase $L_{\beta I}$. Hydrophilic headgroups are represented in black and hydrophobic tails in green, with the last tail bead depicted in red to better visualize the bilayer structure (color online only).

tails as a function of temperature and for different values of the repulsion parameter between the headgroups, a_{hh} (see Eq. (A.5) in Appendix for a definition of this parameter). These quantities are shown in Fig. 13, where the inflection point of the curves has been used to define the phase boundaries.

Interestingly, two gel-phases were found below the main transition temperature, depending on the repulsion parameter between the headgroups. For small repulsion the gel phase is the L_β phase, where the two leaflets are well separated, while for large repulsion the gel phase is an interdigitated $L_{\beta I}$ bilayer. In both cases the lipid tails are not tilted respect to the bilayer normal. Snapshots of typical configurations of the model bilayer in the fluid L_α and gel, L_β and $L_{\beta I}$, phases are shown in Fig. 14. The effect of increasing the head–head repulsion on the gel to liquid crystalline transition temperature was found to be much more pronounced for the $L_\beta \rightarrow L_\alpha$ transition than for $L_{\beta I} \rightarrow L_\alpha$. This can be understood considering that in the interdigitated phase the average distance between the lipid heads is already much larger compared to the noninterdigitated phase, and a further increase of this distance does not have a dramatic effect on the stability of the gel phase. Also, the interdigitated phase is stabilized for lipids with longer tail-length, consistently with experimental results [135]. Since the interdigitated phase is more closely packed than the noninterdigitated phase, the van der Waals energy is greater. This energy gain is proportional to the number of carbon atoms in the phospholipid chain and thus interdigitation becomes energetically more favorable for longer chains. The dependence of the $L_\beta \rightarrow L_\alpha$ transition temperature on lipid tail-length is in agreement with the experimental results of Misquitta and Caffrey [134], who systematically investigated the phase behavior of monoacylglycerol, a single-tail lipid. Fig. 15 shows the phase diagrams of single-tail lipids for various chain lengths [97,98].

Interestingly, Cooke and Deserno [40] did not find an interdigitated gel-phase in their single-tail coarse-grained model (described in Section 2). They attribute this to the fact that the aspect ratio of their model lipids is smaller than

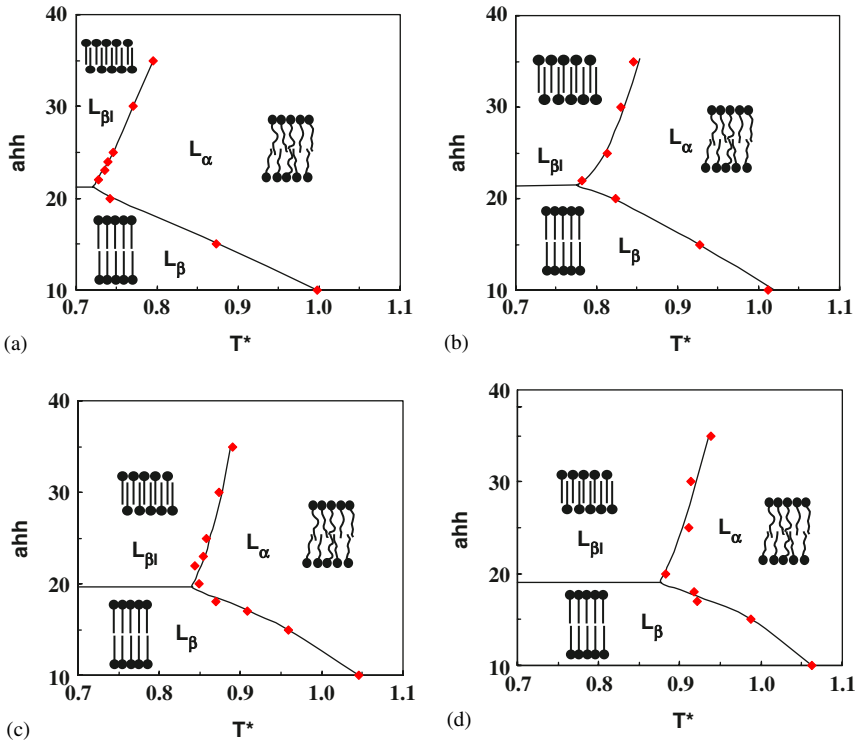

Fig. 15. Phase diagrams as a function of the repulsion parameter between the lipid headgroups a_{hh} and of reduced temperature T^* for lipids of different chain length: (a) 6, (b) 7, (c) 8, and (d) 9 beads in the tail. From the work of Kranenburg et al. [98].

that of the lipids modeled by Smit and co-workers, and that they use Lennard–Jones potentials, which are 'harder' than the ones used in DPD simulations.

Another model study of phase transitions using a mesoscopic model of saturated single-tail lipids was done by Lenz and Schmid [35]. These authors used MC simulations to study bilayer phase changes as a function of temperature and pressure. In the case where the solvent was explicitly modeled, it was found that the gel–fluid phase transition can be observed over a wide pressure range. At high temperature and low pressure, the fluid bilayer dissolves and forms an isotropic phase, while at both high temperature and pressure Lenz and Schmid observe the spontaneous formation of a stack of two fluid bilayers.

3.1.2. Double-tail lipid bilayers

The phase behavior of double-tail coarse-grained lipid bilayers was also studied using coarse-grained models, both minimal [79,98,101] and semi-quantitative [112].

The phase diagram as function of tail length of double-tail lipid bilayers from the DPD simulations of Smit and co-workers [98,101] is shown in Fig. 16. All the phases which characterize reconstituted phospholipid bilayers at different temperatures were observed. The transition pathway from L_c to L_α was seen to depend on lipid tail length. For short tails no $L_{\beta'}$ phase was observed and the transition is directly from L_c to $P_{\beta'}$ and then to L_α. For longer tails, the $L_{\beta'}$ phase was observed in between the L_c and $P_{\beta'}$ phase. This phase behavior well reproduces experimental results for PCs [136,137]. The transition temperatures were seen to increase with increasing tail length, in agreement with experimental data, with the exception of the transition temperature from the L_c phase to the $L_{\beta'}$, which was almost constant with increasing tail length.

Similarly, using the model described in Section 2, Stevens [79] investigated the phase behavior of double tail lipid bilayers as a function of temperature and lipid tail length. The model was studied by MD and the author adopted the (N,P,T) ensemble, in which the cell dimensions can be independently controlled. A zero value of the surface tension was chosen. The model system was able to reproduce a liquid–gel transition: in the gel phase the lipids are tilted and

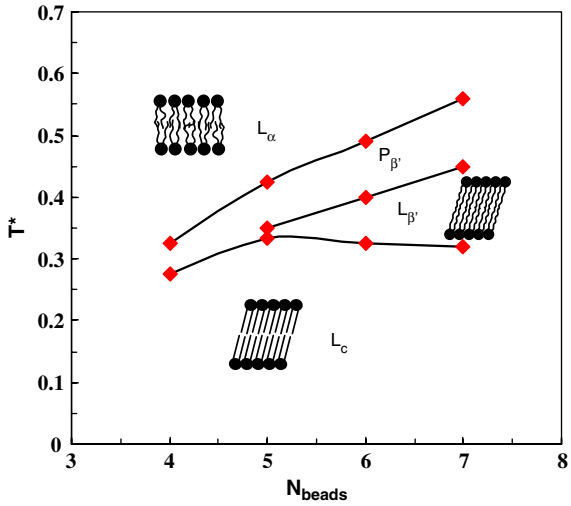

Fig. 16. Phase diagram of bilayers of double-tail coarse-grained lipids as a function of temperature and lipid tail length. From the DPD simulations of Kranenburg et al. [101].

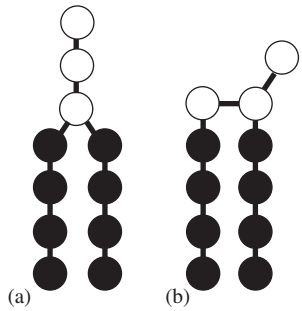

Fig. 17. Coarse-grained model lipids of Smit and co-workers (a) and of Stevens [79] and Illya et al. [93] (b). In both models the lipid tails can have different lengths. Hydrophobic beads are depicted in black and polar (hydrophilic) beads in white.

no interdigitation was found. Also, a phase resembling the ripple phase was observed in large patches of a bilayer consisting of rather long (8 tail beads) lipids. Stevens found a linear increase of the area per lipid and a decrease in the bilayer thickness with increasing temperature at fixed tail length, and an increase of the main transition temperature with increasing tail length. Both these results are in agreement with experimental data and with the results of Smit and co-workers. It is interesting to note that, despite the fact that the model of Smit and co-workers and the model of Stevens differ in the lipid architecture (see Fig. 17), in the functional form of interaction potentials and in the simulation technique with which they are studied, they both display remarkably similar behaviors. This seems to indicate that the phase behavior of lipid bilayers is determined by some general aspects, and does not depend on the details of molecular interactions. Unsaturated lipids were also modeled by Stevens by introducing a kink in one or both the lipid tails. The effect of the double-bond is to decrease the effective lipid length, hence decreasing the bilayer thickness. Also, the kink disrupts the bilayer ordering, thus increasing the area per lipid and decreasing the main transition temperature, in agreement with experimental results.

In contrast to the case of single-tail lipid bilayers, no interdigitated gel phase was found by Smit and co-workers, even for large values of the repulsion parameter between the lipid headgroups [98,101]. This result is indeed consistent with the experimentally observed structure of symmetric PC's bilayers. However, Illya et al. [93] found an interdigitated phase in double-tail lipids studied using DPD for sufficiently large headgroup repulsion. The reason

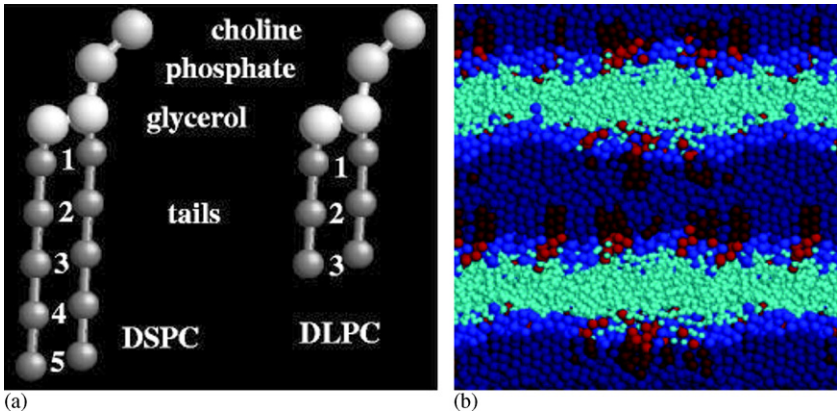

Fig. 18. (a) Illustration of the coarse-grained models for DSPC and DLPC used by Faller and Marrink in [138] and snapshots of a mixed DLPC (red) /DSPC (blue) bilayer. The gel phase domains surrounded by fluid phase are visible in the snapshot in (b). Reprinted with permission from [138]. Copyright 2004 American Chemical Society.

for this difference might be that in the model of Illya et al. the lipids are constructed by linking the two tails each to a head-bead (see Fig. 17(b)), instead than both to the same head-bead as in the model of Smit and co-workers (Fig. 17(a)); this results in a larger headgroup area, which cannot be achieved by only increasing the headgroup repulsion parameter.

Another observation is that, for low values of the headgroup repulsion parameter, the gel phase is the L_β phase, in which the lipid tails are ordered but not tilted with respect to the bilayer normal. An interesting comparison can be done with the model of Marrink and co-workers [112]. These authors investigated the gel to fluid phase transition in coarse-grained DPPC bilayers by cooling and heating bilayer patches composed of up to 8000 lipids. Extrapolating to macroscopic length and time scales, they estimated that the transition temperature from the heating and cooling processes converges to 295 ± 5 K, which is in good agreement, even if somehow lower, than the value of 314 K which is experimentally found for DPPC. The phase transition is characterized by a drop in lateral mobility of the lipids of two orders of magnitude, and by an increase of the same order of magnitude in the lipid rotational correlation time. Also, simulations performed at different levels of hydration indicated that the gel phase is stabilized at low hydration Interestingly, these authors find a gel phase in which the lipid chains are not tilted [112]. Marrink and co-workers show that, if the size of the beads forming the lipids acyl chains is decreased (which in the model of Smit and co-workers would correspond to an increase of the headgroups effective distance), then a tilted gel phase for double tail lipids is observed at low temperatures [112]. This is due to the fact that, in the model of Marrink and co-workers, some entropic disorder of the acyl-chains is implicitly incorporated into the coarse-grained beads when parameterizing the interaction potential. This implicit entropy cannot be removed when the temperature of the system is decreased, unless the bead size is decreased as well.

The phase behavior of binary lipid mixtures was also studied by Faller and Marrink [138], who simulated lipid bilayers made of a mixture of coarse-grained DLPC and DSPC, as illustrated in Fig. 18 and were able to reproduce semiquantitatively the experimental phase behavior of mixtures of phosphatidylcholines of different chain lengths. These authors found that the phase transition from the liquid crystalline to the gel phase shifts to a lower temperature with increasing concentration of short-chain lipids, and that lipids of different chain lengths mix almost perfectly in the liquid phase. Nevertheless, they were not able to observe phase separation in equimolar systems, and attributed this to computational limitations.

We have seen so far that coarse-grained models are able to reproduce experimentally observed structures of lipid bilayers, as well as the effect of lipid architecture on bilayer properties. Are coarse-grained models also able to make quantitative (or semi-quantitative) predictions of these bilayer structural properties, such as the area per lipid or the bilayer thickness? For the models which derive their parameterization from atomistic MD simulations, the physical quantities in simulations are directly derived in real units, and comparison with experimental data is straightforward. For models such as the DPD systems presented above, in which reduced units are used, a mapping is required to convert those into physical units. In DPD simulations, the length scale is usually determined by the coarse-graining level used

Table 1
Bilayer hydrophobic thickness, D_c, and area per lipid, A_L, at different temperatures. DPD simulations on a coarse-grained model of DMPC [109] and experimental values

T (°C)	Phase	D_c (Å)		A_L (Å^2)	
		Sim	Exper	Sim	Exper
10°	$L_{\beta'}$	34.3	30.3[a]	48.6	47.2 [a]
30°	L_α	26.3	25.6[b]	60.4	60.0[b]
50°	L_α	24.3	24.0[b]	64.4	65.4[b]
65°	L_α	23.6	23.4[b]	65.7	68.5[b]

The error on the simulation data is 0.2 Å for D_c and 0.4 Å^2 for A_L.
[a]From [139]. The error for D_c is 0.2 Å, and for A_L 0.5 Å^2.
[b]From [140].

to define a bead. For example, a mapping of three water molecules onto one coarse-grained bead corresponds to a bead-volume of 90 Å^3, which, for a density od 3 (which is the value typically used in DPD simulations), gives a value of the cut-off radius R_c (see Eq. (A.5) in Appendix) of 6.46 Å [89]. To translate the reduced temperature to physical temperature, a linear mapping of the form $T = aT^* + b$ can be adopted [101]. The parameters a and b can be derived by substituting for T and T^* the experimental temperature of a phase transition and the reduced transition temperature of the corresponding coarse-grained model, respectively. For example, the pretransition $L_{\beta'} \rightarrow P_{\beta'}$ and the main transition $P_{\beta'} \rightarrow L_{\alpha'}$ temperatures of a DMPC bilayer could be used. Using these conversion rules for length and temperature, the structural properties of a DMPC lipid bilayer derived from DPD simulations at different temperatures were found to be in good agreement with the corresponding experimental values [109], as shown in Table 1. Small deviations from the experimental values were observed in the case of the area per lipid at high temperature (65 °C), and in the case of the bilayer hydrophobic thickness in the gel phase(10 °C). It is also important to recall that the interaction parameters used in most DPD simulations of lipid bilayers have been tuned to reproduce the compressibility of water and mutual solubilities at room temperature. The DPD model is too simple to expect that, once these parameters have been fitted at a given temperature, one would, for example, reproduce the compressibility of water at other temperatures. Despite this, the effective—and simple—parameterization of the interactions between different beads has proven sufficient to well reproduce the phase behavior of lipid bilayers within a wide range of temperatures.

3.1.3. The rippled gel-phase

As we have already mentioned, for some lipids the transition from the ordered gel phase to the disordered liquid crystalline phase occurs via the so-called rippled phase ($P_{\beta'}$). This phase is characterized by a long-wavelength rippling of the bilayer and an anomalous swelling of the membrane. The rippled phase is observed only in bilayers containing PC's, for which the low temperature phase is the $L_{\beta'}$. Lipids like PEs, for which the low temperature phase is the untilted L_β, do not display a pretransition ([141] and references therein). The temperature interval between the pre-transition $L_{\beta'} \rightarrow P_{\beta'}$ and the main transition $P_{\beta'} \rightarrow L_\alpha$ decreases with increasing chain length. For chains containing more than 20 carbon atoms the pretransition disappears or merges with the main transition [142]. The rippled phase was first observed by Tardieu et al. in 1973 [143]. Several studies, both experimental and theoretical, have followed this first observation, addressing the question of how this corrugated structure may appear. Also, the structure of this phase is still a matter of controversy. The hypothesis is that the shape of the ripple is a asymmetric sawtooth, but in some models it is also proposed that the ripple is a sinusoidal. Explanations about the formation of this phase can be found in variations of the thickness of the bilayer, changes in tilt angle of the hydrophobic chains, and coexistence between the fluid L_α phase and the gel phase $L_{\beta'}$ [136,141,144–153]. Also, it is not very clear if the (anomalous) swelling of a membrane is coupled to the formation of the rippled phase and if the rippled phase only exists in stacked bilayers or if it is also present in a single bilayer system. Experimentally, the rippled phase has a wavelength of the order of 150 Å [154]. Hence, to observe fully developed macroscopic structures of this phase, length scales are necessary which are much longer than what it is accessible even with coarse-grained simulations. However, simulations of coarse-grained lipid bilayers do give evidence of a phase separation into micro domains, which might indicate the onset of a rippled phase [79,100,101].

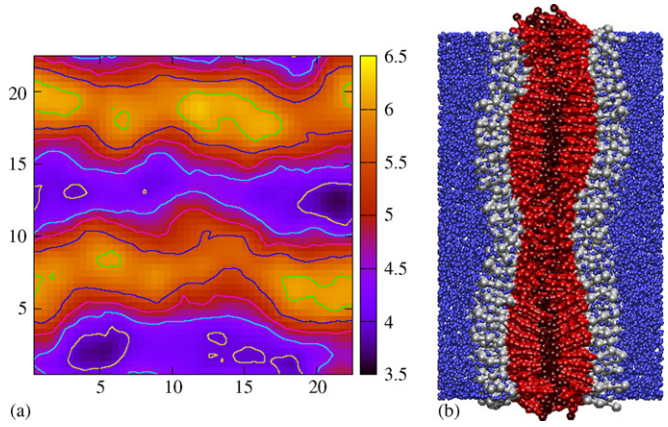

Fig. 19. Structure of the rippled phase. From the simulations of Kranenburg et al. [100,101]. The contourplot (a) shows the thickness of the bilayer as a function of the position in the bilayer plane, where the colors indicate the hydrophobic thickness. Fig. (b) represents a side view of the bilayer, in which the head groups are colored black and the tails gray. The darker color gray is used to indicate the end segments of the tails. The water particles are depicted as smaller spheres.

Using the coarse-grained model previously described, Kranenburg et al. [100,101] systematically studied the structure of the ripple phase as a function of lipid tail length. These authors found that the period of the ripple increases with increasing tail length. Fig. 19 shows the ripple phase in a bilayer of lipids with a tail length of four beads. In some simulations, the ripple was formed diagonally in the bilayer plane to accommodate the longer wave length. Since periodic boundary conditions were applied in all three directions, one might wonder if the observed phase is the rippled phase or just the formation of two domains. Simulations of systems of up to 1800 lipids showed that the striped structure was again formed, this time parallel to the y-axis, indicating that the rippled phase is the stable phase. Once the period of the ripple is optimized, a linear relation between the system size and the number of ripples was observed. These simulations also showed that a key factor in the formation of the rippled phase is the head group interaction. By decreasing this parameter, the L_β phase, in which the tails are not tilted, becomes stable and as a consequence the rippled phase is not formed with increasing temperature. Experimentally this scenario has been observed when the size of the of the lipid head group is decreased [150].

De Vries et al. [155] were the first to report observations of the formation of a ripple phase using atomistic MD simulations. Their results on lecithin bilayers show that packing competition between the head groups and the tails leads to the formation of the ripple phase, which shows a sawtooth shape for bilayers containing more than 128 lipids and a peristaltic shape similar to the one observed by Kranenburg et al. for smaller systems. For this study de Vries et al. have used relatively small system sizes (not more than 400 lipids in total); it would be interesting to study the behavior and shape of the ripple structures for larger system sizes.

3.2. Effect of small molecules on lipid bilayers

Coarse grained models were also used to study the effect of small molecules (for example alcohols, anesthetics, or cholesterol) on the structural, mechanical and thermodynamic properties of the membrane. In the following, we review some of these applications, which range from the formation of the bilayer interdigitated phase, to the formation of bilayer pores, and the occurrence of the liquid-ordered phase.

3.2.1. Alcohols

As we have discussed in the previous section, an interdigitated bilayer phase, $L_{\beta I}$, may appear in some coarse-grained bilayers systems below the main transition temperature. In real systems, the $L_{\beta I}$ phase does not spontaneously form in bilayers of symmetrical chain phospholipids, such as DPPC [156], but it can be induced by changes in the environment, like for example via hydrostatic pressure, changes in the pH of the solution [157], or by incorporation at the membrane interface of small amphiphilic molecules, such as alcohols [158–160], or anesthetics [161]. Interdigitation can also be induced by changes in the lipid architecture, for example by introducing an ester-linkage in the headgroup of the

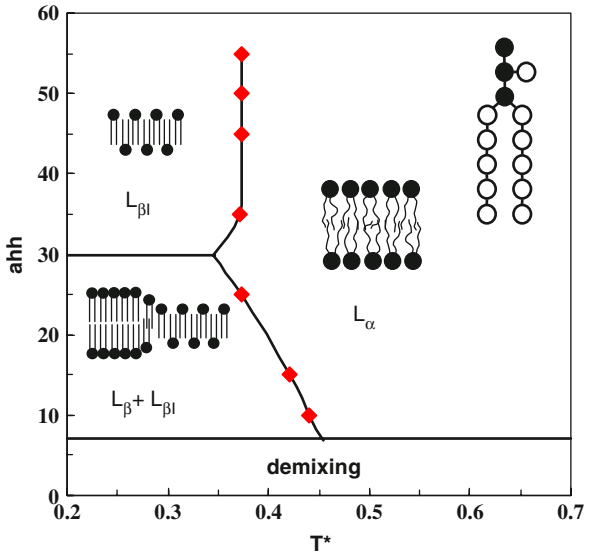

Fig. 20. Phase diagram for a bilayer consisting of the model lipid shown in the inset, which has an additional hydrophobic bead in the headgroup. Hydrophilic beads are depicted in black and hydrophobic ones in white.

phospholipids [162,163]. We have seen in the previous section that spontaneous interdigitation was found for single-tail lipids. Using DPD simulations on coarse-grained models of lipids, Kranenburg et al. studied the mechanism of induced interdigitation in more realistic, double-tail lipid bilayers. Two mechanisms were considered: interdigitation induced by changes in the molecular structure of the lipids forming the bilayer, and interdigitation induced by short-chain alcohols (from methanol to heptanol).

The esterification of an ethyl group linked to the phosphate group in the headgroup of phospholipids leads to the formation of cationic lipids, that can, for example, play an important role in the delivery of DNA to eukaryotic cells. The interdigitation in these bilayers is induced by two effects: charge repulsion of the cationic head groups and steric hindrance in the head group region caused by the presence of the ethyl group. Lewis et al. [162] found that the presence of a positive charge is of main importance for inducing interdigitation and that the steric hindrance facilitates the process. The coarse-grained model used to study the interdigitation induced by a change in the lipid molecular structure is built by adding an additional hydrophobic bead in the lipid headgroup [98]. The phase behavior resulting from the simulations of Kranenburg et al. [98] indicates a possible alternative interpretation of the experimental results just mentioned. The phase diagram shown in Fig. 20 suggests that interdigitation is mainly driven by the presence of the extra hydrophobic bead in the lipid headgroup, which has both the effect of increasing the effective distance between the headgroups and of shielding the lipid tails in the interdigitated phase from the water environment. The headgroup charge, modeled by an increase in the headgroup repulsion parameter a_{hh}, stabilizes the interdigitated phase.

It is known that the presence of alcohol molecules in a lipid bilayer can change the bilayer phase diagram [164–167], as illustrated in Fig. 21(a), which shows the typical phases of a lipid/alcohol bilayer as a function of temperature and alcohol concentration. Experimental studies [168] found that, depending on the concentration, alcohols have two different effects on the transition from the low temperature gel phase to the high temperature fluid phase of lipid bilayers [168]. At low alcohol concentration, the main transition temperature shifts to a lower temperature, while at high concentration the main transition temperature shifts to a higher temperature compared to a pure lipid bilayer. This effect was called the “biphasic effect”. Simon and McIntosh [135] observed the formation of the interdigitated phase at high alcohol concentrations, which explains the biphasic effect. At low concentrations of alcohol the disorder of the lipid tails increases, leading to a lower transition temperature. At high concentrations the more tightly packed interdigitated phase is formed, resulting in an increase of the transition temperature. With a mechanism similar to the one described above for the additional ester-linkage in the lipid head group, the alcohol molecules replace the interfacial water and lateral space is created between the head groups, leading to voids in the hydrophobic core. These voids are energetically unfavorable and thus the system minimizes its the energy by the formation of an interdigitated phase.

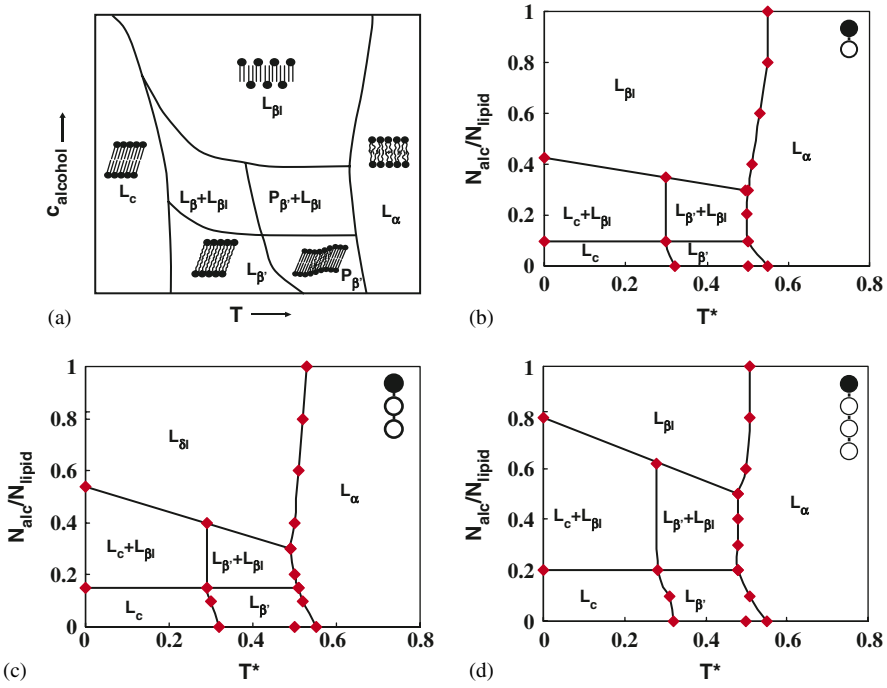

Fig. 21. (a) Schematic representation of the phase diagram of a PC/alcohol mixture as a function of the concentration of alcohol and temperature [164–167]. (b), (c) and (d) are the phase diagrams of coarse-grained lipid bilayers, with model alcohols of different length studied using DPD. The lipids have three hydrophilic head beads and two hydrophobic tails, each of seven beads. The acohol structure is shown in the inset of the figures.

Due to interdigitation, the system gains energy because of the stronger van der Waals interaction [135,165,169] in the interdigitated phase compared to the noninterdigitated case, and increases the entropy by replacing the highly ordered water molecules at the interface by alcohol molecules [135,159,170]. Since the tail ends of the alcohol molecules shield the tail ends of the lipids from the interfacial water, the energy cost in the formation of the interdigitated phase is further lowered.

Kranenburg et al. [99,171] built a coarse-grained model for alcohol molecules. The model alcohol consists of one hydrophilic head bead connected to an hydrophobic tail made of a number of hydrophobic beads which can vary from 1 to 3. The mechanism of alcohol-induced interdigitation was studied with DPD simulations on coarse-grained lipid–alcohol bilayers. These authors were able to reproduce the temperature/composition phase diagram discussed above—as can be seen from Fig. 21. At high temperature, the stable phase is the fluid L_α phase, as it is the case for pure lipid bilayers. At low temperature, various structures were found, depending on temperature and alcohol concentration. At low concentrations, the system behaves as the pure system, with transition from the highly ordered subgel L_c phase via the gel phase $L_{\beta'}$ to the rippled phase $P_{\beta'}$. In all these phases the tails have a tilt with respect to the bilayer normal. At high concentrations of alcohol the rippled phase disappears, and the interdigitated phase $L_{\beta I}$ is formed, in which the tails do not show a tilt. In between these extremes a coexistence region was observed between the rippled phase or the gel phase and the interdigitated phase. The biphasic effect on the main transition from the gel phases (L_β or $L_{\beta'}$) to the fluid phase (L_α) was also observed in these simulations: at a low fraction alcohols/lipids, the transition temperature shifts to a lower temperature. Increasing the alcohol concentration leads to an increased melting temperature. If interdigitation is complete, the melting temperature is almost constant.

Experiments by Nagel et al. [172] showed the coexistence of the $L_{\beta'}$ and $L_{\beta I}$ phase in a DPPC/ethanol system. Mou et al. [173] assumed that this coexistence is due to an inhomogeneous distribution of the alcohol molecules in the bilayer. If alcohol molecules could concentrate in certain regions of the bilayer, the local concentration could go above the critical value, so that a mosaic pattern of localized interdigitation can be formed. Even at very low alcohol concentrations, very narrow domains of the interdigitated phase can form [173]. The simulations of Kranenburg et al.

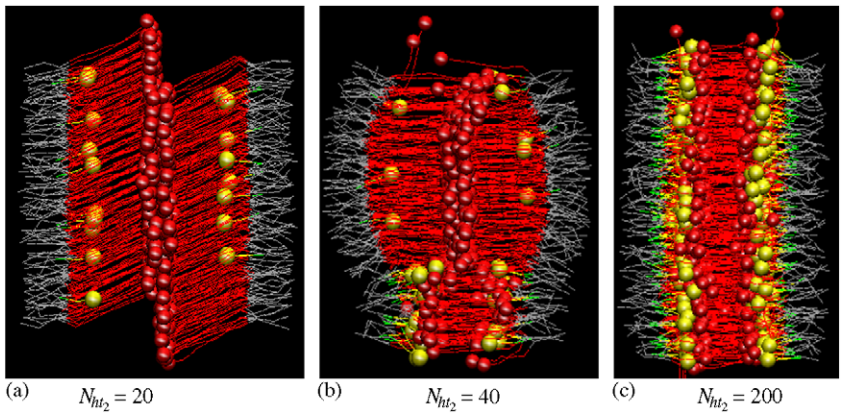

Fig. 22. Snapshots of a bilayer at increasing alcohol concentration (number of alcohol molecules in the bilayer, N_{ht_2}), at a constant temperature below the main transition. The red bonds represent the lipid tails and the gray ones the lipid headgroup. The terminal beads of both the lipids and the alcohols are depicted as larger spheres (red for the lipids and yellow for the alcohols). Color online only.

confirm that the alcohol molecules are indeed inhomogeneously distributed in the lipid bilayer. At a constant temperature, in the observed coexistence region, the mole fraction of alcohols in the interdigitated phase is constant while the mole fraction of alcohols in the noninterdigitated domains increases with increasing number of alcohols. This explains the experimentally observed coexistence region: at a fixed temperature, the region of the bilayer which is interdigitated increases in size while the size on the noninterdigitated one decreases with increasing alcohol concentration, as shown in Fig. 22.

Molecules such as alcohol can be viewed as surfactants; therefore the same type of coarse-grained models used for alcohol may be adopted to study the effect of surfactants on lipid bilayers. Surfactants, for example in household cleaning products, can adsorb at the membrane–water interface of bacteria and may induce the formation of pores in the bilayer, which eventually cause the death of the cell. This important practical issue motivated Groot and Rabone to develop a mesoscopic model for mixed bilayers of lipids and nonionic surfactants [89]. Using DPD simulations, Groot and Rabone studied the diffusion of water through the membrane and showed that permanent holes can be formed at relatively high surfactant concentration. In addition, these simulations show that surfactants reduce both the extensibility and the maximum stress that the bilayer can withstand.

3.2.2. Anesthetics

The mechanism through which anesthetics work on cells via the cell membrane is still a matter of debate. In fact there are two schools, one that believes that the action of anesthetics is mediated by proteins; and the other that thinks that the lipid matrix plays an active role [174,175]. Using the coarse-grained model of Klein and co-workers described in Section 2, Pickholz et al. [122] performed MD simulations to gain insight into the mechanism of drug action on membranes at the molecular level and into the role played by the lipid bilayer. Different anesthetics concentrations were considered. It was found a monotonic increase of the area per lipid with anesthetic concentration and a decrease in the interlamellar spacing; both results are in good agreement with previous atomistic simulations [121,176]. Also, the coarse-grained model well reproduced the most probable location of the anesthetic molecules within the membrane, as well as the increase of the lipid order parameter with anesthetic concentrations, as observed in atomistic simulations and NMR experiments.

3.2.3. Cholesterol

The plasma membrane of mammalian cells contains up to 50 mol % of cholesterol. Because, and in contrast to a phospholipid molecule, cholesterol is essentially rigid and has a relatively smooth hydrophobic section, its interaction with the lipids is of dual nature, which is thought to result in a new bilayer phase called the liquid-ordered phase [177]. The lipids in this phase have fairly ordered gel-like tails, but have translational degrees of freedom characteristic of the fluid phase. Recently, the importance of this liquid-ordered phase has been recognized. A number of physiological phenomena and diseases [178] are thought to be related to the formation of ‘rafts’, namely lipid domains which

have a high cholesterol content. Murtola et al. [138] have developed a implicit solvent coarse grain model for lipid bilayers (DPPC in particular) containing cholesterol with the intent of studying the large scale properties of the bilayer. Murtola et al. [138] modeled the bilayer as a two-dimensional system consisting of two weakly interacting sheets made of point-like particles, where each point represents the center of mass of either a lipid or a cholesterol molecule. The particles can move and interact with one another in two dimensions with continuum coordinates. The model was parameterized using the inverse Monte Carlo method, where the effective interactions between the beads are derived from MD simulations on the corresponding all-atom system. Murtola et al. [138] studied the system at intermediate cholesterol concentrations and found that it phase separates into cholesterol-rich (i.e., the liquid-ordered phase) and cholesterol-poor domains, in agreement with what was suggested by experiments. The advantage of this coarse-grained approach is the speed of the simulations, which is about eight orders of magnitude faster compared to standard MD simulations on atomistic models. Concerning the limitation of the approach, as the authors pointed out themselves, the inverse MC procedure limits the range of validity of the model parameterization. A wrong estimate of the bilayer properties derived from the atomistic MD simulations will be transferred to the coarse-grain model, via the effective interaction potentials. Also, it is not clear in which concentration range the effective potentials are valid. In fact, the authors advise against using the same potentials whenever one crosses a (temperature, composition) phase boundary.

More recently, Izvekov and Voth [179] also studied the effect of cholesterol on DPPC lipid bilayers using an explicit-solvent coarse-grained model. The model is built using the multiscale coarse-graining method which was developed for pure lipid bilayers (see Section 2). The authors considered a one-, four-, and seven-bead model for cholesterol, while water is represented as single beads (as it is usually done in other coarse-grained models). The structural properties of the mixed system were investigate in the (N,P,T) ensemble. The results from the simulations showed a good agreement with those obtained by the equivalent atomistic system.

3.3. Lipid–protein interaction

This section is devoted to the applications of coarse-grained models to the study of the interactions between membrane proteins and lipid bilayers, with particular focus on the issue of hydrophobic mismatch.

3.3.1. Hydrophobic mismatch

To minimize exposure of nonpolar moieties to the water environment, hydrophobic matching between the lipid bilayer hydrophobic thickness and the hydrophobic length of transmembrane proteins has to occur. For a number of years, the hydrophobic matching hypothesis has constituted a matter of debate, both from the theoretical as well as from the experimental point of view [20,180–192]. It has been suggested that the hydrophobic matching is involved in membrane organization and biological functioning. In fact, hydrophobic matching seems to play a role, among others, in the secretory pathway in the Golgi [193–196], and in sequestering proteins with long transmembrane regions [197] into sphingolipids–cholesterol biomembrane domains denoted as ‘rafts’ [198–200]. Biological membranes can compensate for hydrophobic mismatch in a number of ways, which may affect the microscopic and macroscopic structure of the membrane, and hence its biological function. There is some experimental evidence indicating that mismatched proteins cause bilayer deformations in the vicinity of the protein–lipid interface [201–207], thus creating lateral inhomogeneities in the membrane plane, which may have biological relevance. Lateral inhomogeneities may also arise due to the lipid sorting mechanism: in the presence of more than one type of lipid, the protein may prefer to have in its vicinity the lipid species that better match its hydrophobic length [189]. The occurrence of lateral inhomogeneities in the membrane may, among others, cause membrane fusion, as suggested by Nielsen et al. [208], and it may affect passive permeability to small ions or solutes. There may be mismatch effects which are lipid-mediated, such as the tilting (or even bending) of a whole protein/peptide to adapt to a too thin bilayer [181,209–216], or even tilting of the individual helices which form a protein. There is indeed some indirect experimental evidence that this is the case for channel proteins [180] and even proteins like Rhodopsin [217], suggesting that a change of the tilt-angle of the individual helices could cause changes in protein activity.

Results from MC simulations on a lattice model of Sperotto and Mouritsen [218] have indicated that mismatched proteins may cause a perturbation—of the exponential type—of the lipid bilayer, the extent of which is dependent on the degree of hydrophobic mismatch and on the size of the protein (i.e. the curvature of the protein hydrophobic surface in contact with the lipid hydrocarbon chains). However, the lattice model did not account for the fact that a mismatched

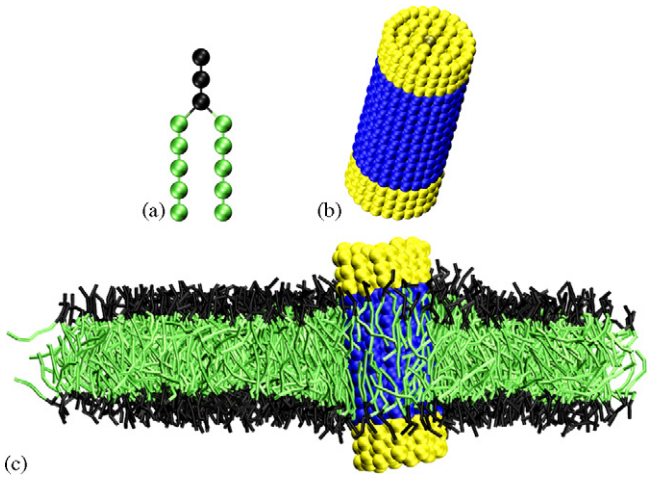

Fig. 23. Schematic representation of: (a) a model-lipid; and (b) a model protein. The figures are not in scale; (c) shows a snapshot from a typical configuration of the assembled bilayer with embedded the model-protein. Reprinted with permission from [109]. Copyright 2005 Biophysical Society.

protein may tilt to better accommodate to the lipid bilayer. By simulations on molecular detailed models it is instead possible to investigate how a protein may perturb the lipid bilayer, and at the same time undergo tilting. Indeed, MD simulations on atomistic models have confirmed too that, within the short time scale of these types of simulations, a protein can induce a deformation of the bilayer under mismatch conditions [219–222]; that the deformation is of the exponential type; and that its extent is protein-size dependent [223]. Also, by atomistic MD simulations it was found that membrane peptides may also tilt if embedded in a mismatched bilayer [224,225].

The use of coarse-grained models allows not only to perform simulations on larger systems and for longer times compared to atomistic simulations, but also to efficiently perform a large number of such runs. Venturoli et al. [109] exploited these advantages to perform a systematic study of the interaction of proteins with lipid bilayers for different mismatch conditions, as a function of protein size and system temperature The aim of these authors was to understand whether proteins—via the cooperative nature of the system, and due to hydrophobic matching—may induce a bilayer deformation rather than tilt with respect to the bilayer normal, and how bilayer deformations and protein tilt may depend on the extent of the mismatch and on the protein size.

Venturoli et al. extended a DPD coarse-grained model for pure lipid bilayers [97] to account for the presence in the membrane of embedded proteins of different sizes and hydrophobic lengths, hence hydrophobic matching conditions. The lipid used in this study consists of three head beads and five beads in each of the two hydrophobic tails. If a bead has the volume of approximately three water molecules, the coarse-grained lipid could be a model for DMPC. The model for a transmembrane protein is constructed by first connecting a varying number of hydrophobic-like beads into a chain, to the ends of which are attached three hydrophilic beads; these chains are then linked together into a bundle of N_P amphipathic bead-chains. By varying the protein hydrophobic sections, i.e., the number of its hydrophobic beads, one can sample different hydrophobic matching conditions. Three typical model-protein sizes were considered, consisting of $N_P = 4, 7$ and 43 chains, respectively. These choice of sizes was motivated having in mind peptides or proteins such as Glycophorin, the M13 peptide from the major coat protein from phage, or α-helical synthetic peptides (modeled by a $N_P = 4$ inclusion), β-helix proteins like gramicidin A (modeled by a $N_P = 7$ inclusion), or larger proteins consisting of transmembrane α-helical peptides that associate in bundles, such as bacteriorhodopsin, the photosynthetic reaction center, or β-barrel proteins, such as aquaglyceroporin (modeled by a $N_P = 43$ inclusion). Fig. 23(a) and (b) show a cartoon of a model lipid and a protein of size $N_P = 43$, respectively. The snapshot of a typical configuration of the assembled bilayer with an embedded protein is shown in Fig. 23(c). The quantities used to characterize mismatch, protein tilt and protein-induced bilayer deformation are illustrated in Fig. 24.

Protein-induced bilayer deformations. Some examples of thickness profiles, $d_L(r)$, for the case of negative and positive mismatch as obtained from the DPD simulations are shown in Fig. 25. The data refer to the three considered

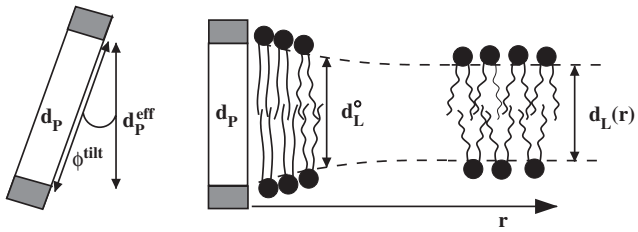

Fig. 24. Schematic illustration which shows the quantities calculated from the simulations of Venturoli et al. [109] described in the text. Pure lipid bilayer hydrophobic thickness (d_L^o); perturbed lipid bilayer hydrophobic thickness ($d_L(r)$) as a function of the distance r from the protein hydrophobic surface; protein hydrophobic length (d_P); tilted-protein hydrophobic length (d_P^{eff}); and protein tilt-angle, (ϕ^{tilt}), with $d_P^{eff} = d_P \cos(\phi^{tilt})$.

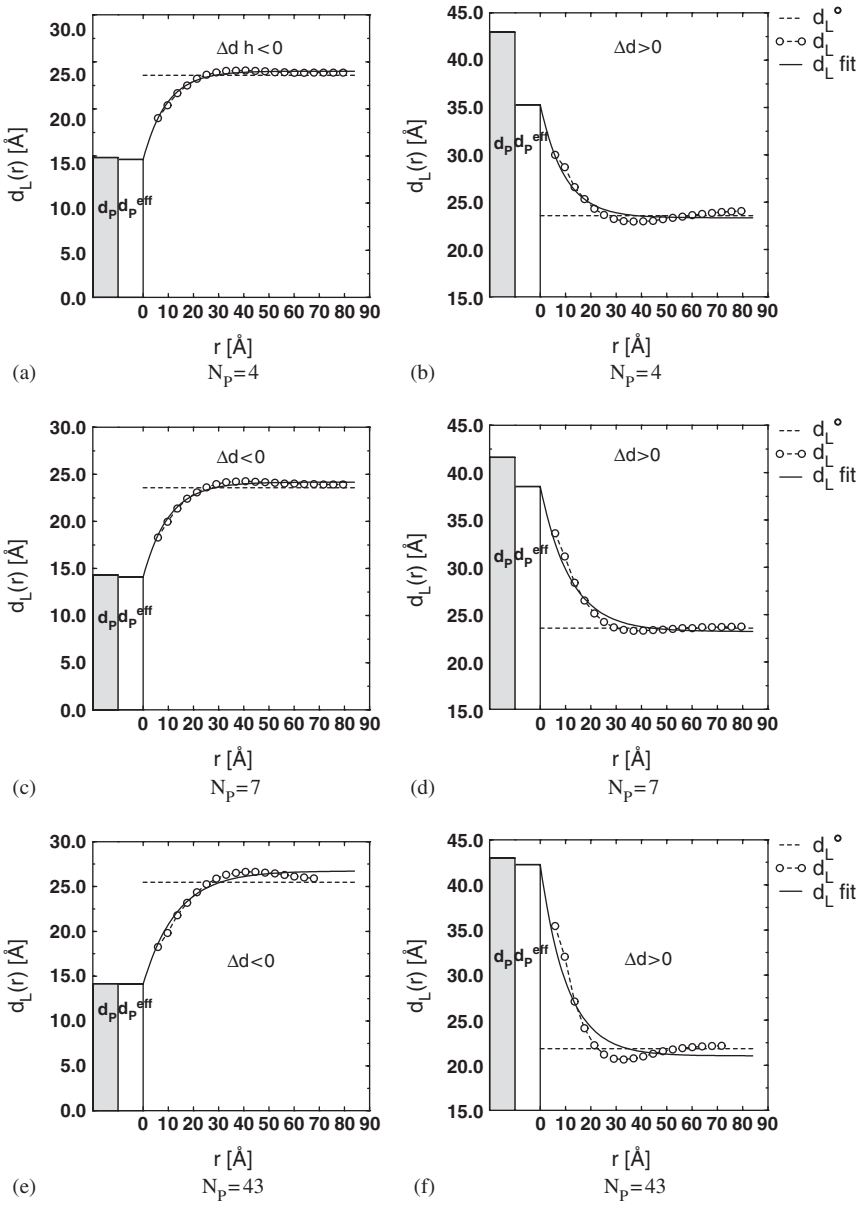

Fig. 25. Bilayer thickness profiles as a function of the distance r from the protein surface for different protein sizes, N_P. The cases for negative (left column) and positive (right column) mismatch, Δd, are shown. d_L^{fit} is the thickness profile fitted using equation (1). From the simulations of Venturoli et al. [109].

protein sizes $N_P = 4$, 7, and 43, and to a temperature well above the melting temperature of the pure system. One can clearly see that, in the case of negative mismatch, the lipids around the protein shrink to match the protein hydrophobic surface, while in the case of positive mismatch the lipids in the vicinity of the protein stretch and become more gel-like than the lipids which are far away from the protein. These results show that, when subjected to hydrophobic mismatch, the protein induces a perturbation of the lipid bilayer in its vicinity, and that the perturbation decays in a manner that depends on hydrophobic mismatch, and on protein size. In the case where the protein-induced bilayer perturbation has an exponential character, the extent of the perturbation can be quantified in terms of a typical coherence length, i.e., the decay length ξ_P, according to [23,218]

$$d_L(r) = d_L^o + (d_P - d_L^o)e^{-r/\xi_P}. \quad (1)$$

In general, this correlation length increases with increasing mismatch (absolute value). Also, the larger the protein, the more pronounced is the extent of the bilayer perturbation—at least in the case of negative mismatch, while positive mismatch is partially compensated by protein tilt. It was found that the smaller the protein, the more pronounced is the tilt. There are few experimental attempts to estimate the extent of the protein-induced bilayer perturbation; nevertheless, the existing ones confirm a qualitative mismatch dependence of the extent of the perturbation [204,207,226–229].

Nielsen et al. [123] carried out MD simulations on a coarse-grained model to analyze the lipid bilayer perturbation around a transmembrane hydrophobic nanotube. The results of these simulations are in qualitative agreement with those obtained by MC simulations on a lattice model [218], atomistic MD simulations [222,223], and the DPD simulations just discussed. Also, Nielsen et al. [208] studied, by MD on a coarse-grained model, the lipid-sorting mechanism which occurs when a protein is embedded in a bilayer formed by a mixture of phospholipids having very different chain lengths. In this case, the extension of the lipid profile around the protein can be 'tuned' simply by changing the concentration of the binary lipid mixture (or, alternatively, the temperature). The simulation results from Nielsen et al. confirm what was already observed in the past by a study which combined fluorescence spectroscopy experiments with MC simulations on a lattice model [189]: the protein selects in its vicinity the lipid type which better matches its hydrophobic surface. Nielsen et al. also suggested that the lipid-sorting mechanism can explain the onset of the fusion process; this could occur via the formation of a meniscus in the vicinity of the protein, which is then the triggering factor for the transition from the bilayer to a nonbilayer phase, as shown in Fig. 26.

The behavior of $d_L(r)$ shown in Fig. 25 for the three protein sizes also indicates that the larger the protein, the more $d_L(r)$ deviates from an exponential function. In fact, in the case of extreme hydrophobic mismatch for large proteins, a *undershooting* or *overshooting* effect is observed (as shown in Fig. 25(e), (f)). Whenever the mismatch is high (low) enough that even the ordered, gel-like (disordered, fluid-like) lipids closest to the protein are not able to match the protein hydrophobic surface, then, in the vicinity of the protein, the lipids might rearrange in a structure resembling the sector of a micelle (*overshooting*) or a structure similar to an inverted micelle (*undershooting*), to maintain the constraint of uniform density in the bilayer core. The *undershooting* and *overshooting* effect was already predicted by membrane elasticity theory [24,230,231]. According to this theory, the reason for this effects is the competition between stretching and bending modes of the membrane, and it is attributed to a damped oscillatory behavior. The effect is particularly pronounced for large proteins, and is expressed in terms of the characteristic decay length, ξ_P, of the membrane thickness relaxation, and of a second characteristic length, ξ_C, corresponding to the wave length of the oscillatory part. The two lengths ξ_P and ξ_C depend on the elastic properties of the membrane. For the cases related to Fig. 25(e), (f), Sperotto et al. [9] have compared the results from elasticity theory with those from the DPD simulations, and found a good agreement between the values of the decay lengths calculated with the two approaches, $\xi_P \approx \xi_C \approx 1$ nm—a remarkable result, considering that the DPD approach refers to discrete lipid models whereas elasticity theory is based on a continuum approach. However, the elasticity theory does not account for the ability of the protein to tilt, while the mesoscopic approach does. The phenomenological elastic model of Nielsen et al. [24] has the same protein-tilt limitation. It is worth stressing that, although the results from phenomenological elastic model studies predicted a nonmonotonic behavior of $d_L(r)$, showing an *overshooting* effect similar to what can be seen in Fig. 25(e), the nonmonotonic behavior observed by Nielsen et al. [24] is most likely due to the boundary conditions (for example, the angle of incidence between the bilayer and the protein) imposed a priori on the system, rather than to the competition between the stretching and bending modes of the bilayer, or to the constraint of uniform bilayer density. With the use of MD simulations on a mesoscopic model for water and lipid bilayers with embedded a nanotube, Nielsen et al. [123] have studied the bilayer deformation in the vicinity of the nanotube—which is allowed to tilt—in

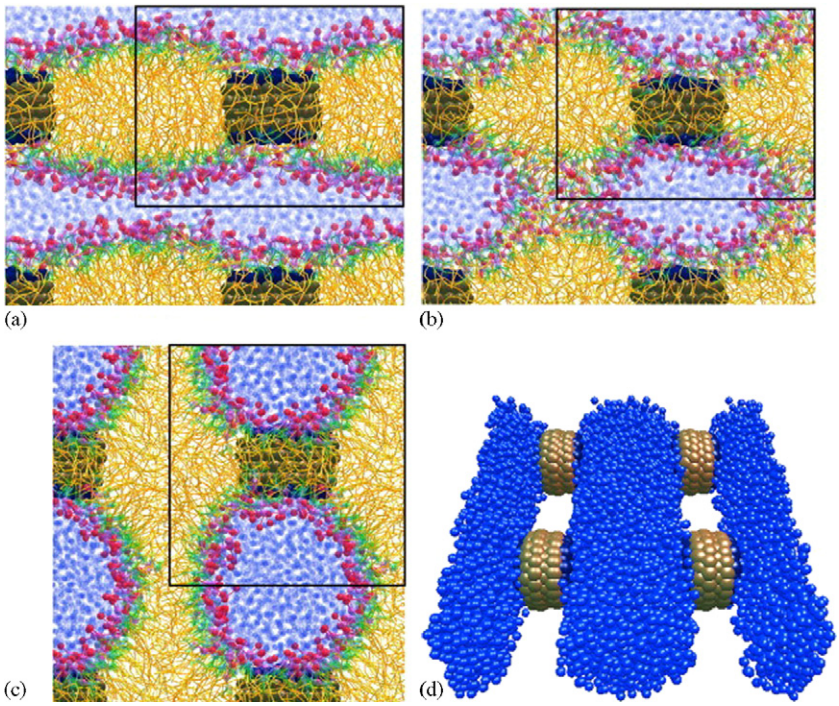

Fig. 26. Snapshots of the L_α-to-inverted phase transition from the simulations of Nielsen et al. [208]: (a) peptide-induced meniscus; (b) water penetration and membrane contact; (c) pore solvation by lipid headgroups; (d) inverted phase. Reprinted with permission from [208]. Copyright 2004 Biophysical Society.

response to hydrophobic mismatch. These authors did not quantify the deformation in terms of a decay length, but focused mainly on the contact angle at the bilayer–nanotube interface, and on the orientation of the lipid molecules in the vicinity of the inclusion. The simulations predicted a nonmonotonic behavior of the lipid thickness profile, $d_L(r)$, around the inclusion, which was attributed to a 'void' effect, consistently with what was suggested by Venturoli et al. The occurrence of a nonmonotonic behavior of $d_L(r)$ was also observed by Brannigan and Brown [232], who used a mesoscopic model for lipid bilayers with an embedded protein and implicit solvent.

Lipid-induced protein tilting. When embedded in a too thin bilayer, a protein may tilt to minimize the exposure of its hydrophobic moieties to the water environment. MD simulations on atomistic models [221,225,224] predicted that, when subjected to positive mismatch, skinny synthetic peptides may tilt (or even bend)—although, at similar mismatch conditions, the degree of tilting varies from system to system. Indeed, experimental studies made to systematically correlate peptide/protein-tilting with mismatch, confirmed what was predicted by the MD simulations. In particular, results from solid state NMR spectroscopy experiments [214,215] and fluorescence spectroscopy experiments [213], showed that, not only the tilt angle of hydrophobic synthetic α-helical peptides, WALP23 and KALP23, and the natural α-helical M13 coat protein, systematically increases with increasing hydrophobic mismatch, but also that different peptide types may tilt differently, even if subjected to the same mismatch. The results from the simulations on the mesoscopic model of Venturoli et al. [109] confirm the hypothesis that proteins tilt in a manner which is mismatch- and protein-size dependent. The higher the (positive) mismatch, the more the protein tilts; also, the larger the protein, the less pronounced is the tilting—as illustrated in Fig. 27. Interestingly, a look at the top snapshot in this figure suggests that the skinny protein (N_p=4) may even bend, as predicted by MD simulations on atomistic models [224,225].

Very recent experimental investigations have confirmed too the protein-size dependence of the protein tilt. Using infrared spectroscopy, Ramakrishnan et al. [216] measured the tilt angle of two β-barrel proteins, OmpA and PhuA. These proteins have approximately the same hydrophobic length, but two very different sizes. It was found that the larger protein tilts systematically less than the smaller one. To compare the functional dependence of the tilt angle on

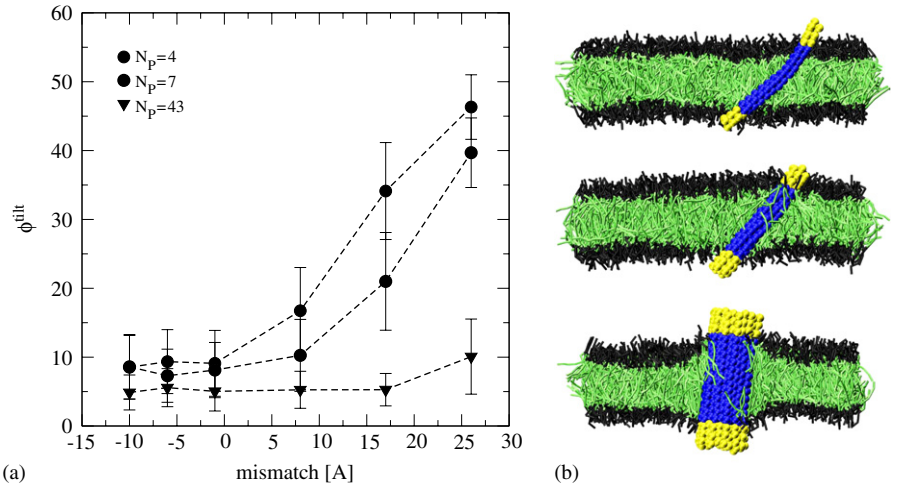

Fig. 27. (a) The protein tilt-angle, ϕ^{tilt} as a function of mismatch, $\Delta d = \tilde{d}_{\text{P}} - d_{\text{L}}^{o}$, for three protein sizes $N_{\text{P}} = 4$, 7 and 43. The dashed lines are only a guideline for the eye. Figure (b) shows snapshots of typical configurations of the bilayer with embedded proteins of different sizes. Reprinted with permission from [109]. Copyright 2005 Biophysical Society.

mismatch predicted by the DPD simulations with experimental measurements, in Fig. 27 the tilt angle is plotted as a function of mismatch, for the three different types of peptides studied experimentally, WALP23, KALP23, and the M13 coat protein peptide, mentioned previously, and for the model peptide with $N_{\text{P}} = 4$. The functional dependences shown in Fig. 28 are very similar for the four cases, suggesting that, although for the same value of hydrophobic mismatch the actual value of the tilt angle may vary from peptide type to peptide type (and may depend on specific features of the peptide, i.e., its sequence), the dependence on mismatch has somehow a more universal nature.

Integral membrane proteins can be made by bundles of α-helices. As previously mentioned, it has been suggested [180] that the activity of these proteins might be affected by changes in the tilt angle of these helices—for example by changing mismatch conditions. Model studies such as the ones presented here can be useful to clarify whether the tilting of helices belonging to bundles is due to intrinsic properties of the helices forming the bundle or, instead, to hydrophobic matching. Also, the functional dependence shown in Fig. 28, together with the protein-size dependence shown in Fig. 27, could be used to predict the tilt angle of a protein made of a bundle of α-helices.

Lipid–protein bilayer in gel phase. Finally, we present results on the behavior of the lipid–protein model system of Venturoli et al. below the melting temperature, i.e. in the gel phase [233]. The results from the simulations are illustrated in two figures. Fig. 29 shows the snapshots of two typical configurations obtained from the simulation of bilayers with embedded a $N_{\text{P}} = 43$ protein. The simulations are done at a reduced temperature corresponding to the $L_{\beta'}$ gel-phase. The pure lipid bilayer in this phase is characterized by a tilted orientation of the lipids, as previously discussed. In Fig. 29(a) is shown the case of a protein subjected to positive mismatch. The response of the protein to the positive mismatch is to tilt to decrease its effective length, with the direction of the tilt oriented parallel to the tilted lipids in the gel-state. A different scenario arises when a protein is subjected to a negative mismatch, as illustrated in the snapshot in Fig. 29(b). In this case, the protein orients antiparallel to the orientation of the lipids; more importantly, the lipids in the vicinity of the protein interdigitate to decrease the bilayer hydrophobic thickness and thus fulfill the matching condition.

By increasing the temperature above the pre-transition temperature, the pure lipid bilayer undergoes a transition from the L'_{β} phase to the 'ripple-like' phase, in which the bilayer assumes a 'peristaltic' shape, alternating thin and thick domains, as discussed in detail in Section 3.1. Interestingly, upon incorporation of a protein, and depending on the mismatch condition, the protein segregates into the domain whose hydrophobic thickness better matches the protein hydrophobic length. This is shown in the snapshots of Fig. 30. For a positive hydrophobic mismatch, (Fig. 30(a)), the protein prefers to segregate in the striated region formed by lipids in the gel-like state. Instead, in the case of negative mismatch, the protein prefers the region where the chains are fluid-like (Fig. 30(b)).

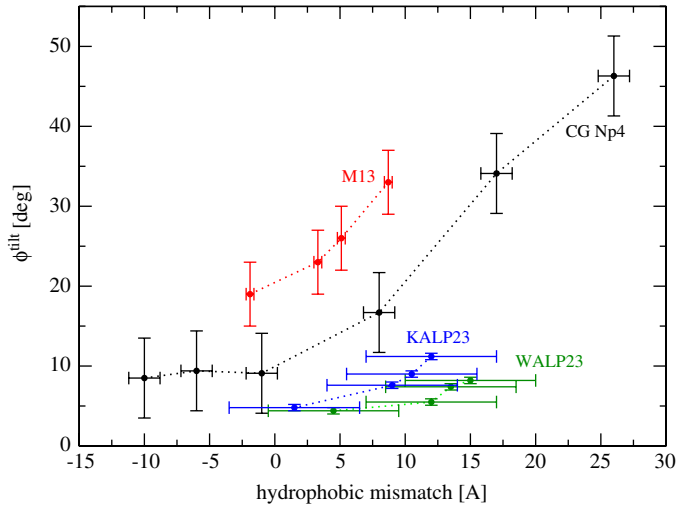

Fig. 28. Protein tilt-angle, ϕ^{tilt}, as a function of mismatch. The simulation data refer to the coarse-grained model-protein corresponding to $N_P = 4$ [109]; the experimental data refer to three different types of α-helical peptides: M13 coat protein peptide [213], KALP23 synthetic peptide [215], and the WALP23 synthetic peptide [214]. The dashed lines are only a guideline to the eye.

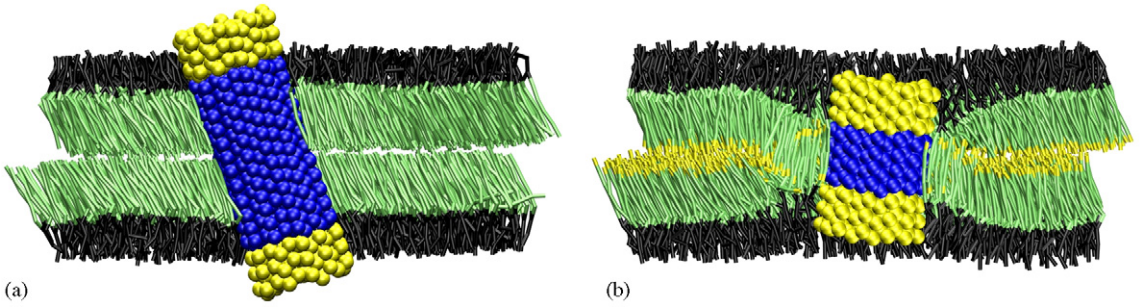

Fig. 29. Snapshots of two typical configurations of a lipid bilayer in the L'_β gel-phase with embedded a protein of size $N_P = 43$. Figure (a) shows the case of the protein subjected to positive mismatch, while figure (b) the case of the protein subjected to negative mismatch. In (b) the terminal tail beads of the lipids are depicted in yellow to better show their position in the bilayer (color online only).

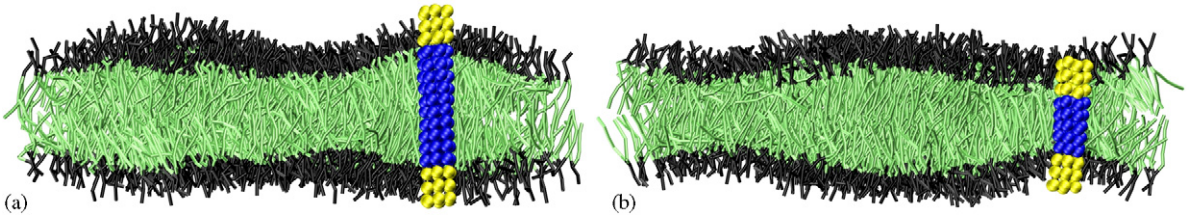

Fig. 30. Snapshots of two typical configurations of lipid–protein bilayer at a temperature in which the bilayer is in the 'striated' phase resembling the P'_β ripple phase: (a) protein subjected to positive mismatch; (b) protein subjected to a negative mismatch. In both cases the protein has size $N_P = 7$.

3.3.2. Protein–protein interaction

The nonspecific lipid-mediated attraction between two cylindrical proteins embedded in a bilayer membrane was studied by Sintes and Baumgärtner [32,33] using Monte Carlo simulations on a mesoscopic model. It was found that the lipid-induced protein–protein attraction mechanism has two regimes: there appears a depletion-induced attraction at short distances, and a fluctuation-induced long range attraction, which originates from the gradients of density and

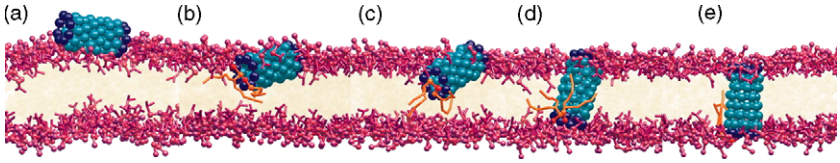

Fig. 31. Snapshots of the spontaneous adsorption of a model 'nanosyringe' into a membrane. From Lopez et al. [234].

orientational fluctuations of the lipids around each protein. Also, to investigate whether the force between two proteins may depend on the shape of the proteins, Sintes and Baumgärtner [34] considered conically shaped proteins (i.e., inclusions that are asymmetric under reflection in the mid-plane of the lipid bilayer), and estimated the forces and the range of interaction between two proteins in the case of the parallel or antiparallel relative orientation. It was found that in both cases (parallel and antiparallel) the interaction is attractive, independent of the interaction-range considered, and of the shape of the proteins—in contrast to what was previously found by elastic theories. Sintes and Baumgärtner attribute the difference between their results and the elastic theories to their somehow 'unrealistic' lipid model.

3.3.3. Protein insertion into membranes

Lopez et al. [234,235] studied, by MD on a coarse-grained model of a DMPC bilayer, the process of spontaneous insertion into the bilayer of a 'functionalized' hydrophobic macromolecule, a 'nanosyringe', which may be a model for a transmembrane channel, a pore, or a carbon nanotube. The macromolecule is modeled by a hydrophobic tube with hydrophilic end caps. The simulation revealed microscopic details of the insertion kinetics, detecting a mechanism by which the lipids assist one of the ends of the nanosyringe to cross the hydrophobic core of the membrane. A two-step process was observed for spontaneous adsorption into the bilayer, as shown in Fig. 31. First the capped tube laterally fuses with the closest leaflet, and then, after plunging into the membrane interior, it rotates to assume a transbilayer orientation. Interestingly, both the presence of the hydrophilic end-sites and hydrophobic matching conditions were seen to be necessary conditions for insertion. Spontaneous percolation of coarse grained water across this model pore was also observed.

Using the same mesoscopic modeling approach, Lopez et al. [236] also studied the spontaneous insertion of antimicrobial polymers into a lipid bilayer. Antimicrobial peptides attack the cell membrane of bacteria, causing its rupture and consequently cell death. The understanding of the mechanism of action of these molecules is clearly of great importance for medical applications. It is generally believed that these peptides attach first to the lipid–water interface through their hydrophobic side, and then insert into the membrane once that their interfacial concentration reaches a critical value [237,238]. The aggregation process results in the formation of membrane pores. The size of these pores may depend, among others, on the hydrophobic mismatch interaction [239,240]. In their model study, Lopez et al. found a possible alternative mechanism of action of antimicrobial molecules, which does not depend on pore formation for membrane leakage. These authors considered a coarse-grained model for the antimicrobial amphiphatic aryl amide dimer, a model for synthetic antimicrobial peptides, and studied its mechanism of insertion into a lipid bilayer as a function of antimicrobial concentration. They found that the antimicrobial molecules spontaneously insert into the lipid bilayer, however, at high concentration, the insertion process becomes cooperative, with molecular rearrangements and interactions between antimicrobial molecules that assist the insertion. Also, no pore formation was observed, and the average orientation of the antimicrobial molecules was found to be parallel to the bilayer plane. Furthermore, Lopez et al. suggested an alternative water transport pathway across the bilayer in which the water molecules 'hop' along the inserted peptides, aided by occasional fluctuations and rearrangement which bring a peptide perpendicular to the bilayer plane.

Srinivas and Klein [241] studied the interaction of a membrane-bound bio-active synthetic molecule with a model membrane by using MD on the coarse-grained model for DMPC described in Section 2. In particular, they have modeled a specific pore-promoting synthetic 'hydraphile', which shows strong ionophoric activity in phospholipid vesicles and E. coli. These hydraphiles are based on a simple threemacrocycle concept, with three 18-crown-6 rings connected by hydrocarbon linkers. The length of the hydrocarbon chains can be varied to match the hydrophobic thickness of a given bilayer. Once inserted into the bilayer, the hydraphile can act as a carrier for ion transport. The details at the molecular level of the hydraphile–membrane interactions still remain to be understood. The results from the simulations provided

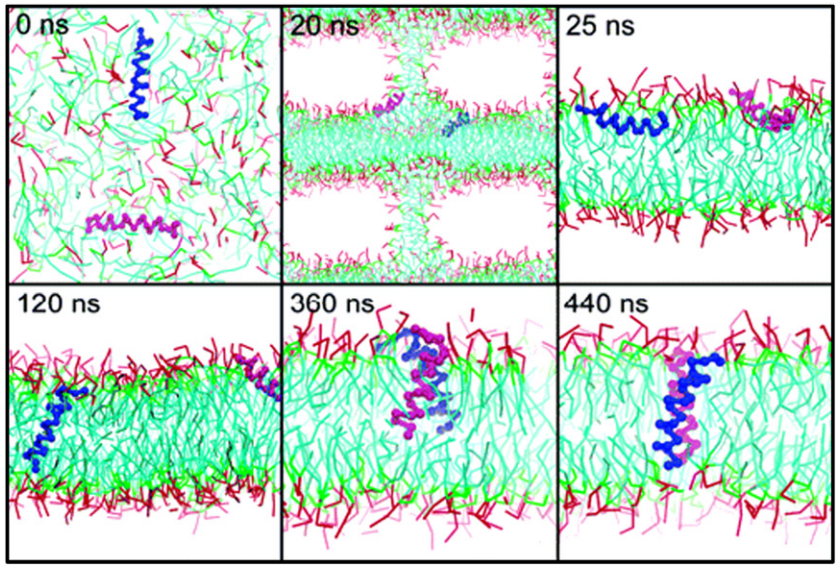

Fig. 32. Self-assembly of a GpA helix dimer in a lipid bilayer. Reprinted with permission from [243]. Copyright 2006 American Chemical Society.

details about the hydraphile–membrane interactions and confirmed that hydraphiles with the appropriate length of the alkyl chain linkers between the crown-ether moieties adopt a membrane-spanning conformation. The resulting picture is consistent with a membrane-spanning model proposed by Leevy et al. [242].

Another interesting application of mesoscopic models to the study of interactions of proteins with lipid bilayers was recently presented by Bond and Samson [243]. These authors extended the mesoscopic model of Marrink et al. [111] to study the insertion and self-assembly into DPPC lipid bilayers of a α-helical protein, Glycophorin A (GpA), and a bacterial β-barrel protein OmpA. The model was studied by MD simulations, and was validated by comparing the simulated self-assembly of protein/detergent micelles to the one obtained by MD simulations on the equivalent atomistic model. In the case of GpA, the results from the simulations (see Fig. 32) indicate that the helices first partition at the lipid–bilayer interface, then insert into the bilayer, and subsequently dimerize. These observations support the two-state model of protein folding. A dynamic equilibrium between the monomers and the dimers of GpA in the bilayer was also observed. A somehow different behavior was seen in the case of the β-barrel OmpA. For this protein, the insertion proceeds via the formation of stalks—as seen in fusion and budding processes (see Section 3.4), where the protein acts as a nucleation site between the lipids which eventually will form the bilayer. The results from this simulation study may help in the understanding of the folding mechanism of membrane proteins and in the prediction of their structure.

3.4. Vesicles fusion, budding and fission

Living cells host a number of biological processes where fusion, budding and fission are involved: for example endo- and exo-cytosis and molecular trafficking within or through the cell all involve shape changes of the outer or inner membrane of the cell [244]. Membrane fusion occurs when two membranes are brought in close contact. Although proteins play a role in the process, the fusion event is thought to be lipid-mediated [245]. Already in 1984 [246], it was suggested that fusion involves the 'stalk' mechanism, according to which fusion can start with the appearance of a stalk between approaching membranes. The mesoscopic approach is well suited to study membrane fusion and fission, because it allows the simulation of large systems, such as vesicles, while maintaining those molecular details which can provide useful insight into the lipid-mediated mechanisms which promote fusion or fission.

Single-component vesicles. Noguchi and Takasu [44] studied by Brownian dynamics on a particle-based implicit solvent model the fusion pathways of two lipid vesicles made of rigid amphiphiles. A 'stalk' intermediate was observed, where a necklike structure connects the outer monolayers of the two vesicles—in accordance with the stalk hypothesis. However, depending on temperature, different fusion mechanisms were observed. At low temperature, the pore-opening

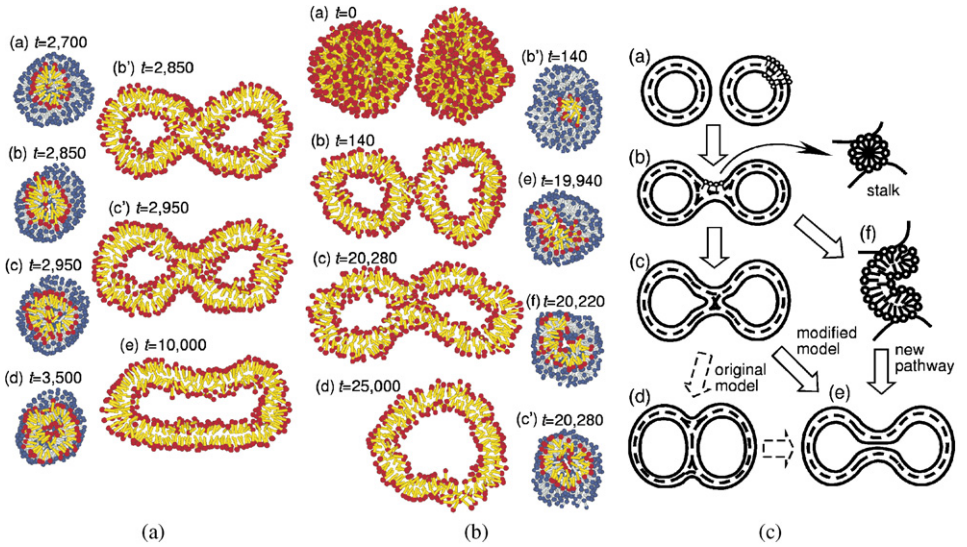

Fig. 33. Snapshots of the fusion pathway of two vesicles at low (a) and high temperature (b). Schematic representation of the different fusion mechanisms (c). Reused with permission from Hiroshi Noguchi and Masako Takasu [44]. Copyright 2001, American Institute of Physics.

follows the pathway of the modified stalk model according to which the pore formation involves the inner monolayers inside the stalk (see Fig. 33(a)). At high temperature, a new pathway of pore opening from stalks may occur, involving stalk-bending around a pre-pore structure (Fig. 33(b)). These authors also observed that the fusion pathway might change if considering vesicles made of flexible amphiphiles.

Using the same modeling approach, Noguchi and Takasu [45] also studied the structural changes in a lipid vesicle induced by mechanical forces. Their studies aimed at reproducing the experimental conditions in which morphological changes in cells are observed, for example during fission. In these simulations the vesicle contains two nanoparticles, one of which is at a fixed position while the other one is moved by a constant force, as in optical-trapping experiments. Upon pulling, pear or tubelike structures form. Then the inner monolayer in the tube-shaped region is deformed, and a cylindrical structure is formed between two vesicles. A further stretching causes a fission near the moved vesicle. The study of lipid vesicles was extended by the same authors to investigate the mechanism of adhesion of nanoparticles—which are simple models for proteins or colloids—to vesicles [46]. Adhesion is involved in biologically relevant phenomena such as endo- or exocytosis [6]. The results from these simulations indicated that the adhering nanoparticle induces morphological changes of the vesicle: budding, formation of two vesicles in which only outer monolayers are connected, and fission. Also, the nanoparticle may promote the fusion process by causing a pore opening in a stalk intermediate.

Müller et al. [247,248] used Monte Carlo simulations on a model for bilayers formed by flexible, single chain block copolymers, to understand the phenomenon of membrane fusion. The authors used the bond fluctuation model of a polymer chain [249] for the description of the lipid molecules. The lipids are composed of hydrophilic and hydrophobic segments, and the solvent by chains of hydrophilic segments. Each segment occupies the lattice cube of a three-dimensional lattice model. The segments are connected by springs and interact with each other via a square well potential. The results from the MC simulations of Müller et al. showed that fusion begins with the formations of stalks—as previously proposed. However, it was also found that the bilayer is destabilized because the stalks catalyze the formation of holes—as previously suggested by Noguchi and Takasu. Müller et al. argue that the energy per unit length of the edge of a hole is reduced when a hole is close to a stalk, and that the stalk will try to surround the hole formed in one bilayer once the hole has appeared.

The intermediate stages of the process of fusion between two small (with a diameter of ca. 15 nm) coarse-grained DPPC vesicles were also investigated by Marrink and Mark [250]. They found that, once the vesicles approach one another within few nanometers (without close contact), the fusion process is triggered by a spontaneous fluctuation in one of the monolayers, which results in few head groups merging with the opposing monolayer, as can be seen in

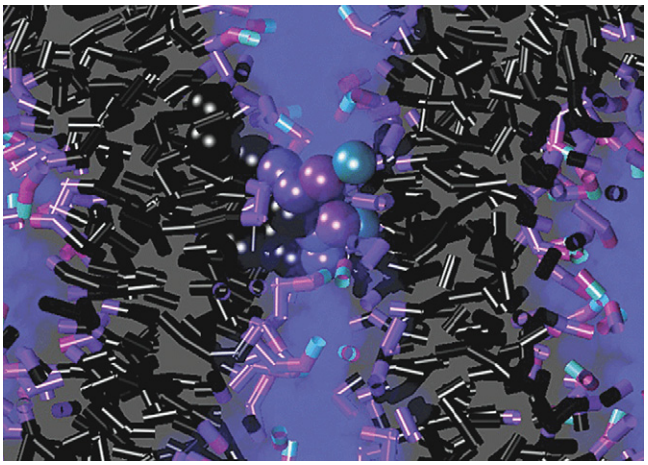

Fig. 34. Snapshot of the initial step in the fusion of two vesicles. The fusion is triggered by the lipids represented as spheres. Reprinted with permission from [250]. Copyright 2003 American Chemical Society.

Fig. 34. Once that the fluctuation occurs, the process proceeds and complete fusion occurs within the nanosecond timescale. The authors detected two fusion pathways, one in agreement with the stalk-pore mechanism [251], according to which a stalk intermediated is formed first, to which a merging of the two monolayers follows, then a small fusion pore forms, and, finally, the rupture of the bilayer occurs, which completes the fusion. A modified stalk-pore mechanisms was also detected, in accordance with previous theoretical predictions and experimental evidences.

Using the modeling approach described in Section 2, Stevens et al. [78] studied the mechanism of fusion of two lipid vesicles, with particular attention to the role of lipid rearrangement at the molecular scale. The two vesicles, made of the same double-tail lipid type, were pushed together by an external force until the outer membranes were in contact. The force was then released and the fusion was allowed to spontaneously proceed. At the edges of the flat contact zone between the two vesicles the membrane is strained due to curvature changes. The authors observed that fusion is triggered by lipids in this contact zone, which tilt and then splay their tails so to span the membranes of both vesicles. Splayed lipids then cluster their tails to form the beginning of a new hydrophobic core and a stalk structure is formed. The stalk grows to an intermediate fusion state and then opens to complete the fusion process.

Shillcock and Lipowsky [252,253] performed a large number of simulations to investigate the statistics of tension-induced fusion of a large vesicle to a flat membrane. Owing to the large system size (a vesicle of 28 nm in diameter and a membrane patch of about $50 \times 50\,\mathrm{nm}^2$) and to the fact that these authors wanted to study the statistics over several realizations of the initial conditions and to follow the system evolution over long times (over 2 μs), the simulation method used was DPD on coarse-grained lipids. Both the vesicle and the flat membrane are composed of the same lipid type, i.e. a coarse-grained lipid with three hydrophilic headbeads and two tails of four hydrophobic beads each, and the solvent is explicitly treated. Shillcock and Lipowsky observed that fusion is tension-induced. When both the vesicle and the flat membrane are in a tensionless state no fusion was observed, instead the vesicle spreads and adheres to the membrane surface, without rupturing. To observe fusion, both the vesicle and the membrane patch should be under an initial positive tension (stretching). The positive tension state is induced by increasing the area per lipid. By performing a large number of fusion attempts, the authors were able to derive the morphology diagram of the fusion process as a function of tension. For low tension fusion was never observed, while for tension which is too high, the flat membrane and the vesicle ruptured. However, even in the region of tension where fusion was observed, not all attempts resulted in fusion, and alternative mechanisms to relax tension (such as rupture and hemifused metastable states) were observed. This indicates that simply applying a uniform tension is not sufficient to reliably drive the fusion event. The authors suggested that applying a local (in space and time) tension could improve the statistics, in a way that would mimic the effect of proteins which are known to aid the fusion process in biological membranes. An interesting observation is that, if fusion happens, then there is a upper time cut-off for the fusion event of about 350 ns, i.e. independently of the applied tension, all successfully completed fusion events were seen to happen within this time window.

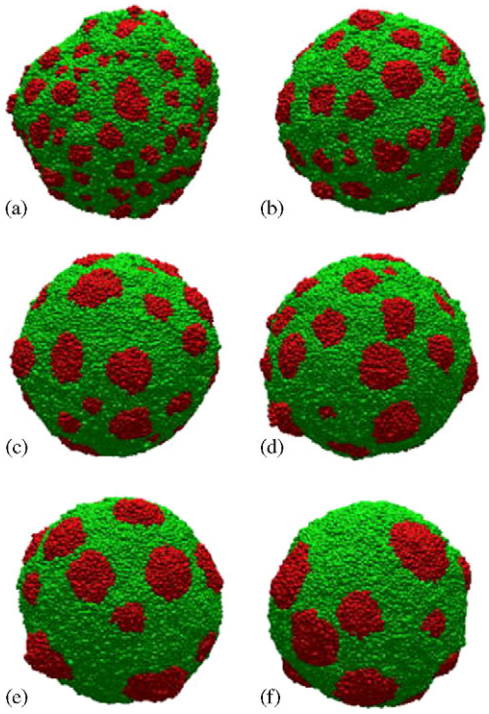

Fig. 35. Snapshots of the formation of a two component phase-separated vesicle. Reused with permission from Mohamed Laradji and Sunil Kumar [108]. Copyright 2005, American Institute of Physics.

Multicomponent vesicles. Membranes formed from multiple lipid components can undergo lateral phase separation into coexisting liquid phases, or domains, with distinct compositions. This process may resemble raft formation in cell membranes. Aspects such as the shape of vesicles, the viscosity of the lipid bilayer, the presence of the solvent, and the area-to-volume constraint (due to the possible vesicle impermeability) in relation to lipid-composition were investigated using coarse-grained models.

Laradji and Sunil Kumar [92,108] performed large-scale DPD simulations of phase separation dynamics of a fluid vesicle made of two lipid components. The lipid molecules are represented by a flexible amphiphilic chain, having one hydrophilic particle and a tail of three hydrophobic particles. By tuning the relative repulsion between lipid molecules, systems composed of two lipid types could be modeled. To study the dynamics of the system, these authors followed a quench from the one-phase region to the fluid–fluid coexistence region (i.e., when the system is fully phase separated). They found that the path through which the system equilibrates depends on the area-to-volume ratio and on composition. However, the late time shape of the vesicles corresponds to that of a surface decorated with caps, as illustrated in Fig. 35. Experimental findings [254] confirm the predictions obtained from those simulations: irrespective of the initial area-to-volume ratio, the main vesicle eventually acquires a spherical shape, which results from the volume constraint. Also, the dynamics at all times is affected by the presence of the solvent. Motivated by the fact that biological membranes have an asymmetric lipid distribution in the two leaflets of the bilayer, Laradji and Sunil Kumar [255] also studied the effect of the lipid asymmetry on the dynamics of phase separation of fluid vesicles made of two lipid components. They found that the local spontaneous curvature of the bilayer induced by an asymmetric distribution of lipids affects both the dynamics and the morphology of the vesicles.

Cook and Deserno [49] used an implicit solvent model to investigate the kinetics of domain formation and the budding process in vesicles made of two lipid types, A and B. What differentiates the two types of lipids is the choice of the value of the range of the attractive interaction (w) between the two lipid types. By choosing the interaction parameter between lipids of the same type smaller than the one between different lipid types, the formation of a domain was observed, with a symmetric transversal distribution of the lipids, i.e. there was approximately the same number of lipids (for each type) in the inner and outer monolayer (see also Fig. 36(b)). Upon cleavage of the domain boundary, budding is induced. Interestingly, Yamamoto and Hyodo [110] found instead that a asymmetric transversal distribution

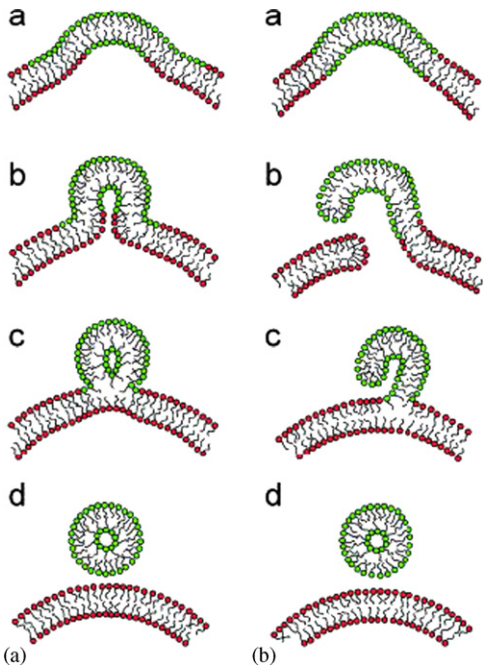

Fig. 36. Schematic drawing illustrating the two possible paths of the budding and fission process. (a) Asymmetric distribution of lipids between the inner and outer monolayer, (b) symmetric distribution. Reused with permission from Satoru Yamamoto and Shi-aki Hyodo [110]. Copyright 2001, American Institute of Physics.

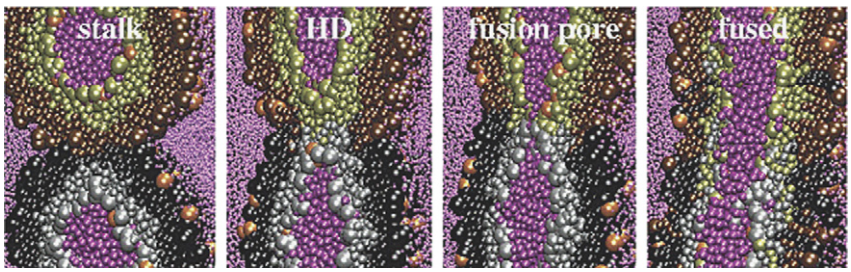

Fig. 37. Snapshots of the fusion pathway of two mixed DPPC/DPPE vesicles. Reprinted with permission from [250]. Copyright 2003 American Chemical Society.

of the lipid types can favor budding and fission. Yamamoto and Hyodo also modeled the two lipid types as having the same shape and size; consisting of a flexible chain made of four beads, where one of the beads represents the head group and the others the lipid acyl chain. To be able to induce segregation of the two components, the effective interaction, modeled by the soft repulsive force typically used in DPD simulations (see Eq. (A.5) in Appendix) between different lipid types was set more repulsive than between alike types.

The results from the simulations of Yamamoto and Hyodo indicate that the domain-formation is a prerequisite for budding, as Cooke et al. [49] suggested more recently. However, the simulation results of Yamamoto and Hyodo show that the local asymmetry in the transversal distribution of the two lipid components can facilitate the budding and fission process. Furthermore, they suggested two possible pathways for budding and fission—as illustrated in Fig. 36—depending on the local asymmetry, or on the occurrence of pronounced thermal undulation of the domains (or an increase of the interfacial energy of the domains), respectively.

The dependence of fusion process on lipid composition was also considered by Marrink and Mark [250], who used a coarse-grained model of mixed DPPC and DPPE or lysoPC (see Fig. 37). These simulations revealed significant

differences in the packing of the lipids between the inner and outer monolayers, and between DPPC, DPPE, and lysoPC. The lipid lateral diffusion rate was found to be faster in the outer than in the inner monolayer. For pure DPPC vesicles, the authors calculated a value of the water permeability coefficient in agreement with experimental data.

4. Concluding remarks

The material properties of biological membranes, and their relation to the biological functioning, have been a subject of experimental and theoretical investigations for decades. Theoretical modeling is a useful tool, either alone or together with experimental studies, to understand the physical behavior of membranes, either natural or reconstituted. However, for decades, there has been a gap between the macroscopic description of biomembranes seen as 'thin elastic sheets', and the microscopic, atomistic description where each atom of the system is considered relevant for the understanding of the membrane physical behavior. While, on the one hand, the macroscopic approach neglects the molecular nature/interactions of the membrane components, which may instead influence the mechanical properties of the membrane, on the other hand, the atomistic approach often takes into account details which are not necessarily relevant for the description of some membrane processes. In this respect, the development of mesoscopic models may help to bridge the macroscopic-microscopic gap. The power of the coarse-grain modeling approach is two-fold. Not only by mesoscopic modeling one can deal with much larger systems (and study them at much longer time scales) than it is possible by 'traditional' atomistic modeling, but one can also make predictions about the influence of molecular details on the behavior of the whole system. Such knowledge may be difficult or even impossible to achieve by experimental methods.

In this review we presented a number of coarse-grained approaches. There is an interesting fundamental question underlying the development of these mesoscopic models and that is whether there is a unique way in going from atomistic simulations to a coarse-grained model. From the previous sections it is clear that every group has their favorite way of coarse-graining a membrane. One of the aims we have set in writing this review was to critically compare the various approaches. The result of this comparison came as a surprise to us and it is that, despite the very different approaches that various groups have used, the resulting coarse-grained models give surprisingly similar and consistent results. From a physicist point of view this is an important result, as it indicates that many of the phenomena that are observed in these complex systems have very generic origins that are not too much dependent on the details of the molecules that form a membrane. If this is correct, there will be many different coarse-grained models that have the same generic behavior, but may differ in certain details. Clearly, depending on which details one would like to retain, a different coarse-graining approach might be chosen.

A related question is how well one should understand a coarse-grained model before applying it to something useful? The idea behind this question is that a coarse-grained model can be seen as a black box to extrapolate an all-atom simulation to longer time and length scales. We feel that the answer has two aspects. First of all, coarse graining implies removal of details and one has to ensure that these details are not essential for the application one would like to understand. Secondly, we hope that this review has shown that studying in detail the behavior of these coarse-grained models helps us to understand the behavior of real membranes; as one can systematically investigate changes of part of the structure of a lipid in a controlled way that it is difficult to achieve in experiments.

The fact that many different coarse-grained models give such a coherent picture on the structure of a membrane is very encouraging. As of yet it is less clear whether the same holds for the dynamics (see e.g. [120]). Most of the models have been tested against structural data, but little dynamics has been included in the validation step. Despite this, the field is at an excellent starting point to use these coarse-graining models to understand many of the exciting processes taking place in biological membranes.

Acknowledgments

This work is partially supported by the EC through the Marie Curie EXT project MEXT-CT-2005-023311 (France). M.M.S. thanks the Center for Biological Sequence Analysis at DTU, Kgs. Lyngby (Denmark), and CECAM, Lyon and the Marie Curie EST project MEST-CT-2005-020491, for hospitality.

Appendix A. Computer simulation methodologies

In this appendix we touch upon the basic ideas of the computational techniques that are usually adopted for particle-based simulations of lipid bilayers. Since there are many good reviews and textbooks that describe MD or MC simulation techniques [256,257], we have kept this discussion very brief and focused on the aspects which are specific to the simulation of membranes. It is important to note that these simulation techniques can be applied both to the study of atomistic-detailed models as well as to the study of coarse-grained models.

Because this review is about simulation methods in relation to modeling of membranes, in this appendix we also define the structural properties which are normally used to characterize lipid bilayers, and show how these properties can be calculated using molecular simulations.

A.1. Molecular simulation techniques

A.1.1. Molecular dynamics

The principles of molecular dynamics are very simple: by knowing the interaction potentials between the 'entities' (i.e., atoms, beads, etc.) in the system, one can compute the forces, and, by solving Newton's equations off motion, one can follow the time evolution of the system. If one has followed a sufficiently large system for sufficiently long time after its equilibration, one can generate the configurations which are used to compute the statistical quantities (structural, thermodynamic and transport) that characterize the system.

In principle, this procedure is straightforward. In practice, the key points here are "sufficiently large" and "sufficiently long". Suppose that the intermolecular potential accurately describes the true interactions in a real membrane, then the MD simulation will well reproduce the behavior of the membrane. Sufficiently large and sufficiently long are then determined by the available computational resources. Very large state of the art simulations can involve as much as 1000 phospholipids molecules and 100,000 water molecules, and span of the order of 100 ns [42]. With such a simulation one can observe the self-assembly of a vesicle [42]. However, for a systematic study that requires, for example, simulations at various temperatures, each of say 100 ns, one has to use much smaller systems, of typically 256 lipids and 10,000 water molecules [155]; this number of molecules would correspond to a bilayer patch with an area of the order of 700 $Å^2$. If we compare these length and time scales with the experimental systems, the limitations of MD simulations on atomistic models become evident. Of course, compared to the very first simulations of a biological membrane, the progress is impressive and more advances are expected as the computational power continues to grow. Despite this, for the coming decades there will still be a large gap between the time and length scales accessible via atomistic molecular dynamics and the ones relevant for some of the properties of real biomembranes.

Alternatively, one can gain many orders of magnitude in time and length scales by looking at membranes at a coarse-grained level, where individual atoms, or even molecules, are grouped together into larger interacting entities. By coarse-grain models, one can thus simulate larger systems and for longer times, than it is possible with all-atom models. Nevertheless, there is a price to be payed: by coarse-graining the systems one looses structural/chemical details which may be relevant for what one wants to investigate; also, some a priori relevant interactions may not be modeled in details, for example the electrostatic interactions.

A.1.2. Monte Carlo

The MC simulation technique [258] is based on the idea of generating a representative set of configurations using trial moves instead of generating configurations by solving Newton's equations of motion for each entity of the system, like it is done in MD. A new configuration of the system is generated, and it is then accepted or rejected depending, for example, on the difference in energy between the configurations. Trial configurations can be generated in many different ways, and this freedom can be used to develop very efficient schemes [257]. For example, from the MD point of view, the flip-flop of lipids (i.e. the diffusion of a lipid from one leaflet of the bilayer to the opposite one) can be seen as a rare event, requiring the crossing of a high energy barrier since the lipid has to move its hydrophilic head from one side of the bilayer to the other across the hydrophobic interior of the bilayer. From the MC point of view, there is no need to 'cross' this barrier, in the sense that one can simply generate a trial configuration, where the actual lipid is located at the opposite leaflet of the bilayer, the energy of which is then compared with the one of the initial configuration. The trial configuration is then accepted or rejected according to a defined probability.

Of course, generating trial configurations of a lipid molecule in a part of the membrane such that this does not result in configurations with unacceptable high energy is a computational challenge [257] and requires special techniques such as configurational-bias MC [219,259–261].

One can also say that the MC simulation method may be used as a short-cut to find the unknown equilibrium structure of the system. For example, for a curved membrane one would expect a different lipid density on the two sides of the membrane. Clearly, a molecular dynamics simulation would require extremely long times if one starts with an initial configuration that is different from the equilibrium distribution. With a MC simulation, one does not have to wait for the flip-flops to spontaneously occur, but the phase space can be explored more efficiently and equilibrium reached in much shorter simulations. The drawback of the MC method is that it gives rise to an artificial dynamics of the system, and therefore it is not suitable to study, for example, transport properties.

A.1.3. Dissipative particle dynamics

The DPD simulation technique was first introduced by Hoogerbrugge and Koelman [262] in 1992 as an off-lattice, coarse-grained model to simulate fluid systems. Using both simulations and theoretical considerations, Hoogerbrugge and Koelman showed that the DPD algorithm obeys the Navier–Stokes equations. The original scheme was modified in 1995 by Español and Warren [263] to ensure that a proper Boltzmann distribution is generated. As DPD is a relatively new technique, we will describe it in some detail.

DPD describes the motion of particles, or beads, which represent the center of mass of a fluid 'droplet', i.e. each DPD particle is a momentum carrying group of molecules. All the degrees of freedom within a bead radius are assumed to have been integrated out, resulting in a coarse-grained representation of fluid elements, and in the possibility to adopt soft interactions between the beads. However, this reduction of degrees of freedom results in a nonphysical dynamic behavior. To reintroduce the correct hydrodynamic behavior, in DPD a dissipative force and a random 'noise', both pairwise additive and momentum conserving, are added to the force acting on a particle. The dissipative and random forces are expressed as

$$\begin{aligned} \mathbf{F}_{ij}^{\mathrm{D}} &= -\eta w^{\mathrm{D}}(r_{ij})(\hat{\mathbf{r}}_{ij}\cdot\mathbf{v}_{ij})\hat{\mathbf{r}}_{ij}, \\ \mathbf{F}_{ij}^{\mathrm{R}} &= \sigma w^{\mathrm{R}}(r_{ij})\zeta_{ij}\hat{\mathbf{r}}_{ij}, \end{aligned} \tag{A.1}$$

where $\hat{\mathbf{r}}_{ij} = (\mathbf{r}_i - \mathbf{r}_j)/|\mathbf{r}_i - \mathbf{r}_j|$ is the unit vector between particles i and j ($r_{ij} = |\mathbf{r}_{ij}|$), $\mathbf{v}_{ij} = \mathbf{v}_i - \mathbf{v}_j$ is the velocity difference between particles i and j, η is a friction coefficient, and σ is the noise amplitude. ζ_{ij} is a random number, with zero mean and unit variance, chosen independently for each pair of particles. The requirement $\zeta_{ij} = \zeta_{ji}$ enforces momentum conservation. The weight functions w^{D} and w^{R} are defined in Eqs. (A.3) and (A.4).

The total force f_i acting on a DPD particle i has thus three contributions [95,262]

$$f_i = \sum_{j\neq i}(\mathbf{F}_{ij}^{\mathrm{C}} + \mathbf{F}_{ij}^{\mathrm{D}} + \mathbf{F}_{ij}^{\mathrm{R}}), \tag{A.2}$$

where $\mathbf{F}_{ij}^{\mathrm{C}}$ is the conservative part of the force.

Español and Warren [263] derived the continuous stochastic differential equation that corresponds to the DPD algorithm, and the associated Fokker–Plank equation governing the temporal evolution of the distribution function of the positions and momenta of the particles. They demonstrated that if the weight functions and coefficients of the dissipative and the random force satisfy the relations

$$\begin{aligned} w^{\mathrm{D}}(r) &= [w^{\mathrm{R}}(r)]^2, \\ \sigma^2 &= 2\eta k_{\mathrm{B}}T, \end{aligned} \tag{A.3}$$

then the steady state solution of the Fokker–Planck equation is the Gibbs canonical distribution. This implies that only the conservative part of the force (or better, the potential U^{C} related to it: $\mathbf{F}^{\mathrm{C}} = -\nabla U^{\mathrm{C}}$) determines the equilibrium averages of the system observables. In this way, DPD can be seen as a momentum-conserving thermostat for MD simulations.

The most common choice for the weight function $w^{\mathrm{R}}(r)$ is in the form of a soft-repulsive interaction

$$w^{\mathrm{R}}(r) = \begin{cases} (1 - r/R_c) & (r < R_c), \\ 0 & (r \geqslant R_c), \end{cases} \tag{A.4}$$

where R_c is a cutoff radius which gives the range of the interaction. $w^{\mathrm{D}}(r)$ follows from Eq. (A.3). For reasons of simplicity, and because of the soft nature of the particles, the conservative force F^{C} is usually chosen with the same functional form as the random and dissipative forces, i.e.,

$$\mathbf{F}_{ij}^{\mathrm{C}} = \begin{cases} a_{ij}(1 - r_{ij}/R_c)\hat{\mathbf{r}}_{ij} & (r_{ij} < R_c), \\ 0 & (r_{ij} \geqslant R_c), \end{cases} \tag{A.5}$$

where the coefficient $a_{ij} > 0$ represents the maximum repulsion strength between particles i and j.

DPD particles move according to the force in Eq. (A.2), in continuous space and discrete time steps. There are two reasons why the integration of the DPD equations of motion may be cumbersome. The first reason is that the velocities depend on the dissipative force, which in turn is itself a function of the particle velocities, hence the integration algorithm should be iterative. Then, because of the random force, the DPD equations of motion are stochastic differential equations, and, in principle, they should be integrated accordingly. Here we will not go into the details of the algorithms proposed to integrate the DPD equations of motion. It is however important to point out that care must be used in choosing the correct integrator and timestep, as extensively discussed by several authors [264–269].

It is worth mentioning that the application of DPD to the study of lipid bilayers [37,88–90] is relatively recent, and that the DPD simulation method was used to investigate a number of different systems outside the membrane field. We refer the reader to Refs. [270,271] for a comprehensive review on DPD and its applications.

A.1.4. Statistical ensemble

Special attention has been devoted to the definition of the ensemble that better reproduces "natural" (or laboratory) conditions of lipid bilayers. A reasonable choice would be to perform simulations at constant temperature and constant pressure. If also the number of particles is kept constant, this corresponds to the canonical (N, V, T) ensemble. However, since membranes may be viewed as an interface, one may need to consider another thermodynamic variable, i.e., the surface tension. Lipid bilayers are self-assembled structures, which, if not constrained by the total area, will adopt a conformation which minimizes the free energy. Because the thermodynamic definition of surface tension is the derivative of the free energy with respect to the area of the interface [272], the free energy minimum for a unconstrained bilayer corresponds to a tensionless state [273]. Experimental results on unilamellar vesicles have indicated that bilayers are, in fact, in a tensionless state [274]. In molecular simulation, for both self-assembled and pre-assembled bilayers, the choice of a fixed number of lipid molecules with fixed area per lipid is usually combined with the use of periodic boundary conditions. Although periodic boundary conditions are meant to reproduce an infinitely large system, the fixed size of the simulation box, and the fixed number of lipids at the interface, impose a constraint on the bilayer area, which results in a finite surface tension. The constraint on the fixed area can be released by performing simulations of membranes at constant pressure or constant surface tension. Surface tension was incorporated into MD simulations to obtain the constant surface tension ensemble (N, V, γ), and the corresponding equations of motion were derived [275,276], and applied to the simulation of phospholipid bilayers [219,277–280]. Alternatively, a series of simulations in the (N, V, T) ensemble can be performed to determine the area per lipid that corresponds to the desired tension, as was done by Goetz and Lipowsky [74]. A different approach consists in imposing a given value of the surface tension through a hybrid scheme which combines DPD or MD with MC [88]. In the following we describe in general terms the fundaments of this approach.

For a system at equilibrium consisting of only two immiscible components (e.g. oil and water) at a fixed composition, the surface tension of the interface between the two fluids is a constant. If surfactants (or lipids) are present, the surface tension will depend on the concentration of surfactants at the interface. The value of the surface tension can thus be controlled by changing the area of the interface (i.e. the surfactant concentration at the interface). Consider a (fluid) system with a constant number of particles N, at constant temperature T, and constant volume V, in which an interface of area A is present, where surfactants are located. The interface gives an additional term to the energy of the system, i.e. the energy associated with the creation of the interface, which is expressed by the surface tension γ multiplied by the area of the interface. The work done on the system by compressing or stretching the interface by $\mathrm{d}A$, is given by $\mathrm{d}W = \gamma \mathrm{d}A$ [272]. The partition function for such a system can then be written as

$$Q = \frac{1}{\Lambda^{3N} N!} \int_V \mathrm{d}\mathbf{r}^N \exp[-\beta(U(\mathbf{r}^N) - \gamma A)], \tag{A.6}$$

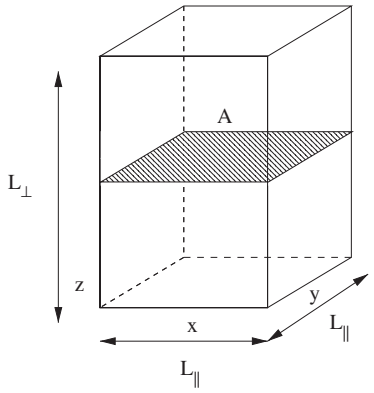

Fig. A.1. Schematic representation of a simulation box for a system with a planar interface parallel to the *xy*-plane. The area of the interface is $A = L_{\parallel}^2$ and the box dimension perpendicular to the interface (z axis) is $L_{\perp}$.

where U denotes the potential energy, γ the surface tension, A the area of the interface and $\beta = 1/k_{\mathrm{B}}T$. $\Lambda = \sqrt{h^2\beta/(2\pi m)}$ is the thermal de Broglie wavelength, with h the Planck's constant.

Consider a simulation box with edges $L_x = L_y = L_{\parallel}$ parallel to the interface (xy plane) and $L_z = L_{\perp}$ perpendicular to the interface (z axis), so that the system volume is $V = L_{\perp}L_{\parallel}^2$ and the area of the interface $A = L_{\parallel}^2$ (see Fig. A.1).

A MC move can then be generated in which the box sizes are rescaled, in such a way that the area and the height of the box are changed but the volume is kept constant, so that no work is done against the external pressure. Such a transformation can be written in the form

$$L'_{\parallel} = \lambda L_{\parallel},$$
$$L'_{\perp} = \frac{1}{\lambda^2} L_{\perp}, \tag{A.7}$$

where λ is the parameter of the transformation. By changing λ, the above expression generates a transformation of coordinates which preserves the total volume of the system, hence no work is made against the external pressure. This introduces an extra degree of freedom represented by the parameter λ. To write the partition function corresponding to this ensemble it is convenient to introduce a set of scaled coordinates $\mathbf{s} \in [0, 1]$, defined as

$$\mathbf{r} = (L_{\parallel}s_x, L_{\parallel}s_y, L_{\perp}s_z). \tag{A.8}$$

By a transformation of the box sizes with λ (Eq. (A.7)) the coordinates of the particles rescale as

$$\mathbf{r}' = \left(\lambda L_{\parallel}s_x, \lambda L_{\parallel}s_y, \frac{1}{\lambda^2} L_{\perp}s_z\right). \tag{A.9}$$

In terms of the scaled coordinates, the partition function of the system takes the expression

$$Q = \frac{V^N}{\Lambda^{3N} N!} \int \mathrm{d}\lambda \int \mathrm{d}\mathbf{s}^N \exp\{-\beta[U(\mathbf{s}^N; \lambda) - \gamma A(\lambda)]\}. \tag{A.10}$$

The probability of finding a configuration with scaled positions $\mathbf{s}^N$ and parameter λ is then given by [257]

$$N(\mathbf{s}^N, \lambda) \propto \exp\{-\beta[U(\mathbf{s}^N; \lambda) - \gamma A(\lambda)]\}. \tag{A.11}$$

In a MC move, an attempt at changing the parameter λ is then accepted with a probability

$$P_{\mathrm{acc}}(\lambda \to \lambda') = \frac{\exp\left\{-\beta\left[U(\mathbf{s}^N; \lambda') - \gamma A(\lambda')\right]\right\}}{\exp\left\{-\beta\left[U(\mathbf{s}^N; \lambda) - \gamma A(\lambda)\right]\right\}}, \tag{A.12}$$

where γ is the imposed surface tension. If we choose the particular value $\gamma = 0$, then the term explicitly depending on the area in Eq. (A.12) drops. The procedure just described can be applied to impose any value of the surface tension.

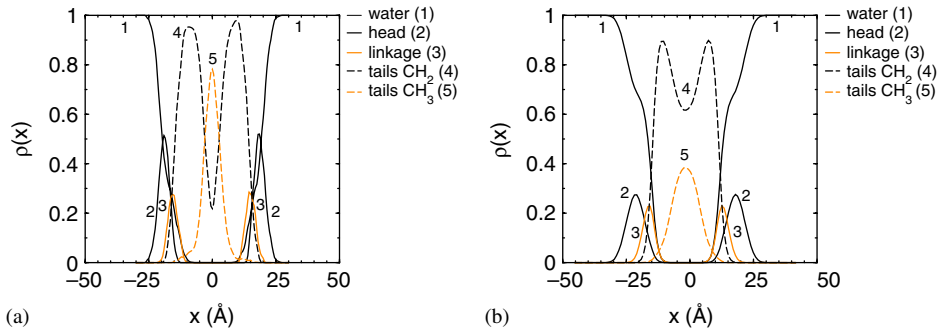

Fig. A.2. Density profiles across a lipid bilayer: (a) from atomistic MD simulations of a DMPC bilayer, where the density profiles of the centers of mass of each group corresponding to a coarse-grained bead are represented; (b) from a coarse grained model of a DMPC bilayer studied using DPD simulations [94].

It is important to remark that the above procedure is applicable if, as assumed, the stress tensor is diagonal, which is true for fluid systems but not for solids.

The MC moves can then be combined with MD, DPD or MC to follow the evolution in phase space of the particles. This 'hybrid' approach has the advantage that one does not have to perform several, time demanding, simulations to locate the interfacial area corresponding to the desired tension. Moreover, by releasing the constraint of a priori chosen area, and allowing dynamic fluctuations, the system is able to explore the phase space and assume the configurational structure that corresponds to the free energy minimum at the given thermodynamic conditions. One of the implications of this extra degree of freedom is that it allows to observe directly structural rearrangements of the bilayer, for example during phase transitions (as described in Section 3.1), in which the area per lipid changes.

A.2. Structural properties of lipid bilayers

The structural properties of a lipid bilayer depend on several parameters. Among others, the morphology of the lipids, the bilayer composition, e.g., whether the bilayer contains more than one lipid type, or other molecules such as cholesterol, proteins or alcohols, and on the thermodynamic state, for example the temperature. Here we briefly describe those observables which can be measured in experiments on simplified membrane systems, and which can also be calculated using molecular simulations. These quantities can be used to parameterize a computational model and test its accuracy, or can be calculated as a result from the simulation of a model system, to give new insights into the behavior of lipid membranes. Moreover, because one of the advantages of molecular simulation is that the positions of the particles in the system are known, one can extract information which is otherwise difficult or even impossible to access by experimental techniques; a good example is a local property like the surface tension profile across the bilayer (see Section A.2.1).

Density profiles. The density distribution of atoms or electrons across a bilayer can be measured experimentally, for example by diffraction techniques [281], and can also be directly calculated from atomistic simulations. The density distribution of the particles of a coarse-grained model system can be calculated too, and compared with the one obtained from simulations on the equivalent atomistic model to verify the ability of the coarse-grained model to reproduce, for example, the internal structure of a bilayer. In Fig. A.2 are shown the density profiles for an atomistic DMPC bilayer and the corresponding coarse-grained system [94]. For the atomistic system the density profiles in Fig. A.2 correspond to the position of the centers of mass of the corresponding coarse-grained beads of the mesoscopic model. Naturally, given the coarse-grain nature of the model, where a number of atoms are lumped into a single coarse-grain bead, one cannot expect an exact overlap between the curves obtained for the coarse-grained model and the atomistic (or experimental) ones. Nevertheless, general features of the density distribution in a bilayer are well reproduced by the coarse-grained model.

Lipid order parameter. The lipid order parameter is a way of quantifying the ordering of the lipid chains. This quantity can be measured experimentally by deuterium substitution NMR spectroscopy [282]. The order parameter is

defined as

$$S = \tfrac{1}{2}\langle 3\cos^2\phi - 1\rangle, \tag{A.13}$$

where ϕ is the angle made by the vector along a given C–H bond with the bilayer normal. If the hydrogen atoms are not represented explicitly (such as in the case of coarse-grained models), the mathematical expression of equation (A.13) can still be used, but the angle ϕ is now defined as the angle between the orientation of the vector along two beads in the chain and the normal to the bilayer plane

$$\cos\phi = \frac{\mathbf{r}_{ij}\cdot\hat{\mathbf{n}}}{r_{ij}}, \tag{A.14}$$

where $\hat{\mathbf{n}}$ is a unit vector normal to the bilayer, and $\mathbf{r}_{ij} = \mathbf{r}_i - \mathbf{r}_j$ is the vector between beads i and j ($r_{ij} = |\mathbf{r}_{ij}|$). The order parameter has value 1 if this vector is, on average, parallel to the bilayer normal, 0 if the orientation is random, and -0.5 if it is, on average, parallel to the bilayer plane. The order parameter for a vector between any two beads in the lipid molecule, or for the entire molecule, can thus be calculated. In particular, the overall order of the chains and the local order can be characterized and monitored, for example as a function of temperature to identify phase transitions from the gel phase—in which the lipid acyl chains are ordered—to the liquid crystalline phase, in which the lipid tails become disordered, as discussed in more detail in Section 3.1.

Area per lipid. The area per lipid projected on the bilayer plane, A_L, can be experimentally estimated from X-ray or neutron scattering experiments [281], or, indirectly, from the lipid order parameter profiles [283]. In simulated bilayers, the area per lipid is usually calculated by dividing the total bilayer projected area by half the number of lipids in the bilayer, since, on average, there is an equal number of lipids in each leaflet. In practice, if the bilayer spans the entire simulation box and it is oriented parallel to one of the orthogonal axis, the area per lipid can be calculated by considering the area of the simulation box parallel to the bilayer and dividing it by half the total number of lipids in the bilayer. It is however important to note that, if the bilayer undergoes large fluctuations and undulations, the value of the area per lipid computed in this way is underestimated (see e.g. [77]).

Bilayer thickness. The lipid bilayer thickness can be estimated from X-ray diffraction measurements, i.e. from the distance between the diffraction peaks referring to the lipid headgroups in the two opposite leaflets of the bilayer. In molecular simulation, the thickness can be computed as the distance between the peaks in the density profile. Alternatively, it can be directly calculated using the positions of the particles by considering the average distance along the bilayer normal between the interfacial part of the molecules in one monolayer and those in the opposite monolayer. Another useful quantity is the lipid end-to-end distance, L_{ee}, defined as the average length of the hydrophobic part of the lipid molecules in the bilayer. In a noninterdigitated bilayer, the hydrophobic thickness of the bilayer D_c, and the end-to-end distance projected onto the bilayer normal, L^n_{ee}, are related by $D_c = 2L^n_{ee}$. However, if the two monolayers are interdigitated, the above relation does not hold [283]. For example, for partially interdigitated bilayers one has $D_c < 2L^n_{ee}$, and for fully interdigitated bilayers $D_c = L^n_{ee}$. To measure the extent of interpenetration of the hydrophobic cores of the lipids on opposite sides of the bilayer, one can calculate the tail overlap, which is defined as $D_{overlap} = (2L^n_{ee} - D_c)/L^n_{ee}$.

A.2.1. Pressure profile

As it is clear from the density profiles (see Fig. A.2), a lipid bilayer is not homogeneous across its thickness, but diplays density variations in going from the bilayer-water interface to the bilayer center. Moreover, different chemical groups are found at different depths in the bilayer. This results in a non-uniform distribution of the lateral pressure across the bilayer, which may have important effects on the biological function of membranes and membrane proteins [284]. For example, the presence in the bilayer of nonbilayer lipids, i.e. lipids which preferentially do not aggregate into a bilayer phase [64], may modulate the distribution of pressure across a bilayer and indirectly affect the function of membrane proteins [284]. Also small molecules, like alcohols or anesthetics, may regulate the activity of transmembrane proteins through a lipid mediated and purely mechanical interaction, via an anesthetic-induced redistribution of the lateral pressure across the bilayer—as proposed by Cantor [174,285–287]. Although the mechanism of action of anesthetics is not yet fully understood [288], experimental findings [175,289] seem to confirm the importance of the lateral pressure in regulating the activity of mechanosensitive transmembrane proteins.

Lindhal and Edholm [290] were the first to calculate the distribution of lateral pressure in a lipid bilayer by atomistic MD simulations. Few years later, Gullingsrud and Schulten [291] performed a systematic MD atomistic study of the

influence of lipid structure on the distribution of lateral pressure, relating it to the gating mechanism of mechanosensitive protein-channels. Also using atomistic MD simulations, Patra [292] studied the effect of cholesterol concentration on the redistribution of lateral pressure in DPPC bilayers. However, atomistic simulations of lateral pressure distribution in lipid bilayers are still relatively few. This might be due to the fact that the local pressure has large fluctuations, and long runs are required to obtain sufficient statistics. The use of coarse-grained models could represent a valid and efficient alternative to the atomistic approach. In fact, studies of pressure profiles in coarse-grained bilayers were done by a number of authors [74,88–90].

Although we will not go into the details of the applications, here we want to provide the reader with a definition of local pressure and its method of calculation.

In homogeneous systems at equilibrium the pressure is constant and equal in each point in space, while for an inhomogeneous system the pressure is a tensor $\mathbf{P}(\mathbf{r})$ that depends on the spatial direction and on the position $\mathbf{r}$ where it is calculated [272,293]. Let us consider a system of two immiscible fluids (e.g. oil/water or vapor/liquid) forming a planar interface normal to the z direction. At equilibrium, mechanical stability requires that the gradient of the pressure tensor is zero everywhere

$$\nabla \cdot \mathbf{P} = \mathbf{0}. \tag{A.15}$$

Shear forces are also zero, and the nondiagonal components of $\mathbf{P}$ vanish; also, because of planar symmetry, the components of the pressure tensor parallel to the interface should be identical. The pressure tensor is then diagonal

$$\mathbf{P}(\mathbf{r}) = \begin{pmatrix} P_{xx}(\mathbf{r}) & 0 & 0 \\ 0 & P_{yy}(\mathbf{r}) & 0 \\ 0 & 0 & P_{zz}(\mathbf{r}) \end{pmatrix}, \tag{A.16}$$

with

$$P_{xx}(\mathbf{r}) = P_{yy}(\mathbf{r}). \tag{A.17}$$

From Eqs. (A.15) and (A.16) we have

$$\frac{\partial P_{xx}}{\partial x}\mathbf{e}_x + \frac{\partial P_{yy}}{\partial y}\mathbf{e}_y + \frac{\partial P_{zz}}{\partial z}\mathbf{e}_z = \mathbf{0}, \tag{A.18}$$

where $\mathbf{e}_\alpha$ ($\alpha = x, y, z$) are the orthogonal basis vectors in the Cartesian space. From Eqs. (A.17) and (A.18) it results that the lateral component of the pressure tensor is a function of z only: $P_L(z) = P_{xx}(z) = P_{yy}(z)$. The normal component is constant throughout the system, and equal to the external pressure: $P_N(z) = P_{zz}(z) = P_{ext}$. The lateral components are also equal to the external pressure in the bulk phases (i.e. far from the interface).

The surface tension is defined as the integral of the difference between the normal and the lateral component of the pressure tensor [294,295]

$$\gamma = \int_{z_1}^{z_2} \mathrm{d}z\,[P_N(z) - P_L(z)] = \int_{z_1}^{z_2} \mathrm{d}\gamma(z), \tag{A.19}$$

where z_1 and z_2 are positions in the bulk phases. The next step is to express this thermodynamic quantity in terms of those microscopic degrees of freedom that can be obtained via molecular simulation. Statistical mechanics provides the necessary tools, as discussed below.

For a homogeneous system, the pressure is a scalar and it can be expressed by the virial equation [296,297]

$$P = \rho k_B T + \frac{1}{3V}\left\langle \sum_{i=1}^{N} \mathbf{r}_i \cdot \mathbf{f}_i \right\rangle, \tag{A.20}$$

where the first term in the right hand side of the above expression is the ideal gas contribution. $\mathbf{f}_i$ is the total internal force on particle i, and the brackets indicate an ensemble average. If the intermolecular forces are pairwise additive,

the above may be written as

$$P = \rho k_B T + \frac{1}{3V}\left\langle \sum_i \sum_{j>i} \mathbf{r}_{ij} \cdot \mathbf{F}_{ij} \right\rangle, \tag{A.21}$$

where $\mathbf{F}_{ij}$ is the force between particles i and j.

For an inhomogeneous system the pressure tensor at position $\mathbf{r}$ can still be expressed in a tensorial form of the virial equation and it can be split in a kinetic $\mathbf{P}^K$ and a potential part $\mathbf{P}^U$ [293],

$$\mathbf{P}(\mathbf{r}) = \mathbf{P}^K(\mathbf{r}) + \mathbf{P}^U(\mathbf{r}). \tag{A.22}$$

The kinetic part can be expressed as a generalization of the ideal gas contribution

$$\mathbf{P}^K(\mathbf{r}) = k_B T\, \rho(\mathbf{r})\hat{\mathbf{1}}, \tag{A.23}$$

where $\rho(\mathbf{r})$ is the density at position $\mathbf{r}$ and $\hat{\mathbf{1}}$ is the 3×3 unit matrix. This kinetic part reflects a single particle property and therefore it is well localized in space. Conversely, there is no unambiguous way of expressing the potential part of the pressure tensor. $\mathbf{P}^U(\mathbf{r})$ is defined as the force acting across a microscopic element of area located at $\mathbf{r}$, but, because the force depends on the position of two particles (for pair additive potentials), there is no unique way to determine which pairs of particles should contribute to the pressure across the microscopic element of area at $\mathbf{r}$, and to reduce the nonlocal two-particle force to a local force at $\mathbf{r}$ [298].

Different methods have been proposed to compute the potential part of the pressure tensor, among others the Irving and Kirkwood method [299] and the Harashima method [300]. Irving and Kirkwood [299] required that, in any definition of the pressure tensor, the local virial should be located near the line connecting the two interacting particles. The various definitions correspond to different choices of the contour which connects the position in which the microscopic pressure tensor is calculated with the position of the particles. For a detailed description of the different methods see [293]. It is important to note that, while the local pressure depends on the calculation method, all methods give the same result for the total pressure (and surface tension) when integrating the local values over the whole system.

We now proceed adopting the Kirkwood–Buff convention [294,301], which takes as contour a straight line. In molecular simulation the system is divided into N_s slabs parallel to the interface. The contribution of each pair of interacting particles to the local pressure tensor is evenly split through all the slabs which intersect the line that connects the two particles (line of centers). The normal and lateral components of the local pressure tensor in slab k, including the kinetic contribution, are then given by

$$P_L(k) = k_B T \langle \rho(k) \rangle - \frac{1}{2V_s}\left\langle \sum_{(i,j)}^{(k)} \frac{x_{ij}^2 + y_{ij}^2}{r_{ij}}\, u'(r_{ij}) \right\rangle, \tag{A.24}$$

$$P_N(k) = k_B T \langle \rho(k) \rangle - \frac{1}{V_s}\left\langle \sum_{(i,j)}^{(k)} \frac{z_{ij}^2}{r_{ij}}\, u'(r_{ij}) \right\rangle, \tag{A.25}$$

where $\rho(k)$ is the average density in slab k, V_s is the volume of a slab, $u'(r)$ is the derivative of the intramolecular potential with respect to r, and the brackets denote an ensemble average. $\sum_{(i,j)}^{(k)}$ means that the summation runs over all pairs of particles (i, j) of which the slab k (partially) contains the line of centers. If a slab k intersects the line of centers between particles i and j, it gets a contribution $1/N_o$ from the pair (i, j), where N_o is the total number of slabs that intersect the line of centers between particle i and j. Periodic boundary conditions are always taken into account in this calculation. The integral in Eq. (A.19) now becomes

$$\gamma = \int_{z_1}^{z_2} [P_N(z) - P_L(z)]\, \mathrm{d}z, \tag{A.26}$$

where Δz_s is the (uniform) width of the slabs.

To better describe and understand the distribution of lateral pressure in lipid bilayers, in Fig. A.3 we show a schematic drawing of a lipid bilayer, and indicate the direction and relative magnitude of the lateral pressure. We also show the lateral pressure profile from a coarse-grained DPD simulation of a DMPC bilayer [233]. Because of the unfavorable

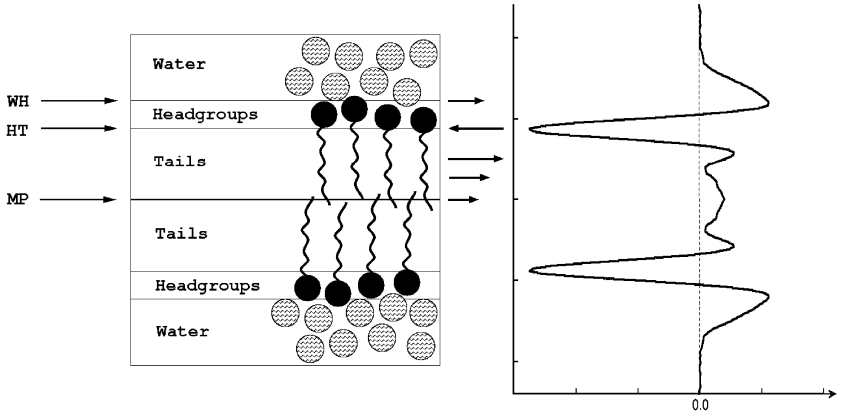

Fig. A.3. Schematic representation of a lipid bilayer. The arrows represent the direction, and relative magnitude, of the lateral pressure. On the right is shown the lateral pressure profile in a coarse-grain DMPC bilayer studied using DPD [233].

interactions at the interface between water and the hydrophobic part of the lipids, a negative (pointing inwards) pressure is exerted, to decrease the area of the interface, hence the area per lipid. On the other hand, steric constraints and entropic disorder in the hydrophobic core of the bilayer exert an outward positive pressure, which tends to expand the bilayer area. The area per lipid is then resulting from the balance between these two opposing forces.

A.2.2. Elastic properties

As discussed in Section 2, the parameters related to the elastic properties of lipid bilayers have been used as input to continuum models of membranes. On the other hand, the elastic properties of lipid bilayers can be derived as a result from simulations on systems which are particle-based, both atomistic and coarse-grained. In this way it is for example possible to study the dependence of mechanical and elastic properties of a membrane on its composition and on the structure of its molecular constituents. However, properties such as membrane thermal undulations are observable only for sufficiently large membrane patches. Long simulation times are also needed, to fully sample the undulation modes, which make atomistic approaches expensive [302,303]. The coarse-grained approach is thus a good alternative, since it allows to bridge length scales ranging from those related to the local motion of molecules, to those of collective membrane undulations in the continuum approximation.

In continuum theories, the Helfrich Hamiltonian of an interface is expressed in terms of the curvature [30,31]

$$\mathscr{H} = \int_S \mathrm{d}A \left[\gamma + \frac{\kappa}{2}(c_1 + c_2 - 2c_0)^2 + \kappa_\mathrm{G} c_1 c_2\right], \tag{A.27}$$

where c_1 and c_2 are the principal curvatures, c_0 is the spontaneous curvature, γ is the surface tension, and κ and κ_G are the bending modulus and the saddle-splay (Gaussian) modulus, respectively.

For membranes which can be described as a continuum interface, the Monge gauge can be used. According to this, the position of the interface is described by its local displacement $h(x, y)$ from the average interface position, so that $h(x, y) = 0$ in the bilayer center. Then, for small curvatures, $c_1 + c_2 = \nabla^2 h$ and $\mathrm{d}A = \mathrm{d}x\,\mathrm{d}y\sqrt{1 + (\nabla h)^2}$. Assuming that the spontaneous curvature c_0 is zero, which is true for self-assembled bilayers, and using the fact that the surface integral over $c_1 c_2$ is zero for a thin film, then Eq. (A.27) can be rewritten as

$$\mathscr{H} = \int \mathrm{d}x\,\mathrm{d}y \left[\frac{\gamma}{2}(\nabla h(x, y))^2 + \frac{\kappa}{2}(\nabla^2 h(x, y))^2\right]. \tag{A.28}$$

Going to Fourier space using $h(\mathbf{r}) = \int \mathrm{d}q\, \tilde{h}(q) \mathrm{e}^{\mathrm{i}\mathbf{q}\cdot\mathbf{r}}$, and considering the energy $\mathscr{E}(q)$ associated to each mode q, expression (A.28) simplifies as

$$\mathscr{E}(q) = \frac{\gamma}{2} q^2 \tilde{h}(q)^2 + \frac{\kappa}{2} q^4 \tilde{h}(q)^2. \tag{A.29}$$

Using the equipartition theorem

$$\langle \mathscr{E}(\tilde{h}(q))\rangle = \frac{1}{A}\frac{k_B T}{2}, \tag{A.30}$$

we have

$$\langle |\tilde{h}(q)^2|\rangle = \frac{k_B T}{A(\kappa q^4 + \gamma q^2)}. \tag{A.31}$$

$\tilde{h}(q)$ can be determined from simulations by Fourier transforming $h(n_x, n_y)$, which is the bilayer height function calculated on a grid. The bending rigidity κ of a bilayer can then be calculated from the fit of Eq. (A.31) for small wave vectors. A characteristic wave vector $q_c = \sqrt{\gamma/\kappa}$ separates the tension regime ($\sim q^{-2}$) from the bending regime ($\sim q^{-4}$). Note that for tensionless bilayers, the term in q^{-2} vanishes.

For length scales comparable to the bilayer thickness, the continuum theory breaks down. At these length scales, molecular protrusions characterize the interface modes. These modes can be described by a protrusion tension σ_{pr}, which is similar in nature to surface tension [304]

$$\langle |\tilde{h}(q)^2|\rangle = \frac{k_B T}{A(\sigma_{pr} q^2)}. \tag{A.32}$$

The area compressibility of a bilayer K_A can be calculated from the dependence of the surface tension γ on the bilayer area A using [302]

$$K_A = A\left(\frac{\partial \gamma}{\partial A}\right). \tag{A.33}$$

Integrating the above equation one obtains

$$\gamma = K_A \ln \frac{A}{A_0}. \tag{A.34}$$

By expanding around the equilibrium area at zero surface tension, A_0, we have

$$\gamma \approx K_A \frac{A - A_0}{A_0}. \tag{A.35}$$

In simulation, the area compressibility can be calculated from the above equation, either by fixing the area of the bilayer and computing the corresponding surface tension (provided the latter has small deviations from the tensionless state), or by considering the spontaneous fluctuations around the equilibrium area of a tensionless bilayer.

References

[1] R.B. Gennis, Biomembranes, Molecular Structure and Function, Springer, New York, 1989.
[2] E.M.D. Gorter, F. Grendel, J. Exper. Med. 41 (1925) 439–443.
[3] J.F. Danielli, H. Davson, J. Cell. Comput. Physiol. 7 (1935) 393–408.
[4] S.J. Singer, G.L. Nicolson, Science 175 (1972) 720–731.
[5] J.N. Israelachvili, Biochim. Biophys. Acta 469 (1977) 221–225.
[6] E. Sackmann, in: R. Lipowsky, E. Sackmann (Eds.), Structure and Dynamics of Membranes, Elsevier, Amsterdam, 1995, pp. 1–65.
[7] S. König, E. Sackmann, Curr. Opin. Colloid Interface Sci. 1 (1996) 78–82.
[8] K.M. Merz Jr., B. Roux, Biological Membranes: A Molecular Perspective from Computation and Experiment, Birkhäuser, Berlin, 1996.
[9] M.M. Sperotto, S. May, A. Baumgärtner, J. Chem. Phys. Lipids 141 (2006) 2–29.
[10] P.R. Cullis, B. de Kruijff, Biochim. Biophys. Acta 559 (1979) 399–420.
[11] J.N. Israelachvili, S. Marcelja, R.G. Horn, Quart. Rev. Biophys. 13 (1980) 121–200.
[12] J.N. Israelachvili, Intermolecular & Surface Forces, Academic Press, San Diego, CA, 1997.
[13] K.V. Damodaran, K.M. Merz Jr., in: K. Lipkowitz, D. Boyd (Eds.), Reviews in Computational Chemistry, VCH Publishers Inc., New York, 1994, pp. 269–298.
[14] C. Tanford, Hydrophobic Effect: Formation of Micelles and Biological Membranes, Wiley, New York, 1980.
[15] J.N. Israelachvili, H. Wennerström, Nature 379 (1996) 219–225.
[16] L. Stryer, Biochemistry, W.H. Freeman and Company, New York, 1995.

[17] B. Alberts, A. Johnson, J. Lewis, M. Raff, K. Roberts, P. Walter, Molecular Biology of the Cell, Garland Science, New York, 2002.
[18] E. Boom, E. Evans, O.G. Mouritsen, Quart. Rev. Biophys. 24 (2001) 293–397.
[19] O.G. Mouritsen, M.M. Sperotto, J. Risbo, Z.Z. Zhang, M.J. Zuckermann, Adv. Comput. Biol. 2 (1996) 15–64.
[20] T. Gil, J.H. Ipsen, O.G. Mouritsen, M.C. Sabra, M.M. Sperotto, M.J. Zuckermann, Biochim. Biophys. Acta 1376 (1998) 245–266.
[21] T. Gil, J.H. Ipsen, Phys. Rev. E 55 (1997) 1713–1721.
[22] S. May, Curr. Opin. Colloid Interface Sci. 5 (2000) 244–249.
[23] D.R. Fattal, A. Ben-Shaul, Biophys. J. 65 (1993) 1795–1809.
[24] C. Nielsen, M. Goulian, O.S. Andersen, Biophys. J. 74 (1998) 1966–1983.
[25] D.P. Tieleman, S.J. Marrink, H.J.C. Berendsen, Biochim. Biophys. Acta 1331 (1997) 235–270.
[26] L. Saiz, M.L. Klein, Acc. Chem. Res. 35 (2002) 482–489.
[27] H.L. Scott, Curr. Opin. Struct. Biol. 12 (4) (2002) 495–502.
[28] G. Brannigan, L.C.L. Lin, F.L.H. Brown, Eur. Biophys. J. Biophys. Lett. 35 (2) (2006) 104–124.
[29] D.R. Nelson, T. Piran, S. Weinberg, Statistical Mechanics of Membranes and Surfaces, second ed., World Scientific, Singapore, 2004.
[30] W. Helfrich, Z. Naturf. 28c (1973) 693.
[31] S.A. Safran, Statistical Thermodynamics of Surfaces, Interfaces and Membranes, Westview Press, Boulder, 1994.
[32] T. Sintes, A. Baumgärtner, Biophys. J. 73 (5) (1997) 2251–2259.
[33] T. Sintes, A. Baumgärtner, Physica A 249 (1998) 571–575.
[34] T. Sintes, A. Baumgärtner, J. Phys. Chem. B 102 (36) (1998) 7050–7057.
[35] O. Lenz, F. Schmid, J. Mol. Liq. 117 (1–3) (2005) 147–152.
[36] G. Ayton, G.A. Voth, Biophys. J. 83 (6) (2002) 3357–3370.
[37] G. Ayton, A.M. Smondyrev, S.G. Bardenhagen, P. McMurtry, G.A. Voth, Biophys. J. 82 (2002) 1226–1238.
[38] J.-M. Drouffe, A.C. Maggs, S. Leibler, Science 254 (1991) 1353–1354.
[39] H. Noguchi, M. Takasu, Phys. Rev. E 6404 (4) (2001).
[40] I.R. Cooke, M. Deserno, J. Chem. Phys. 123 (22) (2005) Art. No. 224710.
[41] S.J. Marrink, E. Lindahl, O. Edholm, A.E. Mark, J. Am. Chem. Soc. 123 (2001) 8638–8639.
[42] A.H. de Vries, A.E. Mark, S.J. Marrink, J. Am. Chem. Soc. 126 (14) (2004) 4488–4489.
[43] R. Goetz, G. Gompper, R. Lipowsky, Phys. Rev. Lett. 82 (1999) 221–224.
[44] H. Noguchi, M. Takasu, J. Chem. Phys. 115 (20) (2001) 9547–9551.
[45] H. Noguchi, M. Takasu, Phys. Rev. E 65 (5) (2002).
[46] H. Noguchi, M. Takasu, Biophys. J. 83 (1) (2002) 299–308.
[47] L. Chernomordik, M. Kozlov, J. Zimmerberg, J. Memb. Biol. 146 (1995) 1–14.
[48] G. Brannigan, P.F. Philips, F.L.H. Brown, Phys. Rev. E 72 (2005) 011915.
[49] I.R. Cooke, K. Kremer, M. Deserno, Phys. Rev. E 72 (1) (2005) Art. No. 011506.
[50] Z.J. Wang, D. Frenkel, J. Chem. Phys. 122 (23) (2005) Art. No. 234711.
[51] Z.J. Wang, D. Frenkel, J. Chem. Phys. 123 (15) (2005) Art. No. 154701.
[52] E. Evans, V. Heinrich, F. Ludwig, W. Rawicz, Biophys. J. 85 (2003) 2342–2350.
[53] P.D. Tieleman, H. Leontiadou, A. Mark, S.J. Marrink, J. Am. Chem. Soc. 125 (2003) 6382–6383.
[54] O. Farago, J. Chem. Phys. 119 (1) (2003) 596–605.
[55] G. Brannigan, F.L.H. Brown, J. Chem. Phys. 120 (2) (2004) 1059–1071.
[56] G. Brannigan, F.L.H. Brown, J. Chem. Phys. 122 (7) (2005).
[57] O. Farago, J. Chem. Phys. 120 (6) (2004) 29340–29350.
[58] R. Lipowsky, E. Sackmann, Structure and Dynamics of Membranes, Elsevier, Amsterdam, 1995.
[59] J.D. Litster, Phys. Lett. A 53 (1975) 193–194.
[60] K. Matsuzaki, Biochem. Soc. Trans. 29 (2001) 598–601.
[61] O. Farago, N. Gronbech-Jensen, P. Pincus, Phys. Rev. Lett. 96 (1) (2006).
[62] C.R. Safinya, Curr. Opin. Struct. Biol. 11 (2001) 440–448.
[63] I.R. Cooke, M. Deserno, Biophys. J. 91 (2006) 487–495.
[64] B. de Kruijff, Nature 386 (1997) 129–130.
[65] A.P. Lyubartsev, A. Laaksonen, Phys. Rev. E 52 (1995) 3730–3737.
[66] A.K. Soper, Chem. Phys. 202 (1996) 295–306.
[67] A.P. Lyubartsev, A. Laaksonen, Lect. Notes Phys. 640 (2004) 219–244.
[68] A.P. Lyubartsev, Eur. Biophys. J. 35 (2005) 53–61.
[69] B. Smit, P.A.J. Hilbers, K. Esselink, L.A.M. Rupert, N.M. van Os, A.G. Schlijper, Nature 348 (1990) 624–625.
[70] B. Smit, A.G. Schlijper, L.A.M. Rupert, N.M. van Os, J. Phys. Chem. 94 (1990) 6933–6935.
[71] S. Karaborni, K. Esselink, P.A.J. Hilbers, B. Smit, J. Karthäuser, N.M. van Os, R. Zana, Science 266 (1994) 254–256.
[72] L. Rekvig, M. Kranenburg, B. Hafskjold, B. Smit, Europhys. Lett. 63 (6) (2003) 902–907.
[73] L. Rekvig, B. Hafskjold, B. Smit, Phys. Rev. Lett. 92 (11) (2004) Art. No. 116101.
[74] R. Goetz, R. Lipowsky, J. Chem. Phys. 108 (17) (1998) 7397–7409.
[75] W.K. den Otter, W. Briels, J. Chem. Phys. 118 (10) (2003) 4712–4720.
[76] W.K. den Otter, J. Chem. Phys. 123 (21) (2005).
[77] A. Imparato, J.C. Shillcock, R. Lipowsky, Europhys. Lett. 69 (4) (2005) 650–656.
[78] M.J. Stevens, J.H. Hoh, T.B. Woolf, Phys. Rev. Lett. 91 (2003) Art. No. 188102.

[79] M.J. Stevens, J. Chem. Phys. 121 (2004) 11942–11948.
[80] M.J. Stevens, J. Am. Chem. Soc. 127 (2005) 15330–15331.
[81] J. Zhang, B. Jing, N. Tokutake, S.L. Regen, J. Am. Chem. Soc. 126 (2004) 10856–10857.
[82] C. Loison, M. Mareschal, K. Kremer, F. Schmid, J. Chem. Phys. 119 (24) (2003) 13138–13148.
[83] C. Loison, M. Mareschal, F. Schmid, J. Chem. Phys. 121 (4) (2004) 1890–1900.
[84] C. Loison, M. Mareschal, F. Schmid, Comput. Phys. Commun. 169 (1–3) (2005) 99–103.
[85] K. Kremer, G. Grest, I. Carmesin, Phys. Rev. Lett. 61 (1988) 566–569.
[86] T. Soddemann, B. Dunweg, K. Kremer, Europ. Phys. J. E 6 (2001) 409–419.
[87] H. Guo, K. Kremer, T. Soddemann, Phys. Rev. E 66 (2002) Art. No. 061503.
[88] M. Venturoli, B. Smit, Phys. Chem. Commun. 2 (1999) Art. No. 10.
[89] R.D. Groot, K.L. Rabone, Biophys. J. 81 (2001) 725–736.
[90] J.C. Shillcock, R. Lipowsky, J. Chem. Phys. 117 (2002) 5048–5061.
[91] S. Yamamoto, Y. Maruyama, S. Hyodo, J. Chem. Phys. 116 (2002) 5842–5849.
[92] M. Laradji, P.B. Sunil Kumar, Phys. Rev. Lett. 93 (19) (2004) Art. No. 198105.
[93] G. Illya, R. Lipowsky, J.C. Shillcock, J. Chem. Phys. 122 (24) (2005) Art. No. 244901.
[94] M. Kranenburg, J.-P. Nicolas, B. Smit, Phys. Chem. Chem. Phys. 6 (16) (2004) 4142–4151.
[95] R.D. Groot, P.B. Warren, J. Chem. Phys. 107 (1997) 4423–4435.
[96] C.M. Wijmans, B. Smit, R.D. Groot, J. Chem. Phys 114 (2001) 7644–7654.
[97] M. Kranenburg, M. Venturoli, B. Smit, Phys. Rev. E 67 (2003) Art. No. 060901.
[98] M. Kranenburg, M. Venturoli, B. Smit, J. Phys. Chem. B 107 (41) (2003) 11491–11501.
[99] M. Kranenburg, M. Vlaar, B. Smit, Biophys. J. 87 (2004) 1596–1605.
[100] M. Kranenburg, C. Laforge, B. Smit, Phys. Chem. Chem. Phys. 6 (2004) 4531–4534.
[101] M. Kranenburg, B. Smit, J. Phys. Chem. B 109 (2005) 6553–6563.
[102] H.I. Petrache, S.W. Dodd, M.F. Brown, Biophys. J. 79 (2000) 3172–3192.
[103] L.J. Lis, M. McAlister, N. Fuller, R.P. Rand, V.A. Parsegian, Biophys. J. 37 (1982) 657–666.
[104] B.A. Lewis, D.M. Engelman, J. Mol. Biol. 166 (1983) 211–217.
[105] R.P. Rand, V.A. Parsegian, Biochim. Biophys. Acta 988 (1989) 351–376.
[106] H.I. Petrache, S. Tristram-Nagle, J.F. Nagle, Chem. Phys. Lipids 95 (1998) 83–94.
[107] J.F. Nagle, M.C. Wiener, Biochim. Biophys. Acta 942 (1988) 1–10.
[108] M. Laradji, P.B. Sunil Kumar, J. Chem. Phys. 123 (22) (2005) Art. No. 224902.
[109] M. Venturoli, B. Smit, M.M. Sperotto, Biophys. J. 88 (2005) 1778–1798.
[110] S. Yamamoto, S. Hyodo, J. Chem. Phys. 118 (7) (2003) 7937–7943.
[111] S.J. Marrink, A.H. de Vries, A.E. Mark, J. Phys. Chem. B 108 (2) (2004) 750–760.
[112] S.J. Marrink, J. Risselada, A.E. Mark, Chem. Phys. Lipids 135 (2) (2005) 223–244.
[113] S.J. Marrink, A.E. Mark, J. Am. Chem. Soc. 125 (49) (2003) 15233–15242.
[114] S.J. Marrink, A.E. Mark, Biophys. J. 87 (6) (2004) 3894–3900.
[115] L. Yang, L. Ding, H.W. Huang, Biochemistry 42 (2003) 6631–6635.
[116] J.C. Shelley, M.Y. Shelley, R.C. Reeder, S. Bandyopadhyay, M.L. Klein, J. Phys. Chem. B 105 (2001) 4464–4470.
[117] J.C. Shelley, M.Y. Shelley, R.C. Reeder, S. Bandyopadhyay, P.B. Moore, M.L. Klein, J. Phys. Chem. B 105 (2001) 9785–9792.
[118] S.O. Nielsen, C.F. Lopez, G. Srinivas, M.L. Klein, J. Phys.: Condens. Matter 16 (15) (2004) R481–R512.
[119] C.F. Lopez, P.B. Moore, J.C. Shelley, M.Y. Shelley, M.L. Klein, Comput. Phys. Commun. 147 (2002) 1–6.
[120] C.F. Lopez, S.O. Nielsen, P.B. Moore, J.C. Shelley, M.L. Klein, J. Phys.: Condens. Matter 14 (2002) 9431–9444.
[121] L. Koubi, M. Tarek, M.L. Klein, D. Scharf, Biophys. J. 78 (2000) 800–811.
[122] M. Pickholz, L. Saiz, M.L. Klein, Biophys. J. 88 (3) (2005) 1524–1534.
[123] S.O. Nielsen, B. Ensing, V. Ortiz, P.B. Moore, M.L. Klein, Biophys. J. 88 (6) (2005) 3822–3828.
[124] S. Izvekov, G.A. Voth, J. Phys. Chem. B 109 (2005) 2469–2473.
[125] S. Izvekov, M. Parrinello, C.J. Burnham, G.A. Voth, J. Chem. Phys. 120 (2004) 10896–10913.
[126] G. Ayton, S.G. Bardenhagen, P. McMurtry, D. Sulsky, G.A. Voth, J. Chem. Phys. 114 (5) (2001) 6913–6924.
[127] G.S. Ayton, G.A. Voth, Biophys. J. 87 (5) (2004) 3299–3311.
[128] G.S. Ayton, H.L. Tepper, D.T. Mirijanian, G.A. Voth, J. Chem. Phys. 120 (9) (2004) 4074–4088.
[129] R. Chang, G.S. Ayton, G.A. Voth, J. Chem. Phys. 122 (24) (2005).
[130] G.S. Ayton, J.L. McWhirter, G.A. Voth, J. Chem. Phys. 124 (6) (2006).
[131] G. Ayton, A.M. Smondyrev, S.G. Bardenhagen, P. McMurtry, G.A. Voth, Biophys. J. 83 (2) (2002) 1026–1038.
[132] R. Koynova, M. Caffrey, Biochim. Biophys. Acta 1376 (1998) 91–145.
[133] J. Stümpel, H. Eibl, A. Niksch, Biochim. Biophys. Acta 727 (1983) 246–254.
[134] Y. Misquitta, M. Caffrey, Biophys. J. 81 (2) (2001) 1047–1058.
[135] S.A. Simon, T.J. McIntosh, Biochim. Biophys. Acta 773 (1984) 169–172.
[136] B.A. Cunningham, A.-D. Brown, D.H. Wolfe, W.P. Williams, A. Brain, Phys. Rev. E 58 (1998) 3662–3672.
[137] B. Tenchov, R. Koynova, G. Rapp, Biophys. J. 80 (2001) 1873–1890.
[138] R. Faller, S.J. Marrink, Langmuir 20 (18) (2004) 7686–7693.
[139] S. Tristram-Nagle, Y. Liu, J. Legleiter, J.F. Nagle, Biophys. J. 83 (2002) 3324–3335.
[140] J.G. Petrov, E.E. Polymeropoulos, H. Möhwald, Langmuir 16 (2000) 6411–7420.

[141] T. Heimburg, Biophys. J. 78 (2000) 1154–1165.
[142] K. Jørgensen, Biochim. Biophys. Acta 1240 (1995) 111–114.
[143] A. Tardieu, V. Luzzatti, F.C. Reman, J. Mol. Biol. 75 (1973) 711–733.
[144] C.M. Chen, T.C. Lubensky, F.C. Mackintosh, Phys. Rev. E 51 (1995) 504–513.
[145] T.C. Lubensky, F.C. MacKintosh, Phys. Rev. Lett. 71 (1993) 1565–1568.
[146] K. Sengupta, V.A. Raghunathan, Y. Hatwalne, Phys. Rev. Lett. 87 (2001) Art. No. 055705.
[147] W.J. Sun, S. TristramNagle, R.M. Suter, J.F. Nagle, Proc. Natl. Acad. Sci. USA 93 (14) (1996) 7008–7012.
[148] M.S. Falkovits, M. Seul, H.L. Frisch, H.M. McConnell, Proc. Natl. Acad. Sci. USA 79 (1982) 3918–3921.
[149] M. Marder, H.L. Frisch, J.S. Langer, H.M. McConnell, Proc. Natl. Acad. Sci. USA 81 (1984) 6559–6561.
[150] P.C. Mason, J.F. Nagle, R.M. Epand, J. Katsaras, Phys. Rev. E 63 (2001) Art. No. 030902(R).
[151] J.F. Nagle, H.I. Petrache, N. Gouliaev, S. Tristram-Nagle, Y. Liu, R.M. Suter, K. Gawrisch, Phys. Rev. E 58 (1998) 7769–7776.
[152] J.F. Nagle, S. Tristram-Nagle, Biochim. Biophys. Acta-Rev. Biomembr. 1469 (3) (2000) 159–195.
[153] M. Rappolt, G. Pabst, G. Rapp, M. Kriechbaum, H. Amenitsch, C. Krenn, S. Bernstorff, P. Laggner, Eur. Biophys. J. 29 (2000) 125–133.
[154] B.A. Canningham, A.-D. Brown, D.H. Wolfe, D.P. Williams, A. Brain, Phys. Rev. E 58 (1998) 3662–3672.
[155] A.H. de Vries, S. Yefimov, A.E. Mark, S.J. Marrink, Proc. Natl. Acad. Sci. USA 102 (15) (2005) 5392–5396.
[156] J.L. Slater, C.H. Huang, Prog. Lipid. Res. 27 (1988) 325–359.
[157] S. Furuike, V.G. Levadny, S.J. Li, M. Yamazaki, Biophys. J. 77 (1999) 2015–2023.
[158] T.J. McIntosh, R.V. McDaniel, S.A. Simon, Biochim. Biophys. Acta 731 (1983) 109–114.
[159] T.J. McIntosh, H. Lin, S. Li, C.-H. Huang, Biochim. Biophys. Acta 1510 (2001) 219–230.
[160] T. Adachi, H. Takahashi, K. Ohki, I. Hatta, Biophys. J. 68 (1995) 1850–1855.
[161] T. Hata, S. Kaneshina, Biophys. Chem. 87 (2000) 25–36.
[162] R.N.A.H. Lewis, I. Winter, M. Kriechbaum, K. Lohner, R.N. McElhaney, Biophys. J. 80 (2001) 1329–3142.
[163] I. Winter, G. Pabst, M. Rappolt, K. Lohner, Chem. Phys. Lip. 112 (2001) 137–150.
[164] P. Nambi, E.S. Rowe, T.J. McIntosh, Biochemistry 27 (1988) 9175–9182.
[165] K. Ohki, K. Tamura, I. Hatta, Biochim. Biophys. Acta 1028 (1990) 215–222.
[166] U. Vierl, L. Löbbecke, N. Nagel, G. Cevc, Biophys. J. 67 (1994) 1067–1079.
[167] L. Löbbecke, G. Cevc, Biochim. Biophys. Acta 1237 (1995) 59–69.
[168] E.S. Rowe, Biochemistry 22 (1983) 3299–3305.
[169] S.E. Feller, C.A. Brown, D.T. Nizza, K. Gawrisch, Biophys. J. 82 (2002) 1396–1404.
[170] E.S. Rowe, J.M. Campion, Biophys. J. 67 (1994) 1888–1895.
[171] M. Kranenburg, B. Smit, FEBS Lett. 568 (1–3) (2004) 15–18.
[172] N.E. Nagel, G. Cevc, S. Kirchner, Biochim. Biophys. Acta 1111 (1992) 263–269.
[173] J. Mou, J. Yang, C. Huang, Z. Shao, Biochemistry 33 (1994) 9981–9985.
[174] R.S. Cantor, Biochemistry 36 (1997) 2339–2344.
[175] E. van den Brink-van der Laan, V. Chupin, J.A. Killian, B. de Kruijff, Biochemistry 43 (2004) 5937–5942.
[176] L. Koubi, M. Tarek, S. Bandyopadhyay, M.L. Klein, D. Scharf, Biophys. J. 81 (2001) 3339–3345.
[177] J.H. Ipsen, G. Karlström, O.G. Mouritsen, H. Wennerström, M.J. Zuckermann, Biochim. Biophys. Acta 905 (1987) 162–172.
[178] J. Fantini, R. Mahfoud, N. Yahi, In Expert reviews in Molecular Medicine, Cambridge University Press, Cambridge, 2002 pp. 1–22.
[179] S. Izvekov, G.A. Voth, J. Chem. Theory. Comput. 2 (2006) 637–648.
[180] A.G. Lee, Biochim. Biophys. Acta 1612 (2003) 1–40.
[181] J.A. Killian, Biochim. Biophys. Acta 1376 (1998) 401–416.
[182] J.A. Killian, T.K.M. Nyholm, Curr. Opin. Struct. Biology 16 (2006) 473–479.
[183] C. Montecucco, G.A. Smith, F. Dabbeni-Sala, A. Johansson, Y.M. Galante, R. Bisson, FEBS Lett. 144 (1982) 145–148.
[184] A. Johansson, G.A. Smith, J. Metcalfe, Biochim. Biophys. Acta 641 (1981) 416–421.
[185] J.R. Abney, J.C. Owicki, in: A. Watts, J.D. Pont (Eds.), Progress in Protein–Lipid Interactions, Elsevier Science Publishers, New York, 1985, pp. 1–60.
[186] O.G. Mouritsen, M. Bloom, M. Biophys. J. 46 (1984) 141–153.
[187] E. Sackmann, in: D. Chapman (Ed.), Biological Membranes, vol. 5, Academic Press, London, 1984, pp. 105–143.
[188] O.G. Mouritsen, M.M. Sperotto, in: M. Jackson (Ed.), Thermodynamics of Membrane Receptors and Channels, CRC Press, Inc., Boca Raton, FL, 1993, pp. 127–181.
[189] F. Dumas, M.M. Sperotto, M.C. Lebrum, J.-F. Tocanne, O.G. Mouritsen, Biophys. J. 73 (1997) 1940–1953.
[190] F. Dumas, M.C. Lebrum, J.-F. Tocanne, FEBS Lett. 485 (1999) 271–277.
[191] R.M. Epand, Biochim. Biophys. Acta 1376 (1998) 353–368.
[192] A.G. Lee, Biochim. Biophys. Acta 1376 (1998) 381–390.
[193] S. Munro, EMBO J. 14 (1995) 4695–4704.
[194] S. Munro, Trends Cell Biol. 8 (1998) 11–15.
[195] M.S. Bretscher, S. Munro, Science 261 (1993) 1280–1281.
[196] H. Pelham, S. Munro, Cell 75 (1993) 603–605.
[197] T.J. McIntosh, A. Vidal, S.A. Simon, Biophys. J. 85 (2003) 1656–1666.
[198] S.K., E. Ikonen, Nature 387 (1997) 569–572.
[199] W.H. Binder, V. Barragan, F.M. Menger, Angew. Chem. Int. Ed. 42 (2003) 5802–5827.
[200] S. Mukherijee, F.R. Maxfield, Ann. Rev. Cell Dev. Biol. 20 (2004) 839–866.

[201] P.C. Jost, O. Hayes Griffith, R.A. Capaldi, G. Vanderkooi, Proc. Natl. Acad. Sci. USA 70 (1973) 480–484.
[202] T.R. Hesketh, G.A. Smith, M.D. Houslay, K.A. McGill, N.J.M. Birdsall, J.C. Metcalfe, G.B. Warren, Biochemistry 15 (1976) 4145–4151.
[203] P. Jost, O.H. Griffith, Ann. N.Y. Acad. Sci. USA 348 (1980) 391–405.
[204] M. Rehorek, N.A. Dencher, M.P. Heyn, Biochemistry 24 (1985) 5980–5988.
[205] B. Piknová, E. Pérochon, J.-F. Tocanne, Eur. J. Biochem. 218 (1993) 385–396.
[206] T.A. Harroun, W.T. Heller, T.M. Weiss, L. Huang, H.W. Yang, Biophys. J. 76 (1999) 937–945.
[207] K. Bryl, K. Yoshihara, Eur. Biophys. J. Biophys. 29 (2001) 628–640.
[208] S.O. Nielsen, C.F. Lopez, I. Ivanov, P.B. Moore, J.C. Shelley, M.L. Klein, Biophys. J. 87 (4) (2004) 2107–2115.
[209] C. Glaubitz, G. Grobner, A. Watts, Biochim. Biophys. Acta 1463 (2000) 151–161.
[210] U. Harzer, B. Bechinger, Biochemistry 39 (2000) 13106–13114.
[211] S. Sharpe, K.R. Barber, C.W.M. Grant, D. Goodyear, M.R. Morrow, Biophys. J. 83 (2002) 345–358.
[212] P.C.A. van der Wel, E. Strandberg, J.A. Killian, R.E. Koeppe II, Biophys. J. 83 (2002) 1479–1488.
[213] R.B.M. Koehorst, R.B. Spruijt, F.J. Vergeldt, M.A. Hemminga, Biophys. J. 87 (2004) 1445–1455.
[214] E. Strandberg, S. Özdirekcan, D.T.S. Rijkers, P.C.A. van der Wel, R.E. Koeppe II, R.M.J. Liskamp, J.A. Killian, Biophys. J. 86 (2004) 3709–3721.
[215] S. Özdirekcan, D.T.S. Rijkers, R.M.J. Liskamp, J.A. Killian, Biochem. 44 (2005) 1004–1012.
[216] M. Ramakrishnan, J. Qu, C.L. Pocanschi, J.H. Kleinschmidt, D. Marsh, Biochemistry 44 (2005) 3515–3523.
[217] K. Gawrish, Private communication.
[218] M. Sperotto, O. Mouritsen, Biophys. J. 59 (1991) 261–270.
[219] S.-W. Chiu, E. Jakobsson, S. Subramaniam, H.L. Scott, Biophys. J. 77 (1999) 2462–2469.
[220] H.I. Petrache, A. Grossfield, K.R. MacKenzie, D.M. Engelman, T.B. Woolf, J. Mol. Biol. 302 (2000) 727–746.
[221] H.I. Petrache, D.M. Zuckerman, J.N. Sachs, J.A. Killian, R.E. Koeppe II, T.B. Woolf, Langmuir 18 (2002) 1340–1351.
[222] M.Ø. Jensen, E. Tajkhorshid, K. Schulten, Structure 9 (2001) 1083–1093.
[223] M.Ø Jensen, O.G. Mouritsen, Biochim. Biophys. Acta: Biomembr. 1666 (2004) 205–226.
[224] K. Belohorcová, J.H. Davis, T.B. Woolf, B. Roux, Biophys. J. 73 (1997) 3039–3055.
[225] L. Shen, D. Bassolino, T. Stouch, Biophys. J. 73 (1997) 3–20.
[226] J.Y.A. Lehtonen, P.K.J. Kinnunen, Biophys. J. 72 (1997) 1247–1257.
[227] A.N.J.A. Ridder, W. Van De Hoef, J. Stam, A. Kuhn, B. De Kruijff, J.A. Killian, Biochem. 41 (2002) 4946–4952.
[228] W.T.M. TM, P.C.A. van der Wel, J.A. Killian, R.E. Koeppe II, H.W. Huang, Biophys. J. 84 (2003) 379–385.
[229] A.N.J.A. Ridder, E.R.J. Spelbrink, J.A.A. Demmers, D.T.S. Rijkers, R.M.J. Liskamp, J. Brunner, A.J.R. Heck, B. Kruijff, J.A. Killian, Biochem. 43 (2004) 4482–4489.
[230] N. Dan, P. Pincus, S.A. Safran, Langmuir 9 (1993) 2768–2771.
[231] S. May, Langmuir 18 (2002) 6356–6364.
[232] G. Brannigan, F.L.H. Brown, Biophys. J. 90 (2006) 1501–1520.
[233] M. Venturoli, Mesoscopic models of lipid bilayers and bilayers with embedded proteins, Ph.D. Thesis, University of Amsterdam, 2005.
[234] C.F. Lopez, S.O. Nielsen, P.B. Moore, M.L. Klein, Proc. Natl. Acad. Sci. USA 101 (13) (2004) 4431–4434.
[235] C.F. Lopez, S.O. Nielsen, B. Ensing, P.B. Moore, M.L. Klein, Biophys. J. 88 (5) (2005) 3083–3094.
[236] C.F. Lopez, S.O. Nielsen, G. Srinivas, W.F. DeGrado, M.L. Klein, J. Chem. Theory Comput. 2 (3) (2006) 649–655.
[237] Y. Shai, Trends. Biochem. Sci. 20 (1995) 460–464.
[238] B. Bechinger, Biochim. Biophys. Acta 1462 (1999) 157–183.
[239] K. He, S.J. Ludke, H.W. Huang, D. Worcester, Biochemistry 34 (1995) 15614–15618.
[240] M. Sperotto, Eur. Biophys. J. 26 (1997) 405–416.
[241] G. Srinivas, M.L. Klein, Nanotechnology 15 (9) (2004) 1289–1295.
[242] W.M. Leevy, G.M. Donato, R. Ferdani, J. Am. Chem. Soc. 124 (31) (2002) 9022–9023.
[243] P.J. Bond, M.S. Sansom, J. Am. Chem. Soc. 128 (8) (2006) 2697–2704.
[244] L.K. Tamm, J. Crane, V. Kiessling, Curr. Op. Struct. Biol. 13 (2003) 453–466.
[245] R. Jahn, H. Grubmuller, Curr. Opin. Cell Biol. 14 (4) (2002) 488–495.
[246] V.S. Markin, M.M. Kozlov, V.L. Borovjagin, Gen. Physiol. Biophys. 3 (1984) 361–377.
[247] M. Müller, K. Katsov, M. Schick, J. Polym. Sci. B 41 (13) (2003) 1441–1450.
[248] M. Müller, K. Katsov, M. Schick, Biophys. J. 85 (3) (2003) 1611–1623.
[249] I. Carmesin, K. Kremer, Macromolecules 21 (1988) 2819–2823.
[250] S.J. Marrink, A.E. Mark, J. Am. Chem. Soc. 125 (37) (2003) 11144–11145.
[251] D.P. Sigel, Biophys. J. 76 (1999) 291–313.
[252] J.C. Shillcock, R. Lipowsky, Nat. Mater. 4 (3) (2005) 225–228.
[253] R. Lipowsky, M. Brinkmann, R. Dimova, C. Haluska, J. Kierfeld, J.C. Shillcock, J. Phys.: Condens. Matter 17 (2005) S2885–S2902.
[254] T. Baumgart, S.T. Hess, W.W. Webb, Nature 425 (2003) 821–824.
[255] M. Laradji, P.B. Sunil Kumar, Phys. Rev. E 73 (2006) Art. No. 040901.
[256] M.P. Allen, D.J. Tildesley, Computer Simulation of Liquids, Clarendon Press, Oxford, 1989.
[257] D. Frenkel, B. Smit, Understanding Molecular Simulations: from Algorithms to Applications, second ed., Academic Press, San Diego, 2002.
[258] O.G. Mouritsen, in: R. Brasseur (Ed.), Molecular Description of Biological Membrane Components by Computer Aided Conformational Analysis, CRC Press, Boca Raton, FL, 1990, pp. 3–83.
[259] D. Frenkel, G.C.A.M. Mooij, B. Smit, J. Phys.: Condens. Matter 4 (1992) 3053–3076.

[260] S.-W. Chiu, M.M. Clark, E. Jakobsson, S. Subramaniam, H.L. Scott, J. Comput. Chem. 20 (1999) 1153–1164.
[261] R.J. Mashl, H.L. Scott, S. Subramaniam, E. Jakobsson, Biophys. J. 81 (2001) 3005–3015.
[262] P.J. Hoogerbrugge, J.M.V.A. Koelman, Europhys. Lett. 19 (1992) 155–160.
[263] P. Español, P.B. Warren, Europhys. Lett. 30 (1995) 191–196.
[264] G. Besold, I. Vattulainen, M. Karttunen, J.M. Polson, Phys. Rev. E 62 (2000) R7611–R7614.
[265] I. Vattulainen, M. Karttunen, G. Besold, J.M. Polson, J. Chem. Phys. 116 (2002) 3967–3979.
[266] P. Nikunen, M. Karttunen, I. Vattulainen, Comput. Phys. Commun. 153 (2003) 407–423.
[267] A.F. Jakobsen, O.G. Mouritsen, G. Besold, J. Chem. Phys. 122 (2005) Art. No. 204901.
[268] M.P. Allen, J. Phys. Chem. B 110 (2006) 3823–3830.
[269] G. De Fabritiis, M. Serrano, P. Español, P.V. Coveney, Physica A 361 (2006) 429–440.
[270] P. Español, SIMU, Chall. Mol. Simul. 4 (2002) 59–77.
[271] P.B. Warren, Curr. Opin. Coll. Interface Sci. 3 (1998) 620–624.
[272] J.S. Rowlinson, B. Widom, Molecular Theory of Capillarity, Clarendon Press, Oxford, 1982.
[273] F. Jähnig, Biophys. J. 71 (1996) 1348–1349.
[274] R. Kwok, E. Evans, Biophys. J. 35 (1981) 637–652.
[275] S.-W. Chiu, M. Clark, S. Subramaniam, H.L. Scott, E. Jakobsson, Biophys. J. 69 (1995) 1230–1245.
[276] R. Zhang, W. Sun, S. Traistram-Nagle, R.L. Headrick, R.M. Suter, J.F. Nagle, Phys. Rev. Lett. 74 (1995) 2832–2835.
[277] S.E. Feller, Y. Zhang, R.W. Pastor, J. Chem. Phys. 103 (1995) 10267–10276.
[278] D.P. Tieleman, H.J.C. Berendsen, J. Chem. Phys. 105 (1996) 4871–4880.
[279] S.E. Feller, R.W. Pastor, J. Chem. Phys. 111 (1999) 1281–1287.
[280] F. Sun, Biophys. J. 85 (2002) 2511–2519.
[281] J.F. Nagle, R. Zhang, S. Tristram-Nagle, W. Sun, H.I. Petrache, R.M. Suter, Biophys. J. 70 (1996) 1419–1431.
[282] J. Seelig, A. Seelig, Q. Rev. Biophys. 13 (1980) 19–61.
[283] J.F. Nagle, Biophys. J. 64 (1993) 1476–1481.
[284] E. van den Brink-van der Laan, R.E. Dalbey, R.A. Demel, J.A. Killian, B. deKruijff, Biochemistry 40 (2001) 9677–9684.
[285] R.S. Cantor, J. Phys. Chem. B 101 (1997) 1723–1725.
[286] R.S. Cantor, Toxicol. Lett. 101 (1998) 451–458.
[287] R.S. Cantor, Chem. Phys. Lipids 101 (1999) 45–56.
[288] K. Tu, M. Tarek, M. Klein, D. Scharf, Biophys. J. 75 (1998) 2123–2134.
[289] E. Perozo, A. Kloda, D.M. Cortes, B. Martinac, Nature Struct. Biol. 9 (2002) 696–703.
[290] E. Lindahl, O. Edholm, J. Chem. Phys. 113 (2000) 3882–3893.
[291] J. Gullingsrud, K. Schulten, Biophys. J. 86 (2004) 3496–3509.
[292] M. Patra, Euro. Biophys. J. 35 (1) (2005) 79–88.
[293] F. Varnik, J. Baschnagel, K. Binder, J. Chem. Phys. 113 (2000) 4444–4453.
[294] J.G. Kirkwood, F.P. Buff, J. Chem. Phys. 17 (1949) 338–343.
[295] S. Ono, S. Kondo, in: S. Flugge (Ed.), Encyclopedia of Physics, vol. 10, Springer, Berlin, 1960.
[296] J.P. Hansen, I.R. McDonald, Theory of Simple Liquids, second ed., Academic Press, London, 1986.
[297] M.P. Allen, D.J. Tildesley, Computer Simulation of Liquids, Clarendon Press, Oxford, 1987.
[298] J.P.R.B. Walton, D.J. Tildesley, J.S. Rowlinson, Mol. Phys. 48 (1983) 1357–1368.
[299] J.H. Irving, J.G. Kirkwood, J. Chem. Phys. 18 (1950) 817–829.
[300] A. Harasima, Adv. Chem. Phys. 1 (1958) 203.
[301] M.J.P. Nijmeijer, A.F. Bakker, C. Bruin, J.H. Sikkenk, J. Chem. Phys. 89 (1988) 3789–3792.
[302] E. Lindahl, O. Edholm, Biophys. J. 79 (2000) 426–433.
[303] S.J. Marrink, A.E. Mark, J. Phys. Chem. B 105 (2001) 6122–6127.
[304] R. Lipowsky, S. Grotehans, Europhys. Lett. 23 (1993) 599–604.